How do birds sing?

sound analysis - mechanical modelling - muscular control

Coen P.H. Elemans

Promotor: prof. dr. ir. Johan L. van Leeuwen
Hoogleraar in de Experimentele Zoölogie

Co-promotoren: dr. Mees Muller
Universitair hoofddocent bij de leerstoelgroep Experimentele Zoölogie

dr. Ole Næsbye Larsen
Universitair hoofddocent aan de Syddansk Universitet, Odense, Denmark

Overige leden promotiecommissie:

prof. dr. Peter Aerts
Universiteit Antwerpen

prof. dr. Johan Bolhuis
Universiteit Utrecht

prof. dr. Carel ten Cate
Universiteit Leiden

prof. dr. Franz Goller
University of Utah, United States of America

prof. dr. ir. Mico Hirschberg
Technische Universiteit Eindhoven / Technische Universiteit Twente

prof. dr. Rolf Hoekstra
Wageningen Universiteit

Dit onderzoek is uitgevoerd binnen de onderzoeksschool WIAS.

How do birds sing?

sound analysis - mechanical modelling - muscular control

Coen P.H. Elemans

Proefschrift ter verkrijging
van de graad van doctor
op gezag van de rector magnificus
van Wageningen Universiteit, Prof. Dr. Ir. L. Speelman,
in het openbaar te verdedigen op vrijdag 12 november 2004
des namiddags te vier uur in de Aula

Elemans, C.P.H. (2004) How do birds sing? sound analysis – mechanical modelling – muscular control
PhD thesis, Experimental Zoology Group, Wageningen University.
P.O. Box 338, 6700 AH Wageningen, The Netherlands.

Subject headings: sound production/biomechanics/vocal control/birdsong/*Streptopelia*/muscle physiology

ISBN: 90-8504-111-2

Wenn nun die Pfeife angezündet,
So sieht man, wie im Augenblick
Der Rauch in freier Luft verschwindet,
Nichts als die Asche bleibt zurück.
So wird des Menschen Ruhm verzehrt
Und dessen Leib in Staub verkehrt.

Unknown poet in J.S. Bach BWV 515a Erbauliche Gedanken eines Tobackrauchers, about 1733-1734.
(Opbouwende gedachten van een tabaksroker, J.S. Bach)

Abstract

Communication is a main key to survival. Many animals use sound to exchange information, which is important in species recognition, sexual selection and consequently in speciation. The animals best known for their vocal virtuosity are birds, which use acoustic signals extensively to communicate. Bird song supplies an important model in the study of learned vocal communication including human speech, animal behaviour and speciation. To produce sound, birds have evolved an organ unique in the animal kingdom; the syrinx, which is located at the bifurcation of the trachea into the bronchi. Although the syrinx was already identified as the sound source in the 18th century, the principle mechanisms that generate the sound are still under debate. Unravelling the physiology of sound production faces tremendous experimental challenges despite improved technologies due to its inaccessible location in the birds' body.

In this thesis, we focussed on the mechanisms underlying sound production and explored three approaches to improve understanding of both sound production and vocal control in birds. First, we explored what sound signals can teach us about the underlying mechanical events using a theoretical signal analysis approach.

Second, we present the first mechanical model of the syrinx that facilitates detailed study of membrane vibrations. As inception we used a relatively simple non-oscine syrinx of the family Columbidae. Our model consisted of a tube with a single membrane in its casing. The adduction of the membrane was controlled by the pressure in a simulated air sac relative to the driving pressure in the tube. We used the Laser Doppler Vibrometry (LDV) technique to measure membrane vibrations, and also measured air sac and bronchial pressures in our model. The functional window for sound production was determined by the position of the membrane. Without an initial complete closure of the tube by the membrane, no membrane oscillations were induced, and no sound was produced. The vibrations of the membrane were coupled to the resonance properties of the distal tube, but membrane material properties and tension also alterd the frequency of the sound.

Third, we studied the contractile properties of the syringeal muscles that control sound production in the ring dove (*Streptopelia risoria*). We showed that the syringeal muscles of ring doves are highly specialised superfast muscles. We simultaneously recorded sound and muscle activity with electromyography *in vivo* and showed that the syringeal muscles gate and frequency-modulate individual sound elements of the trill. Additionally, we measured the *in vitro* contractile properties of the syringeal muscles. These force measurements confirmed the superfast twitch characteristics of the syringeal muscles. The discovery of this special muscle type in the syrinx implied that superfast muscle can no longer be considered a rare adaptation and are probably the main muscle type controlling birdsong.

We also investigated the non-isometric properties of the syringeal muscles in ring doves using the workloop technique. The capabilities of the syringeal muscles strongly supported the notion that they act as antagonists for the positioning of the sound-producing structures, the lateral tympaniform membranes. The morphology of the syringeal muscles at ultra-structural level was typical for muscles that are superfast and require a high endurance. We observed large quantities of mitochondria, sarcoplasmatic reticulum and two T-tubuli per sarcomere in both muscles. Our results provided strong evidence that the syringeal muscles are the main frequency modulating structures of song in ring doves. Furthermore, our *in vitro* results on force modulation serve as essential input to state-of-the art mathematical models of sound production in birds.

Contents

SECTION I

general introduction

chapter **1**

General introduction and outline of thesis

Central motivations to study avian vocal production

Communication is a main key to survival. From the start of multicellular life about one billion years ago, up to now, organisms have evolved modalities to exchange information by a myriad use of colours, sounds, chemicals, movements and even electrical signals. Many animals use sound to exchange information; it is the origin modality for human language (Bradbury & Vehrencamp, 1988). The animals best known for their vocal virtuosity are birds (Catchpole & Slater, 1995). Birds use acoustic signals extensively to communicate, which is important in species recognition, sexual selection and consequently in speciation (Kroodsma & Miller, 1996). In order to reproduce, communication signals must be embedded in successful behavioural patterns. This requires strong interaction between the nervous system, peripheral morphology and environment (Chiel & Beer, 1997). A prime example of this rich interplay is birdsong, where neural instructions drive a highly nonlinear sound-generating system (Fee et al., 1998) that is capable of generating complex acoustic signals over a wide range of timescales (Greenewalt, 1968).

These aspects provide strong central motivations to study bird song. It offers some of the clearest opportunities for examining how coordinated neuromuscular control (Suthers et al, 1999) and peripheral mechanisms contribute to behaviour. Furthermore, bird song supplies a model for signal evolution or co-evolution of multi-modal signals (Cooper & Goller, 2004) and provides an important model in the study of learned vocal communication including human speech (Doupe & Kuhl, 1999), animal behaviour (Chiel & Beer, 1997) and speciation (Podos, 2000).

The diversity of bird song

Birds combine their sounds into intricate strings of syllables that form species-specific songs. Some species have repertoire sizes of over one hundred of separate syllables. Birds can also be plastic with their songs; they can imitate other birds, mobile phones or other sounds, and they also develop dialects. Most information exchanges between conspecific individuals do not consist of elaborate and complicated songs, but of short calls or squeaks. These vocalisations can be divided into several categories based on their function, such as general alarm calls, distress calls, nest calls, flock calls and even pleasure calls.

Bird song is ubiquitous and has influenced many aspects of human civilisations. Maybe first of all, the song complexity and melody of avian vocalists has inspired composers and musicians throughout time and place. Our own famous Western classical composers such as Vivaldi, Beethoven and Schubert used bird songs in their compositions. J.S. Bach wrote a sonate (BWV 963, part 4, in Re majeur: Thema all'Imitatio Gallina Cucoa) in which a cuckoo battles a chicken (and wins). Mozart was likely to be inspired by his pet starling (*Sturnus vulgaris*) to write the controversial 'Ein musikalischer Spass'. Although birds have not evolved their song deliberately to please our ears, we do enjoy the songs of birds. For many people, the song of birds in their gardens provides a strong connection to nature. The vast numbers of enthusiastic birdwatchers increase the awareness of the importance and urgency to conserve important bird areas (IBA's) and as such contribute to the conservation of biodiversity around the world. In the words of Sir David Attenborough (1998), a.k.a. the great communicator: "It is hardly surprising that human beings have studied birds with a greater dedication and intensity than they have lavished on any other group of animal". Aside from

scientific arguments, the latter makes it even more surprising that even up today, the mechanisms underlying sound production in birds are still poorly understood.

What is sound?

Sound is a propagating wave of pressure variation through a medium. These pressure variations are small: they are generally less than 20 Pa, compared with the atmospheric pressure of about 100,000 Pa. For sound to be generated, the regions over which the pressure and density of the medium change, must be much larger than the distance that the molecules travel before colliding with other molecules. Otherwise the molecules would move freely from the crest to the trough of the wave and immediately smear out the wave. A sound wave travels at roughly half the average molecular speed (Feynman et al., 1963). In air of 20°C, the speed of a sound wave is about 340 m/s and in water of 20°C it is about 1500 m/s. The frequency of a sound wave is determined by the number of wave cycles per second, or Hertz. The human ear detects sound frequencies from 20 Hz to 20 kHz. This range is called audible sound or audio. Most birds perceive from 200 Hz to 10 kHz, with maximal sensitivity at 2 kHz (Bradbury & Vehrencamp, 1998).

As sound travels, it transports energy with it. This energy deflects our eardrum allowing us to perceive the wave. The amount of energy in sound waves is generally very low. For example, the acoustic energy of the combined shouts in the EU soccer final would be just enough to fry an egg. A large jet aircraft, however, generates as much acoustic power as the entire world's population screaming all at once (Dowling & Ffowcs Williams, 1983).

How do birds sing?

The amphibians, reptiles, and mammals use their larynx to produce sound. The larynx is located at the rostral end of the trachea and has presumably evolved with the primary function to separate the airways from the digestive tract. In some reptiles, many amphibians, and all mammals the larynx also harbours paired structures, the so-called vocal folds or vocal membranes that can vibrate and generate sound.

The larynx is also present in birds. However, birds have evolved a new organ that is unique in the animal kingdom. Sound is produced in the syrinx, which is located at the bifurcation of the trachea into the bronchi. The first morphological descriptions of the syrinx in the literature appear in the 18th and 19th century by Hérissant (1753) and Cuvier (1802). The morphological diversity of syringeal morphology is enormous and the dichotomous classification of all birds into songbirds or non-songbirds is based on syringeal morphology and not on their vocal abilities: e.g. a parrot is a non-songbird and a crow is a songbird. Apparently the syrinx was a successful key invention in the evolution of birds; there is no trace of it in the reptiles and, as far as we know, the larynx is never used for sound production in birds (Gaunt & Gaunt, 1985).

Although the syrinx was already identified as the sound source in the 18th century, the principle mechanisms that generate the sound are still under debate. Due to its inaccessible location in the birds body, the function of the syrinx was mainly derived from morphological observations and

physiological measurements such as flow, pressure and muscle activity (for reviews see Gaunt & Gaunt (1985), Nottebohm (1976), Goller & Larsen (2002) and many references herein). Sound was believed to be produced by flow-induced vibrations of thin membranous structures named the medial tympaniform membranes. However, direct observations using fibre optics by Goller & Larsen (1997a, 1997b, 2002) changed the dominant idea that the medial tympaniform membranes were the principal sound generators. It is now demonstrated in songbirds that sound is produced by oscillations or collisions of the labia (Goller & Larsen, 1997b, 2002). For non-songbirds, we cannot yet make general statements since the syringeal morphology is more diverse, and only two species have been studied. No name covers the multitude of structures present in the different families that possibly generate sound. However, in the pigeon (*Columba livia*), sound is produced by vibrations of structures named the lateral tympaniform membranes or LTM's (Goller & Larsen, 1997a).

Unravelling the physiology of sound production faces tremendous experimental challenges despite improved technologies. Direct observations only succeeded with anaesthetised birds because of the uncomfortable fibrescopes in their mouth. There are numerous surgical difficulties due to the location of the syrinx deep inside the body. Once all these difficulties have been conquered, the interpretation of *in vivo* signals still requires great care, since transducers are subject to drift, mucous accumulation etc.

Until recently, it was assumed that the central nervous system directly controls all complex features of song (Konishi, 1994). In order to complete the path that leads from the brain to the sound, it was necessary to formulate adequate mathematical models of the sound producing organ - the syrinx - (Fee et al., 1998; Gardner et al., 2001; Laje et al. 2001; Laje & Mindlin, 2002). These mathematical models showed that complex song cannot be attributed solely to equally complex neural instructions, because the nonlinear nature of the syrinx introduced complexity into the vocalizations (Fee et al., 1998; Goller, 1998). The models employ grossly simplified morphology, control and physical principles that underlie bird phonation, but they nevertheless provide insight in the minimal amount of parameters needed to reproduce bird songs (Mindlin et al., 2003). Mathematical modelling of the physical mechanisms of the syrinx is an indispensable complement to the more traditional approach towards the study of motor control of birdsong. Modelling is more profitable than directly correlating neural instructions with acoustic outputs (Suthers & Margoliash, 2002).

Aim and synthesis of thesis

As argued above, the production of sound in birds is still poorly understood, and unravelling the physiology of sound production faces tremendous experimental challenges. In this thesis, we focus on the mechanisms underlying sound production and examine three distinct approaches that aim to improve understanding of both sound production and vocal control in birds.

** Sound analysis*

What information can we obtain about the underlying mechanical events by just looking at the sound signal? We present a theoretical approach to signal analysis that explores the structure of sound signals.

** Mechanical modelling*

We present a mechanical model of the syrinx that allows for more accurate measurements of sound production than *in vivo* studies of the syrinx.

** Muscular control*

In a study on sound production *in vivo*, we focus on muscular control in a model species, the ring dove (*Streptopelia risoria*). We combine *in vivo* measurements of muscle activity with *in vitro* mechanical properties of the two syringeal muscles to study the control mechanisms that alter sound properties such as amplitude and frequency.

Thesis outline

Section I: General introduction

Together with the current chapter, the first section provides an overall introduction to the thesis. In chapter 2, we review the status quo in current quantitative models of the biomechanics of bird sound production. An important aero-acoustic model is a quantitative model of the vocal apparatus by Fletcher (1988) that represents the syrinx (i.e. the portions of the trachea and bronchi with labia and membranes) as a single membrane. This membrane acts as a valve that rapidly closes and opens during phonation. This model can be used as a basis to address comparative morphological and physiological questions. More recently, the syrinx has been modelled as a simple modified oscillator based on models of human phonation (Gardner et al., 2001; Fee et al, 1998; Laje & Mindlin, 2002; Laje et al., 2002; Mindlin et al., 2003). Many features of the sound are captured remarkably well. The parameter values, however, do not represent the distribution of the actual material properties of the syrinx. These models demonstrate the minimum number of parameters required to describe the essential dynamics of the sound signal. Furthermore, we address possible interesting future directions for modelling.

Section II: Sound analysis: from sound to the sound generators

Chapter 3 provides a theoretical approach to sound production by animals. Here, we explore what the sound signals themselves can teach us about the underlying mechanical events. We aim to provide basic assessment tools for sound analysis to identify candidates for sound generators

and modulators, complementary to modelling the dynamics of the specific sound generators. We go back to the basics of signal analysis to explore spectrograms that visualise the time-frequency content of a signal. Spectrograms are commonly used to analyse animal vocalisations. We show that the physiological basis for sound generation and modulation can be assessed using spectrogram analysis. First, we synthesise common features in bird vocalisations such as transients, harmonics, amplitude- and frequency modulation and non-linear events by an array of simple artificial signal modifications (e.g. by introducing nonlinearities such as clipping). To illustrate the explanatory power of the approach, we analyse the sound signal of a real bird. We reconstruct this vocalisation mathematically using the previously described effects of signal modifications. This approach yields not only convenient statistical descriptions, but also aids in formulating hypotheses about the underlying physiological mechanisms. The predictive power of the spectrogram analysis is substantiated by its application to sound production of a simple mechanical model; the drone reed of a bagpipe. We show that many clues (such as collisions) regarding the physiological basis of sound generation can be extracted from spectrograms. However, it proves to be difficult to provide unambiguous proof on the mechanical origin of features found in spectrograms without a priori knowledge of the underlying mechanical events.

Section III: Mechanical modelling of the syrinx

Next, we focus on sound production in birds. We built a simple mechanical model of the syrinx to study the role of pressure and membrane properties on the sound generation. The vibratory behaviour of the labia or membranes in the syrinx determines to a large extent the nature of the produced sound, and these complex movements are largely unknown due to the problems encountered with *in vivo* observations. In chapter 4, we present the first mechanical model of the syrinx that facilitates detailed study of membrane vibrations. As inception we used a relatively simple non-oscine syrinx of the family Columbidae. Our model consists of a tube with a single membrane in its casing. The adduction of the membrane is controlled by the pressure in a simulated air sac relative to the driving pressure in the tube. We used the Laser Doppler Vibrometry (LDV) technique to measure membrane vibrations, and also measured air sac and bronchial pressures in our model. The functional window for sound production is determined by the position of the membrane. Without an initial complete closure of the tube by the membrane, no membrane oscillations are induced, and no sound is produced. The vibrations of the membrane are coupled to the resonance properties of the distal tube, but membrane properties and tension also alter the frequency of the sound. Mechanical modelling provides an excellent opportunity to test the mathematical models of the syrinx.

Section IV: Muscular control of vocal production

In order to generate more than a few stereotyped songs, birds need to have control over the parameters that determine the sound. In this section, we use the insights gained on vocal production in the previous chapters and study vocal control by the syringeal muscles. As a model species, we chose the ring dove (*Streptopela risoria*), which is a domesticated form of the Barbary dove (*S. roseogrisea*). Its song and syringeal morphology are relatively simple, and the song of this species is well studied in a wide context. In chapter 5, we describe biological aspects of the ring dove, such as field characteristics, distribution, habitat, food and voice. Many birdsongs contain sound elements that require extremely fast control. The trill in the coo of the ring dove is a sequence of

short sound elements that may be as short as 10 ms. If their generation is under active control, fast muscle contractions are required that approach the performance limits of vertebrate muscles. In chapter 6, we show that the syringeal muscles of ring doves are so-called superfast muscles. We simultaneously recorded sound and muscle activity with electromyography *in vivo* to show that the syringeal muscles gate and frequency-modulate individual sound elements of the trill. Additionally, we measured the *in vitro* contractile properties of the syringeal muscles. These force measurements confirm the superfast twitch characteristics of the syringeal muscles. The discovery of this special muscle type in the syrinx implies that superfast muscle can no longer be considered a rare adaptation found only in a few highly derived acoustic organs such as in the toadfishes swimbladder and the rattlesnake's tail. Superfast muscles are probably the main muscle type controlling birdsong.

In chapter 7, we investigate the non-isometric properties and the ultra-structure of the syringeal muscles of ring doves. We varied the amplitude and frequency of length changes to measure power and work performance, i.e. we applied the so-called workloop technique. For both the syringeal muscles, i.e. the tracheolateralis and sternotrachealis muscle, the overall relationships between net work and power output versus cycle frequency resemble that of the fastest known vertebrate muscle, the toadfish swimbladder muscle. The two muscles produce positive power at cycle frequencies up to 30-50 Hz. The morphology of the syringeal muscles at ultra-structural level is typical for muscles that are superfast and require a high endurance. We observed large quantities of mitochondria, sarcoplasmatic reticulum and two T-tubuli per sarcomere in both muscles. The capabilities of the syringeal muscles strongly support the notion that they act as antagonists for the positioning of the sound-producing structures, the lateral tympaniform membranes. The highest power output was recorded at a 20 Hz cycle frequency for both muscles, close to the trill rate of 25 Hz in the main vocalisation of doves, the coo. Furthermore, both muscles have their highest power output at the same contraction amplitude of 0.75 mm. We calculated that the stress on the LTM exerted by the muscles is at least five times higher than the stress caused by pressure differences in the respiratory system during 76% of the coo. In the absence of *in vivo* force and strain measurements, *in vitro* workloops provide strong evidence that the syringeal muscles are the main frequency modulating structures of song in ring doves. This conclusion is based on the assumption that muscle performance is adapted to muscle function, and hence performance characteristics obtained *in vitro* can be extrapolated to muscle function *in vivo*. Furthermore, our *in vitro* results on force modulation serve as essential input to state-of-the art mathematical models of sound production in birds.

Section V: General discussion

Finally, chapter 8 summarises and discusses the most important results of this thesis. we discuss the implications of our findings on sound production and control in ringdoves. Furthermore, we indicate directions of further research on the rapidly developing field of vocal production.

Acknowledgements

Larsen, Johan van Leeuwen, Mees Muller and Ulrike Müller are greatly acknowledged for useful discussion and suggestions for improvement of the text.

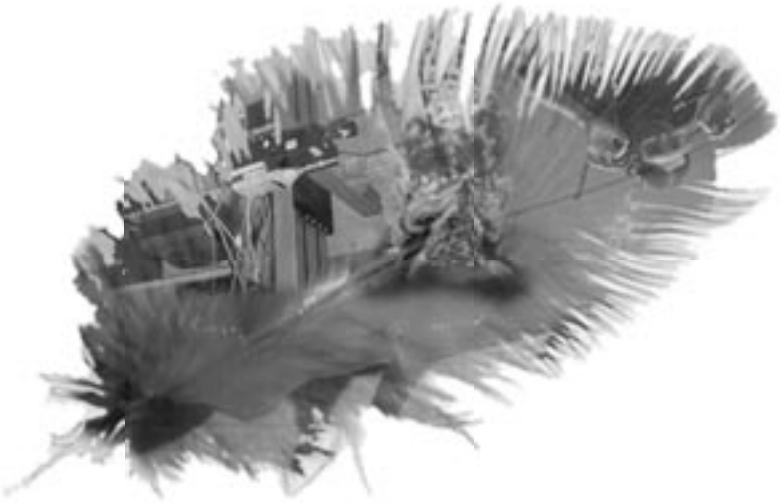

chapter **2**

Quantitative modelling of the biomechanics of the avian syrinx

Published as:
Coen P.H. Elemans, Ole N. Larsen, Marc R. Hoffmann, & Johan L. van Leeuwen (2003) Quantitative modelling of the biomechanics of the avian syrinx. *Animal Biology* **53**,183-193.

Abstract

We review current quantitative models of the biomechanics of bird sound production. A quantitative model of the vocal apparatus was proposed by Fletcher (1988). He represented the syrinx (i.e. the portions of the trachea and bronchi with labia and membranes) as a single membrane. This membrane acts as a valve that rapidly closes and opens during phonation. This model can be used as a basis to address comparative morphological and physiological questions. More recently, the syrinx was modelled as a simple modified oscillator. Many features of the sound were captured remarkably well. The parameter values, however, did not represent the distribution of the actual material properties of the syrinx. These models demonstrated the minimum number of parameters required to describe the essential dynamics of the sound signal. Furthermore, we address possible interesting future directions for modelling.

Introduction

The beauty of the virtuoso singing of birds has inspired composers and scientists for centuries, but only during the last few decades has the understanding of the mechanisms and control of sound production accelerated rapidly. The avian sound source was identified 250 years ago (Hérissant, 1753) as a modification of the airway and was named the syrinx (Huxley, 1877; cited in King, 1989). Syringeal morphology of the extant bird species varies considerably (cf. figure 2.1), and the variation has been used for taxonomic classification, e.g. the distinction between songbirds (oscines) and non-songbirds (non-oscines). For reviews on syrinx morphologies see e.g. Setterwall (1901), Rüppell (1933) and King (1968). Of the over 9600 extant bird species known, almost 4000 species are non-songbirds (Pough et al., 2002) that have no extrinsic syringeal muscles.

Several qualitative models of syringeal function to explain sound generation in birds have been debated (Greenewalt, 1968; Gaunt & Gaunt, 1985; Goller & Larsen, 2002) and many references therein). Recently, Goller & Larsen (1997b, 2002) showed by direct endoscopic observations that in songbirds the actual sources of sound were the vibrating labia acting as pneumatic valves. This 'labial hypothesis' was in contrast to the thin Medial Tympaniform Membranes (MTM's) as being the sound generators, as was previously hypothesised based on morphological observations. Endoscopic observations also suggested that in the pigeon (*Columba livia*) and the cockatiel (*Nymphicus hollandicus*), two non-songbird species, the Lateral Tympaniform Membranes (LTM's) acted as a pneumatic valve in the trachea (Goller & Larsen, 1997a; Larsen & Goller, 1999). Identification of the vibratory sound generators demonstrated that the physical mechanisms underlying sound production in the syrinx were similar to the mechanisms found in the larynx of most tetrapods.

The capability of songbirds to generate more variable songs than non-songbirds does not necessarily imply that the sound elements generated by non-songbirds exhibit less complexity. Signal classifications used in the literature such as tonal sounds, harmonic stacks and chaotic signals (Fitch et al., 2002; Wilden et al., 1998) can be found in both songbirds, e.g. in zebrafinches (Fee et al., 1998), and in non-songbirds, e.g. parrots (Fletcher, 2000). The most likely causes for the generation of the more variable songs in songbirds are their neuromuscular control of the syrinx (Laje & Mindlin, 2002) and proximal structures (beak, tongue) and learning capabilities (Brainard & Doupe, 2000; Suthers et al. 1999; Wild, 1997).

Until about 1990, only a few attempts have been undertaken to describe the physics quantitatively (Brackenbury, 1979; Casey & Gaunt, 1985; Fletcher, 1988). The issue has been given a new impulse due to the direct endoscopic observations in birds by Goller and Larsen. Recently, the efforts of physiologists and physicists have led to a new quantitative approach to the mechanisms underlying songbird sound production by presenting models based on human vocal fold models (Fee et al., 1998; Fee, 2002; Fry, 1998; Gardner et al., 2001; Laje et al., 2002a; Laje & Mindlin, 2002). However, the morphology of the sound system has been either largely ignored or strongly simplified. To answer biological questions, physicists often use powerful quantitative tools that are unknown to biologists. Models can teach us a lot about a system, despite their conceptual, mathematical or physical limits. Not all models are equally suited to answer any given question, so it is paramount to choose a model that can deliver meaningful answers.

In this paper, we discuss the status quo of quantitative modelling of the biomechanics of bird sound production. We consider the strengths and limitations of these models and their applicability to biological questions. It is, however, not our aim to explain the mathematical details of the models.

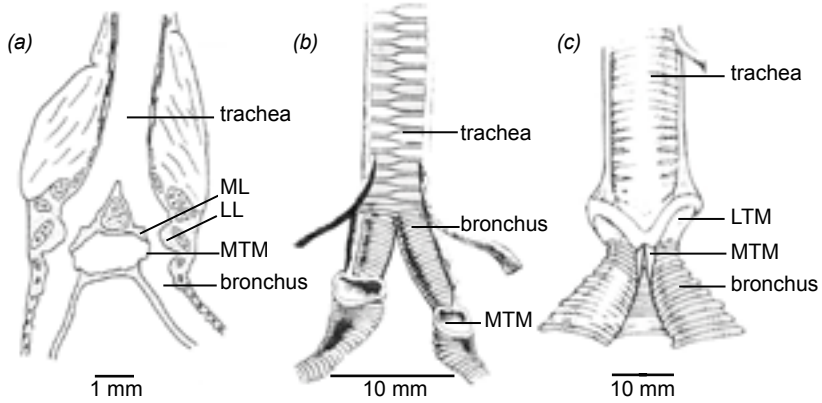

Figure 2.1 Variation in syrinx morphologies. (a) Cross-section through the syrinx of a Brown thrasher (*Toxostoma rufum*), which is a typical Passeriniform syrinx (modified after Suthers et al. (1999). (b) Ventral external view of the syrinx of an oilbird (*Steatornis caripensis*; modified after King, 1989) and (c) of a cormorant (*Phalacrocorax carbo*; modified after King, 1989). ML, Medial Labium; LL, Lateral Labium; LTM, lateral tympaniform membrane; MTM, medial tympaniform membrane.

Review of mathematical syrinx models

In order to provide a clear overview, it is essential to define some terms on the concepts of modelling. A physical model, or mechanical model, is a real object. A mathematical model is a purely mathematical construct. A conceptual physical model is the geometry and the physical principles on which the mathematical model is based. A computational model is the implementation of a mathematical model in a computer programme with which simulations can be made for a selected range of values of the input parameters.

Several mathematical syrinx models are compared in table I. The models use the concept that the sound sources in birds are the MTM's (Brackenbury, 1979; Fletcher, 1988) or labial masses (Fee et al., 1998; Fee, 2002; Fry, 1998; Gardner et al., 2001; Laje et al., 2002a; Laje & Mindlin, 2002). To our knowledge, there is no model specifically constructed based on LTM vibrations. All models aim to explain signal properties (e.g. spectral composition) of the radiated sound from the dynamics of either vibrating membranes or two paired labia in the syrinx. Presently, only one model can account for both the production of pure tone sounds and complex harmonic sounds (Fry, 1998).

The related literature on so-called 'collapsible tubes' is vast. The knowledge and classification of the phenomena of collapsible tubes such as blood vessels is extremely relevant for modelling birdsong production in the near future. We would like to refer to e.g. Bertram & Pedley (1982), since it is beyond the scope of this review to include this subject.

Aero-acoustic models

The prime examples of this type of model are those of Brackenbury (1979) and of Fletcher (1988). Brackenbury (1979) calculated the amplitude of the vibrating syringeal membranes to estimate the radiated power output for crows of a cock *(Gallus domesticus*). However, unrealisti-

Table I Comparison of models in literature. A. Brackenbury (1979b); B. Fletcher (1985); C. Fee et al. (1998); D. Fry (1998); E. Gardner et al. (2001); F. Laje et al. (2002); G. Fee (2002). [1] SD; Spring Damper model, [2] TM; Tympaniform Membrane

Model type	aeroacoustical			modified oscillators			
Model	**A**	**B**	**C**	**D**	**E**	**F**	**G**
Aim of model development							
Neuromuscular control			•	•	•	•	
Morphology							
General mechanisms	•	•					•
Bird group							
Passeriformes (song birds)		•	•	•	•	•	•
Non-songbirds	•						
MTM modelled by							
Moving piston	•						
Edge clamped drum		•					
Labia modelled by							
One/two mass SD[1]			•	•	•	•	
Multiple mass SD[1]							•
Input parameters							
Bronchial pressure	•	•	•	•	•	•	
Complex pressure wave		•					
Labial / membrane stiffness		•		•	•	•	•
Gating of flow						•	
Model output tested							
Generation sounds	•	•	•	•	•	•	
Acoustical power output		•		•			
Amplitude modulation				•			
Pressure gradient over TM[2]		•					

cally large membrane amplitudes of several millimetres were required for the model to produce the measured power levels. The discrepancy probably stems from the physical assumptions that were made to describe the system mathematically. Brackenbury modified a model of Ffowcs Williams & Lovely (1975) and used their theoretical discussion on a vibrating surface panel exposed to a semi-infinite uniform tangential fluid flow. Ffowcs Williams & Lovely (1975) assumed that the moving panel had no influence on the bulk flow. As pointed out by Fletcher (1988), Brackenbury's geometric representation (redrawn in figure 2.2a) in fact did not correspond to the conceptual

physical model used by Ffowcs Williams & Lovely (1975), represented by the drawing shown in figure 2.2b. Contrary to Brackenbury's assumptions, pressure waves are produced in the syrinx as the result of the mutual influence of the membranes or labia and the flow.

Fletcher's model of the avian syrinx (Fletcher, 1988) was essentially a quantification of proposals by Greenewalt (1968). It described sounds induced by moving surfaces, and combined solid mechanics and fluid dynamics. A similar approach was previously used to model reed-driven woodwind instruments. Fletcher modelled the geometry of the vocal system as a serial array of acoustic elements: an air-sac with driving pressure p_G, a certain acoustical resistance (or impedance, assumed to be low with respect to the resistance of the syrinx), a proximal reservoir (representing a bronchus), a syrinx portion modelled as a short tube with a single moving membrane in the wall opposite a ridge, a tube representing the trachea, and a horn (representing mouth and beak, figure 2.2c). In birds, this geometry is three-dimensional, but for simplification the components of the model were taken were one or two-dimensional.

To model the pressure and flow, Fletcher used a force balance between the dynamic pressure forces, the acceleration of the moving membrane and the forces on the membrane due to the difference between the external pressure in the air-sac and the bronchial pressure (resp. p_G and p_B in figure 2.2c).

The syrinx itself was modelled as a tube with one moving membrane and a stiff opposite wall. The longitudinal extension of the membrane was assumed to be much smaller than the length of the trachea. To simplify the calculation of the forces on the membrane, the calculation were split into a down- and an up-stream half. The aerodynamic forces on the membrane due to pressure were calculated only for the upstream half. For the downstream half, the pressure was assumed to equal the pressure in the proximal trachea (p_T). The pressure on the outer side (p_G; representing air-sac pressure) of the membrane was prescribed and was also used to drive the system at the tube entrance.

The trans-membranous pressure difference was the difference between the local pressure inside the tube and the (relatively) steady air-sac pressure. The pressure in the bronchus varied and depended on the impedance Z_G, the flow out of the syrinx U and the pressure differential over the impedance (see figure 2.2c). Nevertheless, quasi-steady flow and incompressibility of the air was assumed: at each time instant the steady Bernoulli equation was applied to relate pressure and velocity (ignoring friction). The membrane in Fletcher's model closed of the tube in its resting position and acted as a valve that rapidly closed and opened during phonation.

The position of the membrane was limited to mimic a collision by setting the damping constant of the membrane κ to a much higher value in the motion equation, when the membrane touched the opposite wall. Brackenbury (1979) assumed a non-linear elasticity to avoid unrealistically large oscillations of the membrane. But Fletcher (1988) found this to cause unspecific "undesirable effects", and instead chose to nonlinearly increase the so-called effective mass of the membrane.

To describe the forcing term in the equation of motion of the membrane, Fletcher summated the forcing terms for the first two dominant modes. This resulted in a harmonically complex driving force for the membrane. This force that drove the oscillation did not simply increase bronchial pressure as measured in birds. It should be noted, however, that the pressure measurements *in vivo* were generally frequency limited.

The tension effects of muscle activity were included in the tension parameter T. In the model, the final tension in the membrane is determined by two factors: the trans-membranous pressure and muscles pulling on the membrane. Active gating of flow by e.g. muscle activity was not im-

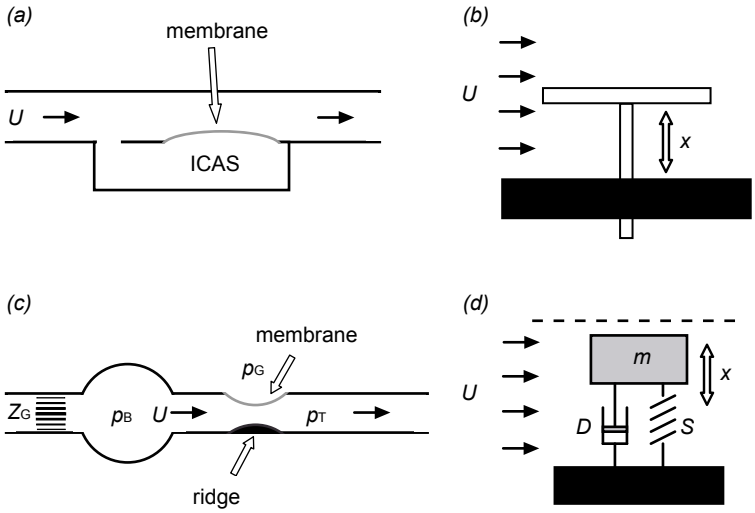

Figure 2.2 Schematic representation of some conceptual physical models used in the literature. (a) Brackenbury's model illustration in Brackenbury (1979) (b) The model used for calculations in Brackenbury (1979) based on Ffowcs Williams & Lovely (1975). (c) The model used for calculations in Fletcher (1988). The horn is not shown. (d) Basic mass-spring-damper model used in Fee et al. (1998), Fry (1998), Gardner et al. (2001), Laje et al. (2002), Laje & Mindlin (2002). Dotted line indicates line of symmetry. Black arrows indicate flow direction in the models. *D*, damper; ICAS, interclavicular air-sac; *m*, mass; p_B, p_G, p_T, pressures; *S*, spring; *x*, displacement; *U*, flow; Z_G, impedance.

plemented.

With this model, Fletcher (1988) produced sounds with a rich harmonic spectrum (or 'voiced' sounds) consisting of integer multiples of the membrane oscillation frequency of about 200 Hz. The power spectrum of the evaluated tracheal pressure exhibited formants around the open- and closed pipe resonances.

The power output of the model was within an order of magnitude of the actually measured values by White (pers. comm. to Fletcher) from an Australian raven (*Corvus mellori*), which had 'typical values' for anatomical and physiological parameters. Ravens belong to the Passeriniformes and thus are songbirds. In fact, the raven syrinx, like that of the American crow (Goller & Larsen 1997b), probably contains labial masses, which - like in the crow - are the likely sound sources, while the modelled thin membranes play a different (not yet established) role in vocalisation. Little is known about the actual mechanical properties of the tissues in the syrinx (Fee, 2002), in contrast to the overall morphology. However, Fletcher's model is constructed as such that it can easily be extended (e.g. Fletcher, 1989).

Modified oscillator models

Another distinct group of mathematical models can be summarised as modified oscillator models (Fee et al., 1998; Fee, 2002; Fry, 1998; Gardner et al., 2001; Laje et al., 2002; Laje & Mindlin, 2002). These models were not designed to include accurately the morphology of the syrinx and its associated air-sacs and muscles, but were developed to understand how simple neural activation patterns can lead to complex (sound) signals (Laje & Mindlin, 2002) in songbirds. The sound

production system of songbirds served as a biological model system for human sound production and its control.

In these modified oscillator models, a labial mass was represented by one-, or two coupled non-linear oscillating masses (figure 2.2d). The flow in these systems was not modelled directly, but the flow induced a pressure force, which drove the oscillators. These models had a relatively small number of free parameters that could still simulate the different classes of signals, ranging from pure sine waves to complex non-linear effects as harmonic stacks, and period doubling (Fee et al., 1998).

The model proposed by Fry (1998) was based upon the line model of acoustic tubes by Kelly & Lochbaum (1962), which has formed the basis of a class of human speech synthesisers (Flanagan, 1972). The syrinx was represented as two sound sources, the two bronchi, each with one mass combined with a spring and a damper. This syrinx model was integrated in a high-parameter system of interconnected acoustical tubes representing the air-sacs, and the trachea. Pure tones were produced when the masses did not occlude the bronchus during vibration, whereas harmonic stacks were produced when the labia in one bronchus collided. This model captured many features of birdsong, but was purely descriptive.

Several one- or two-mass models have been published (Fee et al., 1998; Fee, 2002; Fry, 1998; Gardner et al., 2001; Laje et al., 2002; Laje & Mindlin, 2002) based on classic human vocal fold models (Ishizaka & Flanagan, 1972; Titze, 1988). The motion equation of the oscillator in the model by Gardner et al. (2001), for instance, includes a non-linear dissipation term that kept the motion of the mass in the model within set boundaries (c.f. theory of relaxed oscillation, see Arnold et al., 1999, cited in Gardner et al., 2001). The non-linear term has been omitted in the even simpler successive model (Laje et al., 2002). Laje et al. (2002) and Laje & Mindlin (2002) included active opening and closing of the labia in their model by introducing a force that controls the stationary position of the mass. With simple sweeps of two control parameters - the stiffness of the oscillator and the bronchial pressure - they could mimic the song of the Chingolo (*Zonotrichia capensis*). The values for stiffness did not represent, however, the distribution of the actual material properties of the syrinx.

Perspectives

Mathematical modelling is required to elucidate the mechanisms of sound production and to interpret the experimental data and overwhelming structural complexity found in birds. Modelling can also help to direct experimental research. Keeping the number of parameters low considerably simplifies the exploration of the parameter space. Some of the aforementioned models have relatively few parameters (Fee et al., 1998; Gardner et al., 2001; Laje et al., 2002; Laje & Mindlin, 2002), with only one or two oscillating masses. These basic models provided fundamental insights into how a grossly simplified system operates and could be controlled. They provide also the minimum number of parameters required to describe the essential dynamics of the sound signal. The one- or two-mass models are not primarily designed and suitable to include the diverse morphologies and physiological parameters found in bird species. The approach by Fletcher (1988) seems to be more suitable to be extended for workers interested in these areas. Extensions of his model can be made in various directions. The model calculations were quasi-steady, thus it was assumed that

the pressure terms associated with local variations in U ($\mathrm{d}U/\mathrm{d}t$) are small and could be ignored. Also, viscosity of the flow was ignored (although viscous losses were included in the membrane). While this may be a valid assumption outside the syringeal region, it seems hard to defend for the tiny slit between the membrane and the opposing wall. High velocities are expected, and high velocity gradients are bound to occur during the short moments of slit opening. Thus, friction may indeed play an important role during the most critical phase of phonation as found with physical models of the human larynx (Deverge et al., 2003). Fletcher's model could be extended to account for these effects.

The air-sac pressure external to the vocal membrane was assumed to be identical to the driving pressure of the system. In fact, rapid pressure fluctuations do occur in the interclavicular air-sac as was recently demonstrated for pigeons (Beckers et al. 2003a). Membrane motion is likely to be a combined effect of driving pressures, membrane properties and acoustical properties of the vocal tract. The first two vibrational modes of the membrane were prescribed in Fletcher's model, thereby restricting a priori the motion of the membrane. The validity of this assumption is supported by measurements on the properties of the medial labium in zebrafinches and canaries (Fee, 2002).

Identifying the role of different parts of the vocal apparatus is relevant for solving important morphological and evolutionary questions. This requires an integrative modelling approach. Isolated measurements on different parts cannot provide definite answers to their role in the vocal system. Recently, the role of the medial tympaniform membranes (MTM) and the labia during sound production in songbirds have received much attention (Goller & Larsen, 2002). Correspondence in fundamental frequency between labial vibrations and sound does not necessarily exclude a fundamental role in the system of the MTM's. For instance, the compliance of the MTM's may be essential for the deformation of the syrinx during phonation. Combined measurements and modelling is needed to shed light on this issue.

The distinction made between membranes and labia in songbirds is artificial and actually comprises a continuum of different tissues with a varying mass and stiffness distribution. Based on this idea, Fee (2002) modelled the continuum of labia and adjacent membranes (the MTM) as a matrix of 121 interconnected masses. In fact, this represents a numerical-experimental approach that estimates material parameters of this complex system. This model has not yet been implemented into a syrinx model.

A quantitative model aimed at comprehending the sound-producing system must consider the fluid dynamics and solid dynamics of the sound producing system as inseparable. Numerical modelling of the tissues of the syrinx and the vocal tract combined with Computational Fluid Dynamics (CFD) modelling of the flow of air as used in human phonation research (e.g. de Vries et al., 2003) can be a step towards a more realistic dynamic model that addresses the architectural complexity found in birds. CFD models have the advantage of allowing complex morphologies and material properties to be included. The obvious disadvantage are the large number of required parameters and the computational costs of such a model. It is impossible to explore the parameter space of high-parameter models exhaustively because the number of parameter combinations is too high, although theoretically finite, quickly becomes practically infinite. Nevertheless, to understand the diversity and evolution of syrinx morphology present in birds, high-parameter models can be of interest to explore.

Physical models have only rarely been used in bird-song research. To our knowledge, in only one study (Brittan-Powell et al., 1997) simple plastic tubes with latex membranes were used as syrinx

models to investigate source-resonator coupling. In human phonation research, physical modelling is often used to test the validity of model assumptions (e.g. Hofmans et al., 2003; Deverge et al., 2003) or to develop prosthesis (e.g. Lous et al., 1998; de Vries, 2000).

On the one hand, advances in transducer technology and surgical procedures provide more accurate experimental data about bird song. On the other hand, the continuous increase in computational power facilitates the exploration of relatively complex parameter spaces. Only by combining experimental work with quantitative modelling we are able to answer the many open questions and to make significant progress in understanding the mechanisms by which birds produce sound and control their song.

Acknowledgements

We thank Dr. Ulrike Müller for useful discussion and suggestions for improvements of the text. This study was supported by the Netherlands Organisation for Scientific Research (NWO).

SECTION II

sound analysis

from sound to the sound generator

chapter **3**

Spectrogram analysis of animal sound production

Submitted as:
Elemans, C.P.H., Muller, M. & Heeck, K.
Spectrogram analysis of animal sound production.

Abstract

Spectrograms visualise the time-frequency content of a signal. They are commonly used to analyse animal vocalisations. Here, we show that the physiological basis for sound generation and modulation can be assessed by spectrogram analysis. We start with some basic characteristics of the Fourier transform which is used to construct spectrograms. Second, we addressed common features in bird vocalisations such as transients, harmonics, amplitude- and frequency modulation and non-linear events. We synthesised these spectral features by an array of simple artificial signal modifications (e.g. by introducing nonlinearities such as clipping). Third, to illustrate the explanatory power of the approach, we analysed the sound signal of a real bird. We constructed this vocalisation mathematically using the previously described effects of signal modifications. This approach yielded not only convenient statistical description, but also aided in formulating hypotheses about the underlying physiological mechanisms. Fourth, the predictive power of the spectrogram analysis was substantiated by its application to the sound produced by a simple mechanical model. This paper aims to provide basic assessment tools for sound analysis to identify candidates for sound generators and modulators without modelling the dynamics of the specific sound generators. We show that many clues (such as collisions) can be extracted from spectrograms regarding the physiological basis of sound generation.

Introduction

Throughout the animal kingdom a wide range of biological mechanisms of generating sound have evolved. Sound production by animals is often based on complex mechanical events; ranging from cavitation induced sound by shrimp (Versluis et al., 2000) to the energy conversion of flow to vibrating structures in the larynx of mammals (e.g. Paulsen, 1967). The generated sound may show up as a clear periodic function of time. In many cases, however, a sound track possesses a seemingly aperiodic character (e.g. a sound track of a piece played by a symphony orchestra; see e.g. Von Békésy, 1960). Although in the time domain hardly any structure can be discovered, the frequency domain may reveal a clear composition of periodic signals. Spectral analyses to study the frequency domain are widespread in science and engineering with applications ranging from econometrics to Geographical Information Systems (GIS) and Remote Sensing (e.g. Lilisand & Kiefer, 2000).

A convenient way to visualise a sound track in the frequency domain is a spectrogram, that shows the spectral composition (e.g. amplitude) of a time window sliding over the signal. Spectrograms based on the Fourier Transform are widespread in biological sciences such as animal behaviour and bio-acoustics. Their value (Hall-Graggs, 1979), trade-offs and limitations (e.g. Beecher, 1988; Bradbury & Vehrencamp, 1998; Clark et al, 1987; Spiegel, 1974; Williams & Slater, 1991) have been well studied. Other spectral analysis techniques, such as zero-crossing analysis (Staddon et al, 1978), wavelets (Wakeling et al., 2002), spectral derivatives (Tchernichovski et al., 2001; Tchernichovski & Mitra, 2002), optimal kernel designs (Jones & Baraniuk, 1995), or others (Darden et al., 2003; Mbu Nyamsi et al., 1994) are used to construct different time-frequency representation with for instance a higher time-, and frequency resolution. Except for the use of wavelet analysis, these techniques are not common practice in the biological literature. Various techniques have been developed to correlate sound structure in a spectrogram (Clark et al., 1987; Cortopassi & Bradbury, 2000; Khanna et al., 1997) with various contextual variables, such as habitat, social context, and inter- and intraspecific differences.

A generated sound wave can be modified by resonators such as air sacs (in frogs, birds and mammals), by filtering by cavities (e.g. trachea, bronchi and mouth cavity in most tetrapods), by the acoustic interaction with another source and finally by the environment. The energy in certain frequency bands can be enhanced by resonance coupling or suppressed by energy absorption in e.g. the trachea. Interacting sound sources compose a generally complex sound pattern.

Can the spectrogram be used to make predictions about the nature of the mechanisms of sound production? Generally speaking, the answer would be negative. Systems already exist that can reproduce any sound signal which in a spectrogram would be indistinguishable from the original signal. The loudspeaker consists of only one vibrating membrane and is perfectly capable of reproducing sound signals from wind noise to bird song, from conversations to orchestras. Animals, however, do not use speakers to generate sound. Although apparently a trivial observation, it is the state of the art knowledge of sound producing mechanisms in animals that conveniently reduces the number of possible explanations. By these means, the explanatory power of spectrogram analysis increases substantially. We believe that interpretation of sound spectrograms can be used to gain understanding of the mechanical events and physiological mechanisms that underlie sound production indirectly, when direct observations of these events are not possible.

In the present paper, we aim to relate simple structures in spectrograms to their causal mathematical and, if possible, mechanical events. We will start by studying the shapes and structures in

spectrograms of a selection of mathematically defined sound signals. This provides a basis to interpret signals of which the exact composition and mechanical origin is not a priori known. We wish to contribute to basic assessment tools that help to identify mechanisms for sound production. Secondly, the sound signal of the Bearded vulture (*Gypaetus barbatus* L.) was analysed and mimicked using simple modulation and manipulation principles and discussed in the background of bird vocalisation. Thirdly, we generated sounds with a mechanical model and related experimentally observed mechanical events to characteristics of the spectrogram. The latter two approaches are used sparsely in bio-acoustics, but have proven to be of great help in directing working hypotheses in other fields of biology.

2. From mathematical theory to features in spectrograms

2.1 Notes on Fourier-series and Fourier-transforms

We briefly explain some fundamental and essential features of Fourier-transform techniques, since they are the basis of spectrograms. Further detailed information can be found in many textbooks (e.g. Abramowitz & Stegun, 1970; Hsu, 1967; Main, 1978; Oppenheim & Schafer, 1989; Press et al., 1990; Spiegel, 1974; Van den Enden & Verhoeckx, 2000). For a list of used symbols see Appendix A.

To obtain information about the frequency contents of a continuous time signal, any, infinitely long, periodical signal may be expanded in a Fourier-*series*:

$$y(t) = \frac{a_0}{2} + \sum_{n=1}^{\infty}\left[a_n \cdot \cos\left(\frac{n \cdot 2\pi \cdot t}{T}\right) + b_n \cdot \sin\left(\frac{n \cdot 2\pi \cdot t}{T}\right)\right], \qquad (1)$$

where t is time, T is the time constant or period length, n is a positive integer, and a_n and b_n are the so-called Fourier-coefficients:

$$a_n = \frac{2}{T} \cdot \int_{c}^{c+T} y(t) \cdot \cos\left(\frac{n \cdot 2\pi \cdot t}{T}\right) dt \text{ and } b_n = \frac{2}{T} \cdot \int_{c}^{c+T} y(t) \cdot \sin\left(\frac{n \cdot 2\pi \cdot t}{T}\right) dt \,. \qquad (2a,b)$$

Thus, by summating a number of sine waves with certain harmonically-related frequencies, and the appropriate phase and amplitude, any infinitely long, periodic signal can be completely reconstructed. In fact, the 'ideal' aim of spectral analysis is to show such Fourier series. The spectrum would then contain bars of finite length (coefficients an and bn, representing e.g. amplitude) at particular frequencies. This representation of spectral decomposition with the Fourier coefficients as bars we often find as schematic drawings (e.g. Bradbury & Vehrencamp, 1998; Greenewalt, 1968; Lavenex, 1999; Van den Enden & Verhoeckx, 2000). However, most time signals are not periodic and also not infinitely long. For such signals, the theory of Fourier-*series* is no longer applicable and has been expanded to Fourier-*transforms*. We will illustrate the consequences of non-periodicity and finite length of time signals by considering simple time signals.

The Fourier-*transform* for continuous functions is defined as:

$$F[y(t)] = Y(\omega) = \int_{-\infty}^{\infty} y(t) \cdot e^{-i \cdot \omega \cdot t}\, dt \,, \qquad (3)$$

where $F[y(t)]$ and $Y(\omega)$ represent the Fourier transform of function $y(t)$, and ω is the angular frequency. This formula transforms a time-signal $y(t)$ into a complex frequency-signal $Y(\omega)$.

The amplitude-spectrum of this signal is: $Y_{\text{ampl}}(\omega) = |Y(\omega)|$, and the power-spectrum is: $Y_{pow}(\omega) = Y(\omega) \cdot Y^*(\omega)$. In engineering textbooks, $Y_{\text{pow}}(\omega)$ is defined as $0.5 \cdot Y(\omega) \cdot Y^*(\omega)$. The continuous time signal $y(t)$ is thus transformed into a continuous function $Y(\omega)$, instead of expanded into a series with an integer number of coefficients. This is a reversible process with the use of the inverse Fourier transform. Some algorithms designed to make better estimates of the power spectrum of a time signal use time averaging methods. Such estimates cannot be used, however, to reconstruct the time signal (Gittes & Schmidt, 1998).

The rectangular pulse is a basal function in Fourier-transform theory. The time function has either the value 0 or the arbitrary amplitude A (figure 3.1a): $y(t) = A \quad (|t| < \tau)$, $\quad y(t) = 0 \quad (|t| > \tau)$. This same function can be represented in the frequency domain using the Fourier-transform [eqn (3)]:

$$Y_{ampl}(\omega) = 2 \cdot A \cdot \tau \cdot \left| \frac{\sin(\omega \cdot \tau)}{\omega \cdot \tau} \right| = 2 \cdot A \cdot \tau \cdot |\text{sinc}(\omega \cdot \tau)| \ . \tag{4}$$

The part $\dfrac{\sin(\omega \cdot \tau)}{\omega \cdot \tau}$ is called the sinc function (figure 3.1a2). An amplitude spectrum with traces of sinc functions is characteristic of many Fourier-transformed functions. Eqn (4) is normalised by dividing by τ:

$$\overline{Y}_{ampl}(\omega) = \frac{Y_{ampl}(\omega)}{\tau} = 2 \cdot A \cdot |\text{sinc}(\omega \cdot \tau)| \tag{5}$$

To illustrate the transition from Fourier series to Fourier transform, and the differences between them, we will now consider a simple cosine function $y(t) = A \cos(\omega_s \cdot t)$ with frequency ω_s (figure 3.1b). If we consider a single period $(t \in [-\frac{1}{2}T, \frac{1}{2}T])$, the Fourier series of a cosine function is: $Y(\omega_s) = A$, $Y(-\omega_s) = A$.

In words, the Fourier series consists of one term with frequency ω_s and finite amplitude A and also has a solution at negative frequencies (figure 3.1b1).

The Fourier transform for $y(t)$ between the instants $-\tau$ and $+\tau$ is:

$$Y_{ampl}(\omega) = A \cdot \left[\frac{\sin\{\tau \cdot (\omega + \omega_s)\}}{\omega + \omega_s} + \frac{\sin\{\tau \cdot (\omega - \omega_s)\}}{\omega - \omega_s} \right]. \tag{6}$$

The Fourier transform resembles a sinc function (figure 3.1c), when a single period is considered. Again, we obtain the *normalised* amplitude spectrum $Y_{\text{ampl}}(\omega)$, if we divide $Y_{\text{ampl}}(\omega)$ by τ in eqn (6). By increasing the number of periods considered (figure 3.2), however, the Fourier-*transform* becomes more similar to the solution of the Fourier-*series* of a single period in figure 3.1. The Fourier-transform of an infinitely long cosine function is:

$$Y_{ampl}(\omega) = \pi \cdot A \cdot \delta(\omega + \omega_s) + \pi \cdot A \cdot \delta(\omega - \omega_s) \ , \tag{7}$$

where δ is the delta function or Dirac pulse (figure 3.1d): $\int_{-\infty}^{\infty} \delta_{(t)} dt = \int_{-\varepsilon}^{\varepsilon} \delta_{(t)} dt = 1$, for $\varepsilon > 0$.

These examples show that for the Fourier-transform, the frequency-signal is basically built up of sinc-functions, and as $\tau \rightarrow \infty$, the Fourier-*transform* approaches a Fourier-*series* (Appendix B).

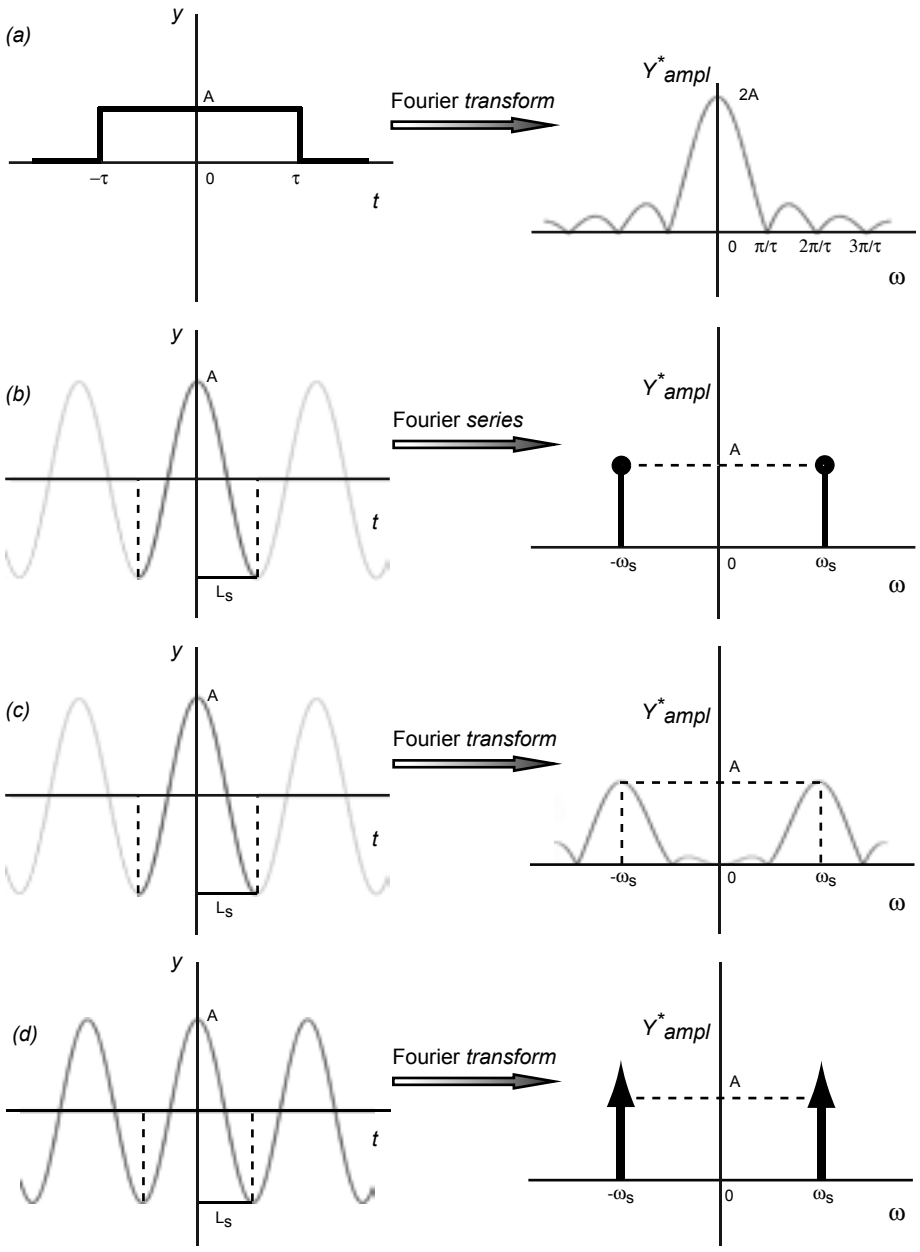

Figure 3.1 Fourier transforms and series. (a) Fourier transform of a symmetrical step-function. (b) Fourier series of a single period of a cosine-function. Although only a single period is considered, the cosine-function may thought to be infinitely long. The dots indicate finite amplitude of the bars. (c) Fourier transform of a single period of a cosine-function. (d) Fourier transform of an infinitely long cosine-function. The arrows indicate infinite amplitude of the bars. A = amplitude, T_s = period, t = time, ω = angular frequency, ω_s = cycle frequency of signal. Left panels: time domain. Right panels: Frequency domain

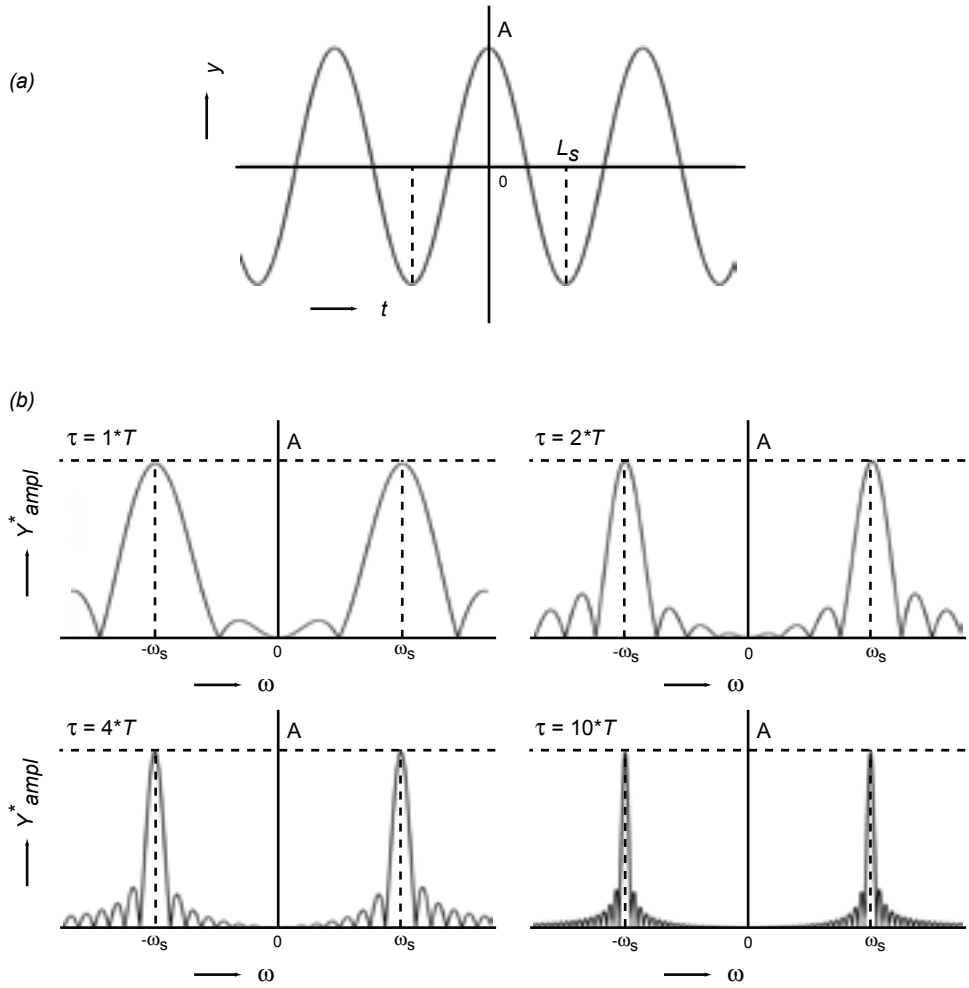

Figure 3.2 Effect on Fourier transform with increasing number of considered periods. (a) Time domain. (b) Normalised function in frequency domain for increasing number of periods (τ) considered, from upper left corner clockwise; 1, 2, 5 and 10 periods.

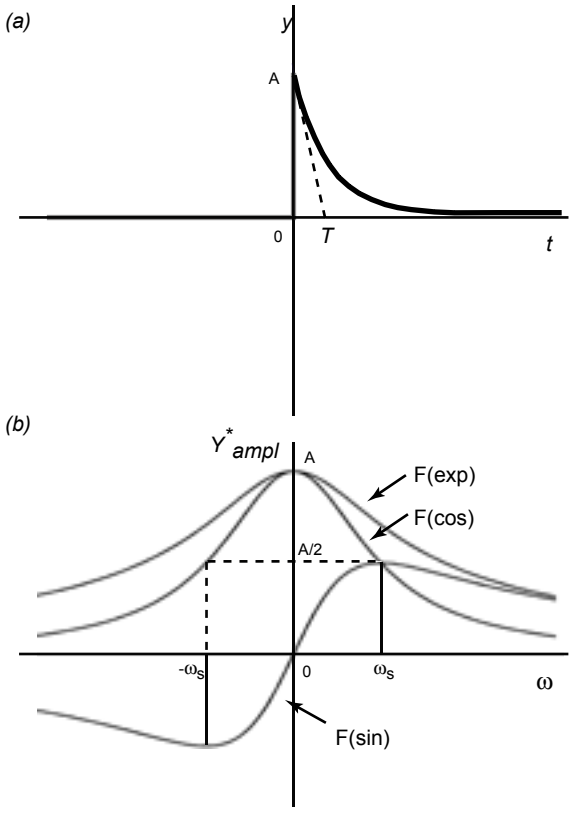

Figure 3.3 Functions that are discontinuous around zero. (a) Exponential function in time domain. (b) Amplitude spectra in frequency domain of exponential, sine and cosine-functions starting at $t = 0$.

The Fourier-transforms of periodic functions that start at $t = 0$ are also continuous functions of angular frequency (ω). So, apart from their values at $\omega=\omega_s$, these functions possess values for any ω, thus including negative frequencies. To show this, consider the exponential function (figure 3.3a):

$$y(t) = A \cdot \exp(-\omega_s \cdot t), \qquad (t > 0); \qquad y(t) = 0, \qquad (t < 0), \tag{8}$$

and its Fourier transform: (9)

$$\mathrm{F}[y(t)] \;=\; Y(\omega) = \frac{A}{\omega_s + i\omega} = \frac{A \cdot \omega_s}{\omega_s^2 + \omega^2} + i \cdot \frac{-A \cdot \omega}{\omega_s^2 + \omega^2} = F[A \cdot \cos(\omega_s \cdot t)] - i \cdot F[A \cdot \sin(\omega_s \cdot t)]$$

The amplitude spectrum is displayed in figure 3.3b. Remarkably, even pure sine- or cosine-functions which start at $t = 0$, possess spectra embracing all frequencies and not only those of the sinusoidal function in question (figure 3.3b). This is due to the discontinuity at $t = 0$. The amplitude of the ever continuing sine function is multiplied by the Heaviside unit step at $t = 0$. The Fourier transform of the product of two functions equals the convolution of their separate Fourier transforms. Clearly, the transform of the step causes the spectral enrichment.

2.2 Spectrogram construction

In case of sampling at equidistant time-intervals, the following lemma, known as the Nyquist theorem, holds: reconstruction of the original time signal from its samples, is only possible if the sample frequency is at least twice the highest frequency component of the signal. If this condition is not met, Fourier transform of the time series will show non-existing components. This phenomenon is called aliasing. (Oppenheim & Schafer, 1989; Press et al., 1990; Van den Enden & Verhoeckx, 2000). This can be avoided by analogue low pass filtering of the signal *before* the sampling process takes place. The sample frequency should be set to at least 2 (in practise even 3 to 5, depending on allowed phase distortion) times higher than the upper cut-off frequency of the filter, depending on the attenuation rate of the analogue filter. The computer processes a digital time signal (sound-track) that is a discrete signal in both time and amplitude. It is the product of (1) the original, continuous sound signal, (2) the sample aperture time and (3) a window-signal representing the sample duration. The calculated frequency signal is the convolution of these three time signals.

The algorithms that calculate the Fourier transform of a series are called Discrete Fourier Transform (DFT) algorithms. Their common presumption about the input series is that it is repeated ad infinitum. The DFT algorithms come in two varieties. The oldest form, considered as slow nowadays, uses the formulas of the Fourier Transform and accepts any number of samples. The other group is formed by the Fast Fourier Transform (FFT) algorithms. These algorithms reduce the number of calculations in a transformation by utilizing symmetry properties of the transformation formulas. As a consequence the number of samples (*nfft*) that can be transformed is limited to a power of two in case of the often used Danielson-Lanczos algorithm (Danielson & Lanczos, 1942) [also known as Cooley-Tucky (Cooley & Tucky, 1965) algorithm]. Many other, fast algorithms exist that reduce the computational burden of the transformation by exploring other symmetries than powers of two (e.g. Johnson & Burrus, 1984; Nussbaumer & Quandalle, 1979). The frequency resolution of the FFT is $f_{sample}/nfft$ or $1/(nfft \cdot T_{sample})$.

Several conditions have to be fulfilled to accomplish these calculations properly. Otherwise, frequency components do not appear as discrete lines in the spectrum, but tend to become spread around the real frequency component. This phenomenon is called 'leakage'. For sine waves, leakage always occurs when: signal frequency = $k \cdot$(sample frequency / *nfft*), (k =0,1,2,... *nfft*/2). With an integer ratio between sample frequency and *nfft*, the signal to noise ratio dramatically decreases to -600 dB. In practice, the above condition is seldom fulfilled.

All our spectra are calculated by means of FFT. To be able to use the standard Cooley-Tucky FFT the number of data-points needs to be a power of two and to accommodate any number of samples zero-padding was used. Due to the zero-padding the number of samples is increased from *nfft* to *m*, which should be a power of two, and the new resolution becomes f_{sample}/m. The frequency axis needs to be multiplied with $nfft/m$ to correct for the zero-padding affect. Hardware frequency analysers, like spectrographs, used multiple analogue hardware filters and had only two fixed frequency resolution settings, filters with a pass-band of either 45Hz or 300Hz (e.g. Greenewalt, 1968). This resulted in the terms narrow-band and broad-band spectrograms.

As mentioned before, the FFT decomposes any infinite signal in sine waves with certain amplitude (or power), frequency and relative phase. In a normal spectrogram, only the amplitude (or power) of the FFT analysis is displayed, also called the *amplitude* spectrogram (Léonard, 2000). The relative phase information of the FFT can be equivalently used to construct a phase-time

representation, which is called a *phase* spectrogram (Léonard, 1997, Léonard, 2000; Léonard et al., 2000). To our knowledge, the phase spectrogram has not been used in published animal sound studies, but could become useful in the future.

3. A mathematical description of several features in spectrograms

Extensive terminology has been developed to describe the most common sound features in spectrograms. Examples found extensively in literature are 'pure tone', 'harmonic stacks', 'broadband pulse', 'amplitude- and frequency modulation', 'sidebands' and 'noise'. We will generate a selection of these common features by simple permutations of sine waves in the time domain. The advantage of mathematically defined signals is that the emergence of spectral features can be explained without ambiguity due to error or variation introduced by measurements.

3.1 Transients

At the boundaries of vocal syllables, sudden on- and offsets of e.g. echolocation clicks in bats, birds and toothed whales, the spectrum changes abruptly. At the transient onset of a tone the spectrum can exhibit sinc-like functions, comparable to figure 3.1a. Sharp transients result in a spectrum that contains energy over a broad range of frequencies or, in the limit case, energy equally spread over all frequencies (cf. figure 3.19 in Bradbury & Vehrencamp, 1998). The spectrogram will show this as broad vertical band. Signals that contain transients should preferably be digitised at very high sample rates, if the signals are hard to obtain (e.g. difficult field conditions, rare species) to avoid artefacts in the spectrogram later on. This also allows for the development of specific filters once the signal is sampled.

3.2 Harmonics

Harmonics are integer multiples of the base frequency or fundamental frequency. All non-sinusoidal, but periodic, time-functions generate harmonics in their spectrum (e.g. Bradbury & Vehrencamp, 1998). Since perfect sine waves are rare in nature, harmonics are ubiquitous. In some special cases, it is possible to calculate analytically the harmonic content of a signal in a Fourier series. The resulting parameter values provide a convenient statistic for comparison. As a first example, we consider the absolute value of a sinusoidal signal, also referred to as 'full wave rectification' of the signal:

$$y(t) = \left| A \cdot \sin\left(\omega_s \cdot t\right) \right| = A \cdot \left[\frac{2}{\pi} - \frac{4}{\pi} \left(\frac{\cos\left(2 \cdot \omega_s \cdot t\right)}{1 \cdot 3} + \frac{\cos\left(4 \cdot \omega_s \cdot t\right)}{3 \cdot 5} + \frac{\cos\left(6 \cdot \omega_s \cdot t\right)}{5 \cdot 7} + \ldots \right) \right] \quad (10)$$

The time signal (figure 3.4a) can be expanded into a series consisting of multiples of $2\omega_s$: [cos ($2\omega_s$...) + cos ($4\omega_s$...) + ... in eqn (10)]. A comparable expansion for a cosine function also shows only multiples of $2\omega_s$ (see Appendix C1). Full wave rectifying thus results in a fundamental frequency of $2\omega_s$ and not ω_s. In the spectrogram (figure 3.4a) a harmonic stack with odd and even harmonics can be recognised. The amplitude of the harmonics is defined by eqn (10).

We can also generate harmonic structures in a spectrogram by clipping of the sinusoidal signal at a level $\pm A_c$:

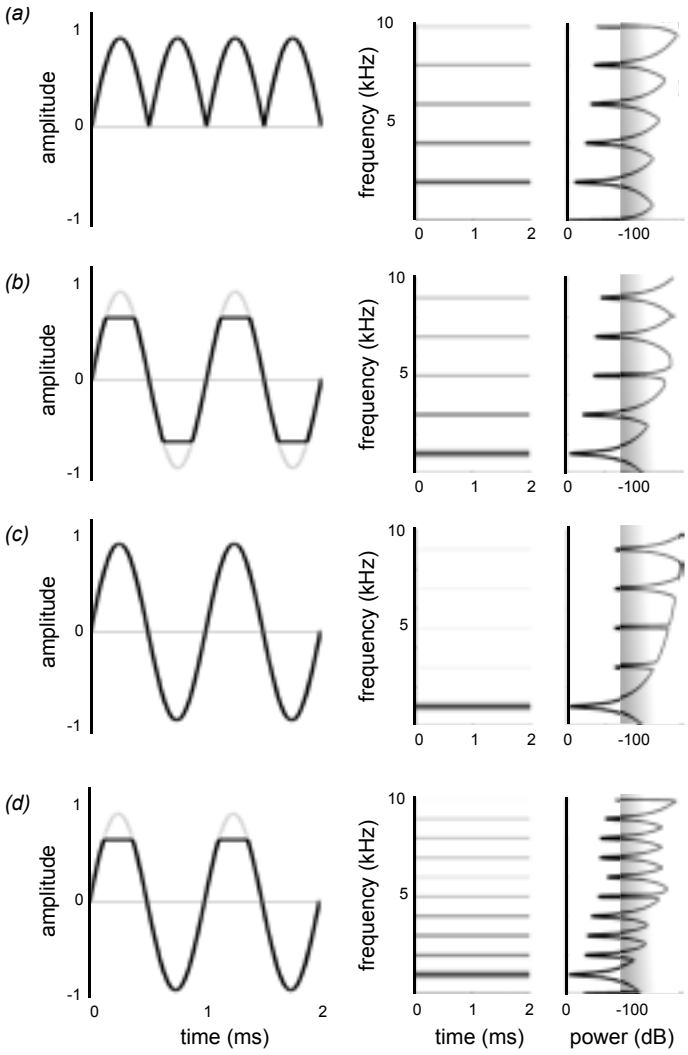

Figure 3.4 Effects of nonlinearity on sinusoidal time-signals. From left to right; the time signal and associated spectrogram and amplitude spectrum. The shaded bars indicates edge of the displayed dynamic range in the spectrogram. (a) Full wave rectified sine wave. The fundamental frequency doubles and both odd and even harmonics occur. (b) Sine wave clipped symmetrically at $A_c = 0.7 \cdot A$. Only odd harmonics occur in the power spectrum. (c) Sine wave clipped symmetrically at $A_c = 0.99 \cdot A$. Even in the latter case, harmonics occur. (d) Sine wave clipped asymmetrically at $A_c = 0.7 \cdot A$. Both odd and even harmonics occur. $\omega_C = 3$ kHz; $F_s = 40$ kHz, *nfft* = 1024.

$$y(t) = A \sin(\omega_s \cdot t), \quad -A_c < y < A_c, \quad A_c \in [0, A] \tag{11}$$

$$y(t) = A_c, \quad |y| \geq |A_c| \tag{12}$$

We will refer to this case as symmetrical clipping (figure 3.4b). See Appendix C2 for the analyti-

cal solution of the Fourier integrals. Clipping can also occur asymmetrically, i.e. for only $-A_c < y$ or $y < A_c$. Here, the boundary A_c is absolute, and in that sense 'hard', in contrast to 'soft', where clipping is implemented with a smooth transition at the clipping level, e.g. with a non-linear term or look-up table. This would also result in a harmonic stack in the spectrogram, but with less energy in the higher frequencies. Even for $A_c = 0.99A$, harmonics are still visible in the spectrogram (figure 3.4c). This implies that the slightest clipping of a sound track recorded from an animal may result in false harmonics in the spectrogram. While symmetrical clipping results in the occurrence of odd harmonics (figure 3.4b and 4c), asymmetrical clipping results in both odd and even harmonics (figure 3.4d).

In this context, periodic pulse trains can be considered as a special case of clipping. If the clipping level A_c would converge to 0 for the asymmetrically clipped sine wave in figure 3.4d, we get a special case of the time signal in figure 3.4a, with a 'silent' interval of amplitude 0 between adjacent pulses. Thus, periodic pulse trains also create harmonics (Watkins, 1967).

3.3 Modulations

A widespread phenomenon in animal vocalisation is modulation. Animals may modulate a carrier signal in various ways: amplitude modulation (AM), frequency modulation (FM) and phase modulation (PM). To generate modulations, we extend the analysis to (linear or non-linear) interactions between sine waves.

3.3.1 Amplitude-modulation

The simplest type of modulation is a sinusoidal amplitude modulation of a sinusoidal carrier signal:

$$y(t) = A \cdot \left(1 + m \cdot y_{AM}\right) \cdot \cos\left(\omega_C \cdot t\right) \text{ for } \omega_{AM} < \omega_C, \tag{13}$$

where $y_{AM}(t) = \cos(\omega_{AM} \cdot t)$.

Here, $y(t)$ is the modulated time signal, m is the modulation-depth of the signal amplitude, $y_{AM}(t)$ is the modulating signal, ω_{AM} is the modulation frequency and ω_C is the carrier-frequency. These equations can be expanded from a product of cosines into a sum of cosines (Spiegel, 1974):

$$\begin{aligned} y(t) &= A \cdot \cos\left(\omega_C \cdot t\right) + A \cdot m \cdot \cos\left(\omega_{AM} \cdot t\right) \cdot \cos\left(\omega_C \cdot t\right) = \\ &= A \cdot \cos\left(\omega_C \cdot t\right) + \frac{A \cdot m}{2} \cdot \left[\cos\left(\{\omega_C + \omega_{AM}\} \cdot t\right) + \cos\left(\{\omega_C - \omega_{AM}\} \cdot t\right)\right] \end{aligned} \tag{14}$$

Three frequencies emerge: the carrier-frequency and the sum- and difference-frequencies of carrier- and modulation signal (figure 3.5a). Note that the modulation-frequency (ω_{AM}) itself is not visible in the spectrum. The modulation signal (and a component at $f = 0$) appears when a DC offset is added to eqn (13) (Bradbury & Vehrencamp, 1998; Lavenex, 1999; Nowicki & Capricana, 1986a, 1986b). In animal sound tracks, the frequency of the modulation signal is often very low compared with the carrier-frequency (Stein, 1968; Watkins, 1967). Then, the sum- and difference-frequencies are invisible in the spectrogram and amplitude modulation is only visible in the time signal.

Both carrier and modulation signal can be either sinusoidal or non-sinusoidal, resulting in four possible principle interactions (figure 3.5a-d). The carrier signal used in figure 3.5 was 3 kHz, and the modulation signal 400 Hz. Non-linearity was introduced to either the modulating or carrier

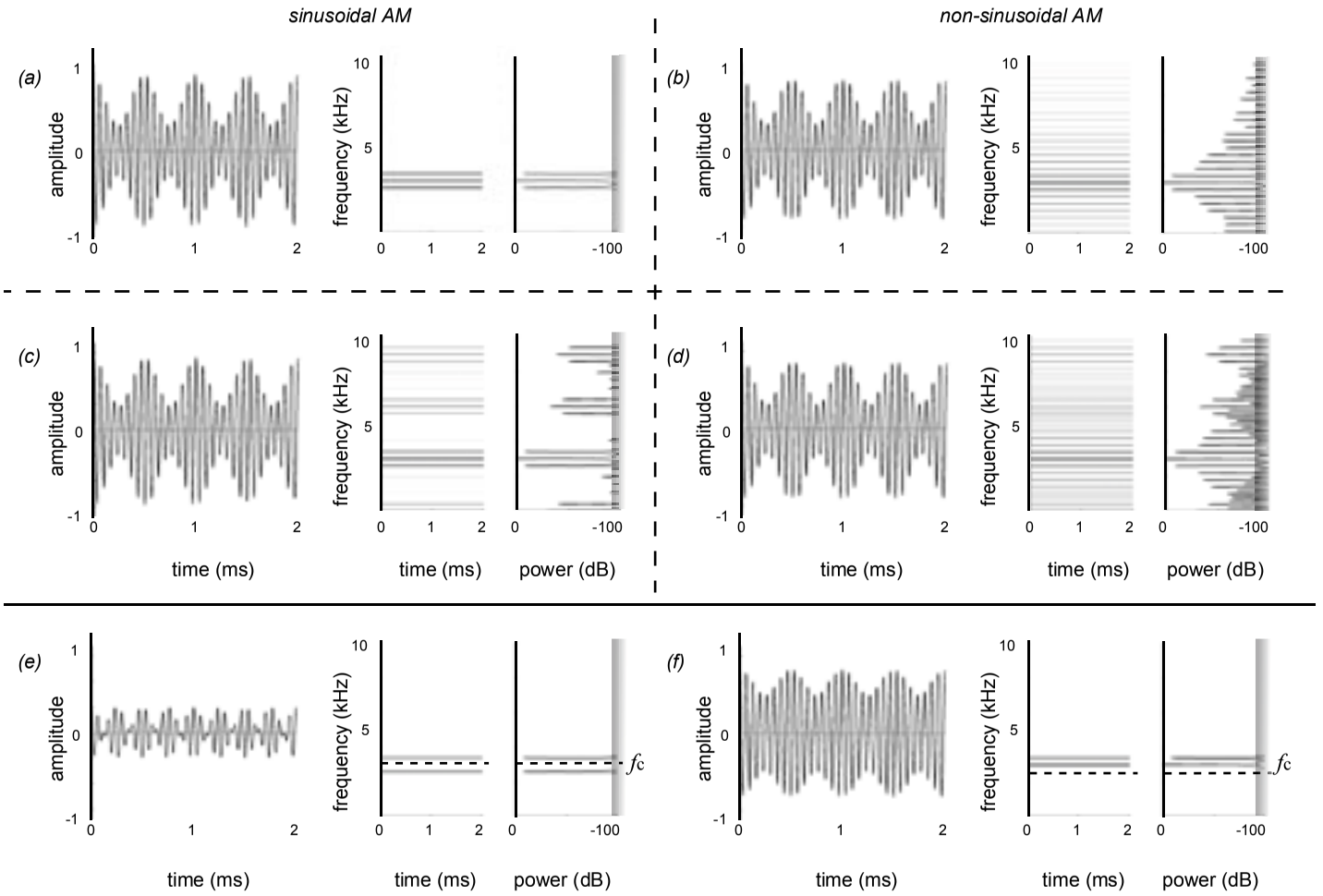

Figure 3.5 Amplitude modulation. (a)-(d) four possible interactions with different carrier and modulation waveforms. (a) Simplest form of AM as described in eqn (13) resulting in the carrier-frequency and two side-frequencies. (b) Non-sinusoidal modulation or, (c) carrier frequeny. (d) Intermodulation. (e) Double Side Band modulation [eqn (15)]. The carrier-frequency has disappeared, here only the side-frequencies emerge. (f) Single Side Band modulation [eqn (16)]. The carrier-frequency and one side-frequency remain. The latter example can be varied in different ways. ω_C= 3 kHz; ω_{AM}= 400 Hz. F_s = 40 kHz; *nfft* = 1024.

signal, or both, by soft clipping. Despite minute changes in the time domain, the spectra are *very different*. If the modulation signal is non-sinusoidal and the carrier signal is sinusoidal (figure 3.5b), the frequency spectrum above the carrier frequency is an in amplitude scaled duplicate of the spectrum of the modulating signal. The spectrum below the carrier is the mirror image. With a non-sinusoidal carrier signal and a sinusoidal modulation signal, sum and difference frequencies appear around the individual bands of the harmonic stack of the carrier signal (figure 3.5c). When both signals are non-sinusoidal, many frequency bands appear around every band of the harmonic stack (figure 3.5d). In a technical context this phenomenon is called *intermodulation*.

Another type of amplitude modulation is obtained by removing the carrier-frequency from eqn (14):

$$y(t) = A \cdot m \cdot \cos\left(\omega_{AM} \cdot t\right) \cdot \cos\left(\omega_C \cdot t\right) = \frac{A \cdot m}{2} \cdot \left[\cos\left(\{\omega_C + \omega_{AM}\} \cdot t\right) + \cos\left(\{\omega_C - \omega_{AM}\} \cdot t\right)\right] \quad (15)$$

This type of modulation is known as Double Side Band modulation (DSB; see Appendix C3) or Amplitude Modulation with suppressed carrier (figure 3.5e). It is obtained for any product of sine- and cosine functions by applying simple goniometric rules (Spiegel, 1974). It can also be interpreted as the sum of two sinusoidal signals of equal amplitude, but with different frequencies. In the two types of amplitude modulation given by eqn (14) and eqn (15), the modulation-signal is not present in the spectrum of the modulated carrier-signal. It can be restored by demodulation by a non-linear network as used in AM radios. In Single Side Band modulation (SSB; see Appendix C4), subsequently, also one of the sideband frequencies ω_C-ω_{AM} or ω_C+ω_{AM} is removed (figure 3.5f) from eqn (15):

$$y(t) = \frac{A \cdot m}{2} \cdot \cos\left(\{\omega_C \pm \omega_{AM}\} \cdot t\right) \quad (16)$$

Since the carrier does not contain any additional information, only one sideband is transmitted and radio receivers for SSB need to regenerate the carrier frequency ω_C before demodulation. Although this type of AM might not seem directly relevant to biological systems, it is important to realize that each sideband at its own contains all the information of an AM signal.

The characteristic amplitude envelope in figure 3.5f is often referred to as 'beating' (e.g. Lavenex, 1990; Bradbury & Vehrencamp, 1998). This spectrum containing two fixed components can be the result of either addition of two sinusoidal signals or the application of Double Side Band modulation.

Summarising, three conclusions can be drawn from the above formulae. First, amplitude modulation always requires interaction between two or more signals. Second, AM is obtained by adding up signals as well as multiplication. In the context of mathematical operation, the terms 'linear' and 'nonlinear' for respective addition and multiplication sinusoidal signals are indiscriminate and inappropriate. Multiplication still results in a *linear* system but not in a *time-invariant* system. Third, the different types of AM generate very different and intricate spectra, while it is difficult to distinguish between the signals in the time domain.

Figure 3.6 Frequency modulation. (a) Normal FM as described in eqn (25), with ω_C= 3 kHz and ω_{FM}= 5 Hz and (b) with ω_{FM}= 250 Hz. This results in a spectrum with a carrier-frequency and multiple sidebands of frequencies. (c) Progressive FM with varying ω_C and (d) with varying ω_{FM}. (e) Multiple signals. For the exact composition see Appendix C6.

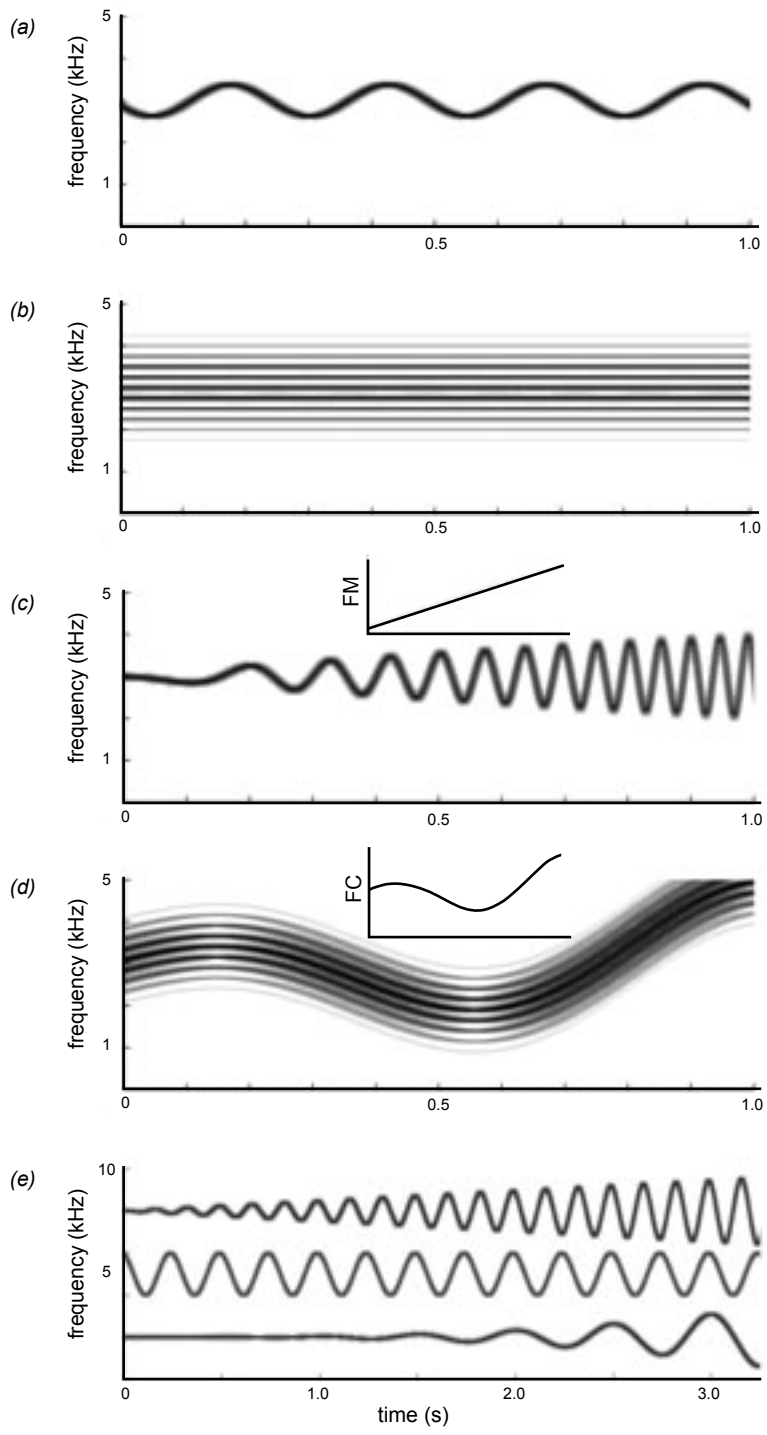
(a)
frequency (kHz)
5
1
0
0.5
1.0
(b)
frequency (kHz)
5
1
0
0.5
1.0
(c)
FM
frequency (kHz)
5
1
0
0.5
1.0
(d)
FC
frequency (kHz)
5
1
0
0.5
1.0
(e)
frequency (kHz)
10
5
0
1.0
2.0
3.0
time (s)

3.3.2 Angular-modulation

Instead of the two side-frequencies that emerge from sinusoidal amplitude modulation, frequency-modulation gives rise to multiple sidebands of frequencies. At low modulation frequencies these sidebands are not visible in the spectrogram (figure 3.6a), but at high modulation frequencies the differences between carrier and FM signal are high enough to visualise the bands (figure 3.6b) dependent of the bandwidth settings of the spectrogram.

Frequency Modulation (FM) and Phase Modulation (PM) are considered to be particular forms of so-called angular modulation (Ziemer & Tranter, 1990). Angular modulation can be represented by:

$$y(t) = A \cdot \sin(\omega_t \cdot t + \varphi_t) \tag{17}$$

In this context, sinusoidal frequency modulation is described by using $\omega_t = \omega_C + m \cdot \cos(p \cdot t)$, and $\varphi_t = 0$ in eqn (17), where, ω_C is the angular frequency of the carrier and p is the angular frequency of the modulation. For phase modulation with sinusoidal modulation we write $\omega_t = \omega_C$, and $\varphi_t = \varphi_{max} \cdot \cos(p \cdot t)$ in eqn (17), where φ_{max} is the peak value of the phase deviation. The expression for the instantaneous angular frequency $\omega = d\varphi / dt$, relates FM to PM. The ratio between angular frequencies of the carrier over the modulation, m/p, is the so-called modulation index of a FM signal. Interestingly, the relation of angular modulation [eqn (17)] can be expanded into underlying Bessel functions that describe the amplitude of each of the individual sidebands created (See Appendix C5). Since a sideband vanishes completely at particular values of m/p, Bessel functions can be used for precise calibration of the modulation process.

In many vocalisations, the modulation increases in time. This is called progressive FM (Appendix C6) and can be modelled by various means; e.g. the carrier frequency (figure 3.6c) or the modulation index (figure 3.6d) that varies in time.

3.4. Fingerprints of nonlinear dynamics

Many sounds in vertebrate animals are produced by structures that can be modelled as nonlinear oscillators. These oscillators exhibit specific dynamics of which some signatures can be observed in spectrograms (Fee et al., 1998; Fitch et al., 2002; Fletcher, 2000; Wilden et al., 1998). Examples are sudden frequency jumps or doublings, or transitions from harmonic stacks to subharmonics to deterministic chaos (that could mistakenly be considered as noise) in spectrograms. These signatures in spectrograms of animal vocalisations are increasingly reported (Wilden et al, 1998).

Nonlinear oscillators exhibit a conversion from AM to PM, when the coefficients in their describing differential equations are excitation dependent (Kharkevitch, 1962). For large drive amplitudes, this system is also subject to the transition from a deterministic to a chaotic oscillator, in the case of which any correspondence between the excitation and the resulting spectra is lost. In biological systems a profound source of non-linearity is the non-Hookian relation between applied force and elongation in elastic tissue. We will illustrate this AM to PM conversion for an electric circuit, i.e. a nonlinear-RLC series circuit that is voltage excited. A second order differential equation describes the system dynamics:

$$L\frac{d^2Q}{dt^2} + R\frac{dQ}{dt} + \frac{1}{C_{(Q)}}Q = U\cos\omega t \ , \tag{18}$$

where L is the inductance (Henry) in the circuit, Q is the charge (Coulomb), R is the resistance

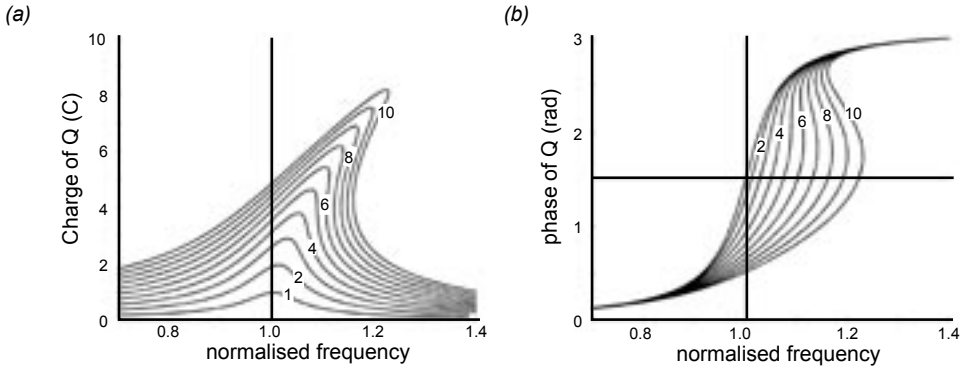

Figure 3.7 Transition from amplitude modulation to phase modulation for a nonlinear oscillator. (a) With a higher amplitude of charge Q, the curve shifts. (b) Phase shift as a function of ω^2/ω_0; B = 1, 2, 3, ...10, λ = 0.01 and d = 0.1 in equations C28 and C29 (Appendix C7).

(Ohm, Ω) and $C_{(Q)}$ is the capacitance (Farad). The input function is a sinusoidal time function [$U{\cdot}\cos(\omega{\cdot}t)$] in Volts. We consider the capacitance (C) in the circuit to be a function of its charge (Q), which is a common kind of non-linearity in RLC circuits. We rewrite eqn. (18) to:

$$\frac{d^2Q}{dt^2}+\frac{R}{L}\frac{dQ}{dt}+\omega_0{}^2F_{(Q)}=\frac{U}{L}\cos\omega t=B\cos\omega t \qquad F_{(Q)}=Q+\lambda Q^3 \qquad \frac{R}{L}=\omega_0 d \quad (19)$$

Differential equations with this 3rd order nonlinearity are known as Duffing equations (Duffing, 1918). To show the AM to PM conversion of this system, we concentrated only on the terms ω_0 concerning the fundamental (Appendix C7). Figure 3.7a shows the amplitude of the charge as a function of normalised frequency. When the excitation increases, the frequency shifts to a higher value. The phase of the charge oscillation is also strongly dependent on the excitation amplitude (figure 3.7b). The AM to PM conversion is evident even in the simplest of all nonlinear differential equation.

3.5 Generation of multiple signals

With the mathematical principles that were derived above, signals can be generated that contain harmonics, side bands and frequency modulations of an exactly known mathematical origin. In general, spectrograms of animal sounds may have a complex character, including several modulated carrier frequencies. figure 3.6e shows an example of a synthetically generated signal with combinations of eqns (14), (17) and (C17). Visual inspection of the spectrogram and careful listening to the sound reveals the separate signals. Visual inspection of the time signal, however, gives the impression of aperiodicity. We can use syllables of the various signals, as described above, to mimic sound tracks recorded from animals.

4. Examples of spectrogram analysis

We demonstrated that many features found in spectrograms of animals can be generated with permutations and interactions of simple sine waves. How does this help us in analysing the mechanics or unravelling the mechanisms that generate natural sounds? We will demonstrate the diagnostic value of the theoretical approach by two examples, the vocalisation of a bird, and sound produced by a simple mechanical model.

4.1 Simulating animal sounds; the bearded vulture

Reconstructing a signal helps in making predictions about the underlying mechanical events and provides parameters for statistical analysis. To illustrate this, we analysed and reconstructed the screech of a Bearded vulture (*Gypaetus barbatus* L.) using parts of multiple signals. This species was chosen for the interesting features of the sound signal. The time signal (obtained from the Internet: *www.birding.dk*) and its corresponding spectrogram are shown in figure 3.8a1 and 8b1. Some features of the spectrogram can be explained immediately with above theory.

Many bands are present that converge towards one band at 1000 ms. In the middle of box a (figure 3.8b1), bands are visible at 2400, 3100, 3700, 4350, 5000 and 5650 Hz, separated by about 650 Hz. If this would be part of a harmonic stack with a fundamental of 650 Hz, we expect that the harmonics would be spaced at integer multiples of 650Hz (i.e. 1300, 1950, 2600, 3250, 3900, 4550, 5200 and 5850 Hz, respectively). These expected multiples, however, do not coincide with the observed frequencies. Alternatively, the signal could be caused by amplitude modulation, which would require two or more sidebands around a carrier frequency. AM with a carrier frequency of 4550 Hz (or 3900 Hz) and a non-sinusoidal modulation frequency of 650 Hz, generates side bands at the observed frequencies. Also the convergence of the sidebands towards one carrier (figure 3.8b1 box b) makes amplitude modulation with a non-sinusoidal modulation signal a very plausible hypothesis. The bands in the spectrogram would be sidebands, (technically also harmonics of the two sidebands in true AM) with one being the carrier frequency. In part (2) and (3) of the spectrogram, we observe a carrier that is frequency-modulated from 3 to 1.5 kHz with some harmonic contents at odd and even multiples. Particularly fast modulations are indicated by arrows on the x-axis in figure 3.8b1. We made the distinction between part (2) and (3) due to the amplitude modulation visible in the time domain.

We used the observations noted above to simulate the vulture's signal. The results of the simulation are shown in figure 3.8a2 and 3.8b2. The first part (1) is a non-sinusoidal AM of a sinusoidal carrier. The carrier signal was constructed with combinations of exponential power functions and the modulation signal was an asymmetrically clipped sine wave. The resulting time signal was clipped asymmetrically to obtain the harmonics in part (2) and (3) of the signal. The AM also results in the sum and difference frequencies in part (1) (see arrow in figure 3.8b1). This procedure can be extended and improved until the desired match with the original signal is made. Listening to these sounds revealed a close match.

This procedure provided us with direct statistics useful for a comparative approach and to focus on potential mechanisms for generating the signal. We can now formulate and discuss the hypothetical origin of the signal interactions.

In songbirds, amplitude modulation has previously been reported in the black-capped chickadee (*Parus atricapillus*) by Nowicki & Capricana (1986a, 1986b). This species belongs to the Order

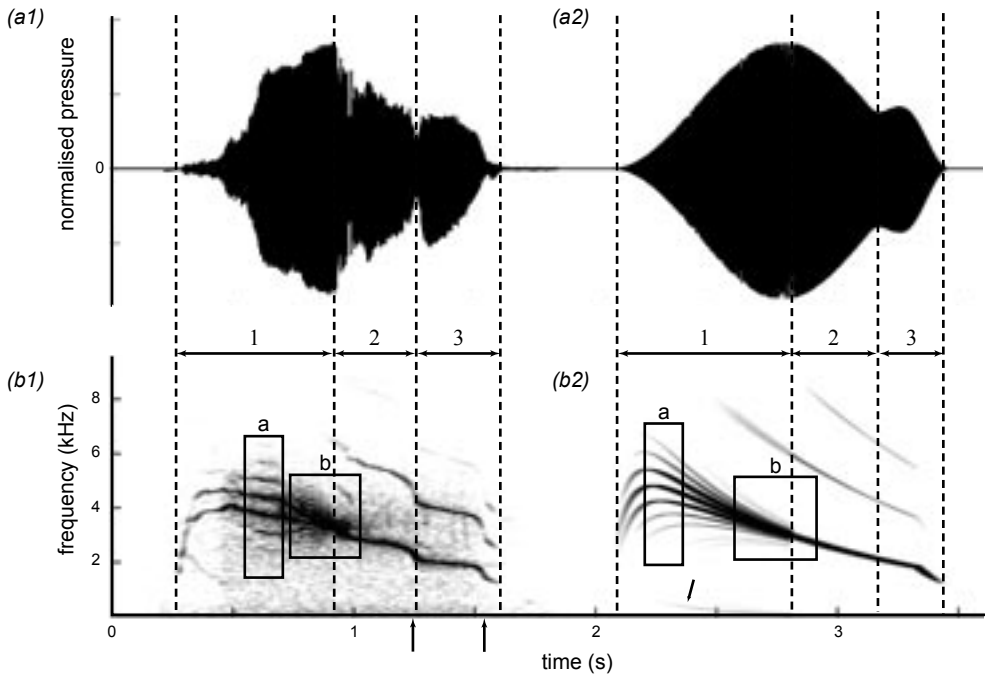

Figure 3.8 The screech of the bearded vulture (*Gypaetus barbatus*) (left) and simulated signal (right). (a) time traces and (b) spectrogram. See text for further explanation.

Passeriniformes (the songbirds) that have two, bilateral syringeal apertures. By denervation of both sides of the syrinx, Nowicki & Capricana (1986a, 1986b) provided evidence that both apertures produced a carrier with a different frequency. AM was the result of coupling between the left and right parts of the syrinx. In non-songbirds, amplitude modulation is reported in parts of the contact calls and in mimicked English vowel sounds (Lavenex, 1999) in budgerigars (*Melopsittacus undulatus*). The bearded vulture, belongs to the order Falconiformes (Sibley & Monroe, 1990), and is also considered a non-songbird. In general, non-songbirds have a syrinx with only one syringeal aperture (King, 1968) formed by two tympaniform membranes, except oilbirds, nightjars and some tropical swifts that have two bronchial apertures (King, 1968; Suthers & Hector, 1982; Suthers & Hector, 1985). Vibrating tympaniform membranes were the most important sound generator in two non-songbirds; the pigeon (*Columba livia*) and the cockatiel (*Nymphicus hollandicus*) (Goller & Larsen, 1997; Larsen & Goller, 1999). In the light of these findings, we hypothesise that also in the bearded vulture the tympaniform membranes generate the sound. What mechanism can cause the AM?

Interference by nonlinearity in the recording equipment of two or more simultaneously vocalising individuals in recordings can cause sidebands (Frommolt, 1999). But let us assume that the AM is generated without these types of interference.

A possibility is that two separate mechanisms generate the carrier and the modulation signal, i.e. the tympaniform membranes generated the carrier frequency that was modulated by a second mechanism or structure. In the ring dove (*Streptopelia risoria*), extremely fast syringeal muscles

modulate the sound by pulling the syringeal membranes (i.e. lateral tympaniform membranes or LTM) out of the tracheal lumen (Elemans et al., 2004). The fastest known vertebrate striated muscles, however, contract up to 270 Hz (Fine et al., 2001) with a low power output as a trade-off for speed (Rome et al., 1996). In both the budgerigar and the bearded vulture, however, modulation frequencies are in the order of 100-700 Hz (Lavenex, 1999; Stein, 1968), which is too high for any known muscular contraction in vertebrates. Another possible explanation is that more downstream structures interact with the carrier produced in the syrinx, such as flow induced laryngeal movement.

Some types of oscillators provide both the carrier and the modulation, which makes the separation of carrier and modulation signal into different mechanisms not appropriate. For instance, some electronic oscillators have a linear relationship between amplitude and supply voltage, which makes them good amplitude modulators. In the non-oscine syrinx, AM could be generated for instance by the flow or pressure that excites the syringeal membranes.

Another explanation could be that the two tympaniform membranes vibrate at different frequencies. This phenomenon is called 'biphonation' and has been studied in various normal human vocalisations and pathologies (Mergell & Herzel, 1997; Tigges et al, 1997). It is mainly due to some asymmetry in the elastic tissue properties of the membranes and the amount of coupling between the vocal folds and the vocal tract (Mergell & Herzel, 1997). So, although biphonation occurs only under specific conditions, it is plausible that the physiology and morphology of different species has evolved to meet them.

All these hypotheses are not easily tested for a singing bird. To find the origin of the AM, we need detailed information on the vibratory behaviour of the sound generators. Direct measurements of syringeal vibration are very challenging, due to the technical difficulties involved. Larsen & Goller (1999) succeeded for the first time in measuring syrinx motions using a photo-transisitor that measured light reflections from the LTMs as a measure of vibration amplitude, which showed that the LTM vibrated. To answer questions about AM, more detailed measurements need to be conducted.

4.2 An example of a mechanical model; the bagpipe reed

Mechanical models are another useful tool to increase understanding of underlying mechanical events and serve to test the accuracy of mathematical models (e.g. de Vries, 2003). In contrast to in vivo measurements of sound generators in biological systems, accurate measurements of the mechanical events can be done at relative low effort. Additionally, parameters can be changed that are fixed in the biological system, such as material properties.

A simple mechanical model that generates sound is a drone reed from a bagpipe consisting of a cane tube (*Arundo donax* L.). The cane tube is closed on one side and transversally and longitudinally cut to form a blade (figure 3.9a). Abduction of the blade widens the slit in the tube (figure 3.9a and 9b). The player does not manipulate the blade directly with its mouth such is the case in a clarinet or saxophone. The drone is connected to the chanter, of which the resonance properties are determined by the player by closing and opening holes. The blade of the reed and the air in the reed tube are coupled oscillators. The design of the blade and its exact geometry has been subject to many hundreds of years of cultural evolution (Baines, 1973). In a bagpipe, a pressure load is applied via the bag to induce vibrations of the reed. We mounted the reed in the sidewall of an acrylate cylinder (inner diameter 34 mm) to mimic the bag and to allow for optical access. The cane tube was open on one side (not visible in figure 3.9a) and formed an outlet. The pressure in the cylinder

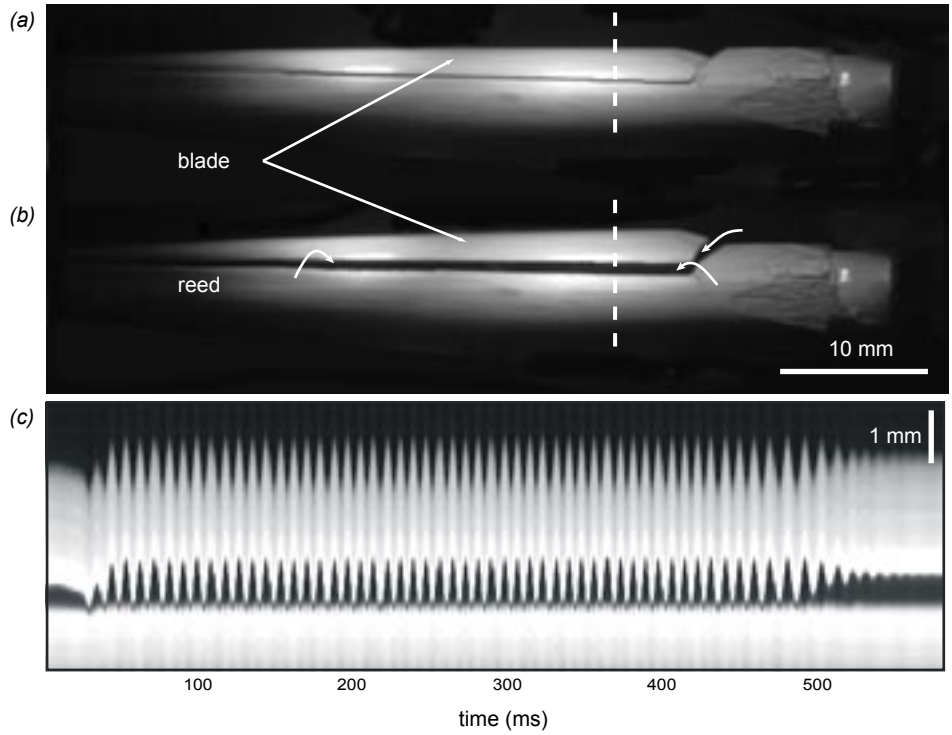

Figure 3.9 The drone model. The position of the blade of the blade movement with when fully closed (a) and open (b) taken from the high-speed recordings. The arrows indicate the air flow that runs from the right through the tube towards the outlet (on the left, not shown). (c) Visualisation of the blade movement. The intensity of the digital images at the dotted line in (a) and (b) was plotted as a function of time. Oscillation period is 4 ms.

could be regulated with pressurised air. Sound was recorded with a condenser microphone (Brüel and Kjær 4939; Preamplifier 2670) at 30 cm from the tube-outlet of the reed in a semi-anechoic room at Wageningen University. The signal was amplified and band-pass filtered (20Hz (40 dB/dec) -10kHz (40 dB/dec), Nexus amplifier; Brüel and Kjær). Gauge pressure was measured about 10 mm from the end of the blade inside the tube with a cathetertip pressure transducer (Millar SPC 350, diameter of tip 1.6mm) and low-pass filtered (10kHz) with a custom-built analogue filter. Pressures were measured relative to the ambient pressure. All signals were digitised at 30 kHz using a 12-bit PCI-MIO16E-4 AD-converter (National Instruments) on a Pentium III 700MHz Workstation. After digitising, the pressure signal was band-pass filtered (100Hz-10kHz) with a 3rd order Butterworth digital filter using zero-phase implementation (Oppenheim & Schafer, 1989). Monochrome, digital high-speed video recordings of the moving blade were made at 2 kHz (Redlake MotionPro). The video system was synchronised with the sound and pressure signals with a time difference less than 0.5 ms. The width of the opening between the blade and the reed was measured from the high-speed images at a fixed position (figure 3.9a and 9b). Width opening as a function of time was up-sampled from 2 to 30 kHz by cubic spline-interpolation (de Boor, 1987; Press et al., 1990) through the time data. Signal acquisition and analysis software was developed in

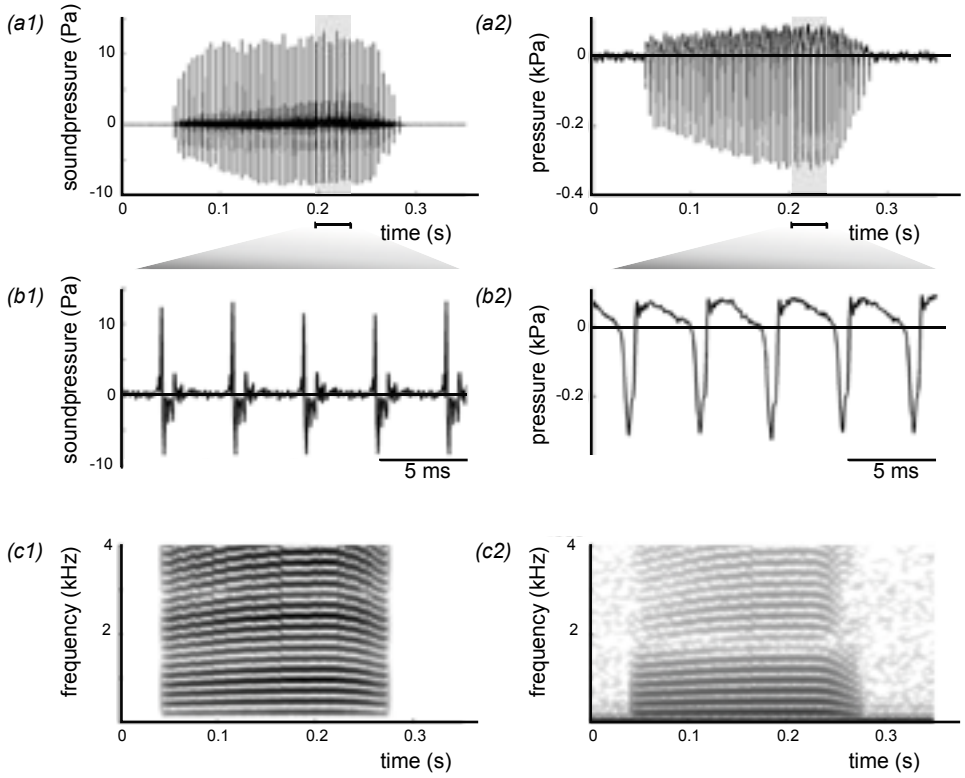

Figure 3.10 Results of reed-like mechanical model. Sound pressure at 30 cm from the tube outlet (left) and pressure measured in the tube (right) (a) time traces and (b) detail of (a). (c) spectrogram of (a). F_s = 30kHz; *nfft*= 1024; df = 29.4 Hz; dt = 17ms.

Matlab 6.5 (The Mathworks).

Time traces and spectrograms of the pressures in-, and outside the tube of a typical recording are shown in figure 3.10. The sound pressure trace varied in amplitude from 12 to -9 Pa (figure 3.10a1). The pressure in the tube varied from about 80 to -350 Pa (figure 3.10a2) around atmospheric pressure. Both the sound pressure (figure 3.10b1) and the pressure in the tube (figure 10b2) exhibited a consistently repeating pattern with a period of 4 ms. Since both pressure functions were non-sinusoidal but repetitive, it was likely that odd and even harmonics of the 250 Hz fundamental will occur in their spectra as long as the time window for the FFT is sufficiently long to capture more than a single period.

Calculated spectrograms (figure 3.10c) consisted indeed of a harmonic stack with a fundamental of 250 Hz and harmonics at evenly spaced odd and even integer multiples (500, 750, 1000, ... Hz). The harmonic stack was found in both spectrograms (figure 3.10c) but their spectra were different since the waveforms differed in shape and amplitude.

What can we conclude from these signals using the mathematical theory presented in section 2? The simplest way to generate a harmonic stack structure is by either asymmetrical clipping or full wave rectifying as described above. A more complex way to generate the structure in the spectro-

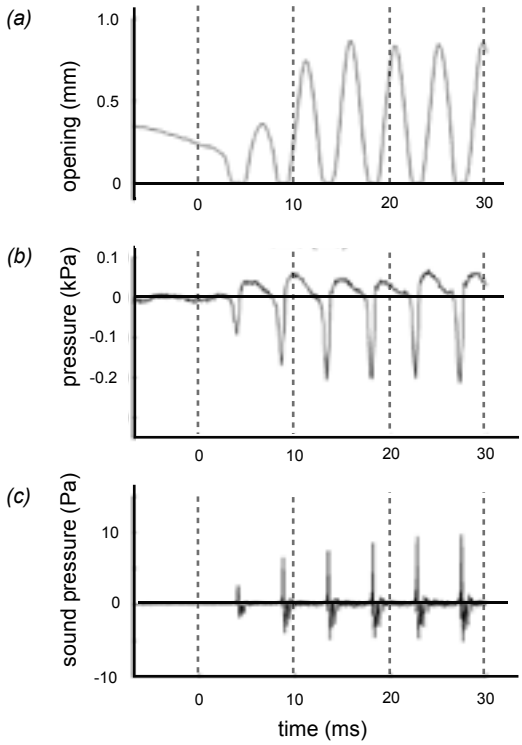

Figure 3.11 Detail of onset of sound production. (a) Width of the reed opening. (b) Pressure in the tube and (c) sound pressure.

gram is by non-sinusoidal AM or FM with application of specific filtering. For example, AM with a sinusoidal carrier of 3 kHz and a non-sinusoidal modulation signal with a fundamental of 250 Hz generates multiple side-bands as shown in figure 3.5b. In this case, the sidebands overlap exactly (since 3000/250=12, an integer) and could generate a structure similar to figure 3.10c. Additionally, a specific filter could match the spectra. The hypothesis that the signal is generated with AM, however, can be rejected because the bands in the spectrogram remain harmonically related also when the lowest band shows slight frequency modulation at the last 400ms. The harmonic relation during FM demonstrates that the most parsimonious explanation is that the lowest band is the true fundamental frequency of the harmonic stack.

We showed that a harmonic structure could be generated if somewhere in the system there is a form of clipping, or more broadly defined, a unilateral restriction. The structure in the spectrogram could indicate a unilateral restriction in the sound generator. Note that even when the signal was generated by AM of some sort, it would require a non-sinusoidal modulation frequency and thus some non-linearity.

During sound production, the blade periodically narrows (figure 3.9a) and widens (figure 3.9b) the slit. The motion of the blade as a function of time during one bout is visualised in figure 3.9c. The high-speed video recordings showed that the blade vibrated in its basal mode and was clearly restricted in its movement by the tube (figure 3.11a). Since the pressure in the acrylate cylinder is

above ambient room pressure, the air flowed (indicated by arrows in figure 3.9a) from the acrylate chamber, through the cane tube into the room. During collision between the blade and the tube, the pressure in the tube decreased from 0 Pa to -300 Pa and then increased sharply (figure 3.10b2). When the blade closed the passage of air, the air in the tube moved on due to its momentum. The local density of the air close to the blade decreased and pressure dropped below ambient pressure. Inertia of the air caused this rapid decrease in pressure. Subsequently, air was sucked through the outlet of the tube, which increased pressure until the blade was pushed upwards. At this stage, air flowed again through the opening of the blade. The movement of the blade is determined by intrinsic mechanical properties and geometry. The movement of the blade and the other mechanical events are locked in periodicity and display limit cycle behaviour comparable to the vocal folds.

Summarising, the analysis of the structure in the spectrogram helped to hypothesise about the clipping event and thus directed the search for identification of the sound source. The spectrogram, however, failed to explain the physical relation between the measured signals. The origin of the harmonics in the spectrogram is the periodicity of the waveform in figure 3.10b. Understanding the measured signals required much more knowledge of the flow dynamics and aero-acoustics of the system (see e.g. Deverge et al., 2003; Fabre & Hirschberg, 2000; Verge et al. 1997a, 1997b).

5. Discussion

5.1 Direct measurements from spectrograms

In this paper, we provide an overview on the essential details of the Fourier Transform to construct spectrograms. Since the FFT algorithm always provides a numerical answer, it is the methodological details that provide credibility to its use. As argued by Darden et al. (2003), measuring parameters directly from spectrograms does not provide data suitable for qualitative frequency analysis, let alone quantitative analysis. To be accurate, time parameters such as syllable onset and duration should be measured from the time signal and not from the spectrogram. Also frequency measurements or noise estimates directly from plotted spectrogram should be taken with care and preferably avoided. The clicks of echolocating bats and birds, for example, show up as vertical bands in the spectrogram when the settings of the spectrogram or sample frequency are incorrect. Parameters measured directly from the spectrogram, such as the height of the displayed 'vertical grey band', based on colour intensity in the spectrogram do not provide accurate information about the signal. Since spectrograms display a fixed dynamic range of the amplitude of the spectral analysis, a spectrogram has an amplitude cut-off. When the dynamic range is set to e.g. 50 dB, this means that all frequency components with amplitude less than -50 dB relative to a reference value, e.g. the strongest amplitude component, are not displayed. For a quantitative comparison between spectrograms, recordings should be calibrated and the recording settings should be kept similar. Especially in field settings, varying noise conditions can result in recordings principally unsuitable for quantitative comparison.

Despite these limitations, spectrograms remain a very useful qualitative representation of sound signals, which are easily used and quickly constructed. They provide a description of the spectral contents of any signal and are therefore an important tool to gain insight in the composition of a signal.

5.2 Reconstructing spectral features

Many of the features found in spectrograms of animal vocalisations can be generated with simple descriptions of time domain waveforms. The reconstruction of sounds can provide statistics for a quantitative comparison of sounds (Nelson, 2004) and is useful in the process of generating hypotheses about sound production. It comprises a purely descriptive approach of spectral composition of sound, but does not predict sound or complete songs on basis of dynamics of the sound generators (e.g. for birds: Elemans et al, 2003; Fee et al., 1998; Fletcher, 1988, 2000; Fitch et al., 2002, Gardner et al., 2001; Laje & Mindlin, 2002; Mindlin et al., 2003). These studies assess the dynamics of sound generation and control and need physiological input parameters that are not available for many species. As demonstrated in this paper, a spectrogram of any vocalisation already provides many clues about its generation. We contributed to an overview of assessment tools that help to identify mechanisms in sound production, such as clipping, amplitude- and frequency modulation, directly from the available spectrogram.

5.3 Mechanical models of sound production

Finally, we demonstrated the use of simple mechanical models to study essentials of sound generation. The use of mechanical models is often used to test the validity of model assumptions in human studies (e.g. Deverge et al., 2003; Hofmans et al., 2003) or to develop prostheses (e.g. Lous et al., 1998; de Vries et al., 2003). To our knowledge, in only one study (Brittan-Powell et al., 1997) simple plastic tubes with latex membranes were used to model the syrinx to investigate source-resonator coupling. The use of more complex mechanical models can be very useful to solve problems such as amplitude modulation in the budgerigar (Lavenex, 1999) or in the bearded vulture. Here it is essential to investigate possible asymmetric vibration dynamics of the two membranes, which is hard to realise in a spontaneously singing bird. We prefer to start by analysing the dynamics of relatively simple models as presented here.

5.4 From spectrogram to mechanics of the sound generators

We related simple structures in spectrograms to their causal mathematical events. To interpret these mathematical permutations in the light of meaningful physical events, additional knowledge of sound generation is needed. On the basis of the spectrogram of an unknown signal, it is in principle not possible to get insight in physical events that caused this signal. It is feasible, however, to identify immediate signatures of repetition, modulations, transients and nonlinear behaviour. Combined with knowledge from other scientific fields, the spectrogram becomes a powerful diagnostic tool to understand sound producing and modulating mechanisms. No single discipline can provide all the requirements to understand sound production inside a complex organism, where many factors remain unknown. Most hypotheses are not easily tested. About the role of morphology in sound generation, Greenewalt (1968) stated: 'Unfortunately it is not easy to make the transition from an anatomical structure, no matter how detailed, to a description of its functional operation.' From the viewpoint of acoustic analysis, Gaunt & Gaunt (1985) made the remark that 'If (avian) voice is modulated even in part by nonsyringeal mechanisms, then syringeal function cannot be deduced from acoustic analysis of the call alone, regardless of the sophistication of the analysis. Acoustic evidence alone may fit contradictory models equally well.' The spectrogram provides important clues about the origin of animal sounds. But just as morphological studies and studies of system dynamics, detailed study of the spectrogram provides only a partial insight in the sound producing system.

Acknowledgements

The authors thank Johan van Leeuwen for comments on the manuscript. We thank Mr. Bjarne Nielsen for his permission to use sounds from *www.birding.dk*. The investigations were (in part) supported by the Research council for Earth and Life Sciences (ALW) with financial aid from the Netherlands Organisation for Scientific Research (NWO).

Appendix A. Abbreviations and units of the parameters used

A	amplitude	[m]	
A_c	clipping amplitude	[m]	
a_n	Fourier coefficient	[m]	
AM	Amplitude Modulation		
b_n	Fourier coefficient	[m]	
c	starting point on time axis of signal considered in Fourier-series	[s]	
C	capacitance	[F]	
DFFT	Discrete Fourier Transform		
DSB	Double Side Band modulation		
f	frequency	[s^{-1}],	$f = 1/T$
$F[y(t)]$	Fourier transform of function $y(t)$	[m]	
FFT	Fast Fourier Transform		
FM	Frequency Modulation		
i	imaginary unit = $\sqrt{(-1)}$		
J_n	Bessel function of n^{th} order.		
L	inductance	[H]	
L_s	half time constant	[s],	$L_s = T/2$
m	modulation depth of amplitude modulation		
n	modulation index of frequency modulation; integer (n=0,1,2,3...)		
nfft	number of samples for DFFT		
p	angular cycle frequency in angular modulation		
PM	Phase Modulation		
Q	charge	[C]	
R	resistance	[Ω]	
SBB	Single Side Band modulation		
T	time constant	[s]	
t	time	[s]	
$Y(\omega)$	Fourier-transform of $y(t)$, $\overline{Y}(\omega)$ = normalised function	[m]	
Y_{ampl}	$Y_{ampl}(\omega)$ = amplitudespectrum, $\overline{Y}_{ampl}(\omega)$ = normalised function	[m]	
Y_{pow}	$Y_{pow}(\omega)$ = powerspectrum,		
δ	delta function (Dirac function)		
λ	system parameter Duffing equations		
τ	limiting time	[s]	
φ_t	phase in angular modulation		
ω	angular frequency	[rad·s^{-1}]	
ω_C	carrier frequency	[rad·s^{-1}]	
ω_{AM}	angular frequency of amplitude modulating signal	[rad·s^{-1}]	
ω_{FM}	angular frequency of frequency modulating signal	[rad·s^{-1}]	
ω_s	angular frequency of signal s	[rad·s^{-1}]	
ω_t	angular frequency in angular modulation	[rad·s^{-1}]	

Appendix B. Parsevals identity

Considering the conservation of total power in a vibrating system, a central theorem is Parsevals identity, which states that the total power in a system is spread about all components at different frequencies:

$$\int_{-\infty}^{\infty} \left| y(x) \right|^2 dx = \frac{1}{2 \cdot \pi} \cdot \int_{-\infty}^{\infty} \left| Y(\omega) \right|^2 d\omega \,, \tag{B1}$$

which becomes for a Fourier-series:

$$\frac{2}{T} \cdot \int_{-\frac{1}{2}T}^{\frac{1}{2}T} \{ y(x) \}^2 dx = \frac{a_0^2}{2} + \sum_{n=1}^{\infty} \left(a_n^2 + b_n^2 \right). \tag{B2}$$

Appendix C. Derivations

(C1) Fourier-series of a full wave rectified cosine function

$$\text{Let } y(t) = A \cdot \cos\left(\omega_s \cdot t \right) = A \cdot \sin\left(\omega_s \cdot t + \frac{\pi}{2} \right). \tag{C1}$$

Substitution of the new argument of the above sine-function in the Fourier-series of the full wave rectified sine-function given by eqn (10), leads to the Fourier-series of a full wave rectified cosine-function:

$$y(t) = \left| A \cdot \cos\left(\omega_s \cdot t \right) \right| = A \cdot \left[\frac{2}{\pi} + \frac{4}{\pi} \left(\frac{\cos\left(2 \cdot \omega_s \cdot t \right)}{1 \cdot 3} - \frac{\cos\left(4 \cdot \omega_s \cdot t \right)}{3 \cdot 5} + \frac{\cos\left(6 \cdot \omega_s \cdot t \right)}{5 \cdot 7} + \ldots \right) \right] \tag{C2}$$

Note that also here only even harmonics occur and that the fundamental frequency has disappeared.

(C2) Analytical solver of the harmonic contents of a clipped sinusoidal signal.

We start from a signal:

$$y(t) = A \cdot \sin\left(\omega_s \cdot t \right) = A \cdot \sin\left(\frac{\pi}{L_s} \cdot t \right), \ \left| y \right| < A_c \qquad A_c \in [0, A] \tag{C3}$$

$$y(t) = A_c \,, \ \left| y \right| \geq A_c \tag{C4}$$

A_c is the level at which the signal is clipped and $L_s = ½ \cdot T_s$. For a half-range expansion of this odd function, it rules: (1) there are only sin-components in the Fourier series, (2) the amplitudes a_n (n=0,1,2...) in the Fourier series are zero, so only the b_n amplitudes remain:

$$y(t) = \sum_{n=1}^{\infty} b_n \cdot \sin\left(\frac{n \cdot \pi \cdot t}{L_s} \right) \tag{C5}$$

The amplitude b_n of this half-range expansion is:

$$b_n = \frac{2}{L_s} \cdot \int_0^{L_s} y(t) \cdot \sin\left(\frac{n \cdot \pi \cdot t}{L_s} \right) dt \tag{C6}$$

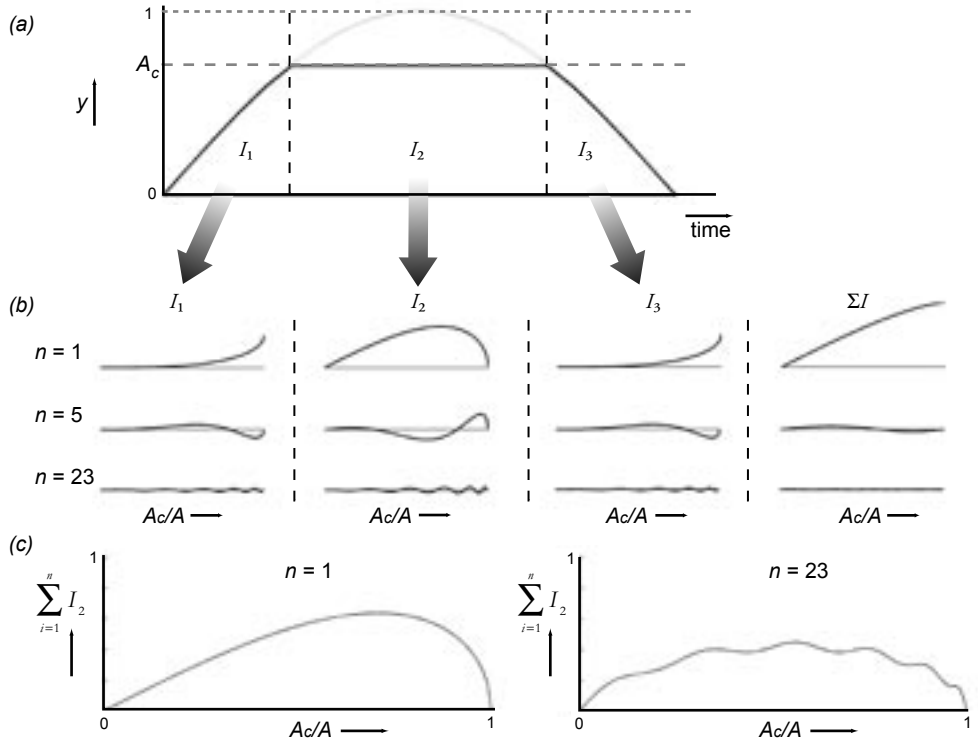

Figure 3.C (a) Half-range expansion of a clipped sinusoidal signal. A = amplitude, A_c = amplitude of clipping-level, τ = clipping-time, L = half-period. (b) The Fourier-integrals of the coefficient b_n as a function of A_c for n = 1, 5 and 25. (c) $\sum_{i=1}^{n} I_2$ for n = 1, and $\sum_{i=1}^{n} I_2$ for n = 23.

Using the instants τ_1 and τ_2 at which the clipping level is reached, we can split up this integral in three parts (figure 3.Ca):

$$b_n = \frac{2 \cdot A}{L_s} \cdot \int_0^{\tau 1} \sin\left(\frac{\pi \cdot t}{L_s}\right) \cdot \sin\left(\frac{n \cdot \pi \cdot t}{L_s}\right) dt + \frac{2 \cdot A_c}{L_s} \cdot \int_{\tau 1}^{\tau 2} \sin\left(\frac{n \cdot \pi \cdot t}{L_s}\right) dt + \frac{2 \cdot A}{L_s} \cdot \int_{\tau 2}^{L} \sin\left(\frac{\pi \cdot t}{L_s}\right) \cdot \sin\left(\frac{n \cdot \pi \cdot t}{L_s}\right) dt$$
$$= I_1 + I_2 + I_3 \qquad \text{(C7)}$$

in which:

$$\tau_1 = \frac{L_s}{\pi} \cdot \arcsin\left(\frac{A_c}{A}\right) \qquad \tau_2 = L_s - \tau_1 \qquad \text{(C8)}$$

Substituting $y(t)$ and τ in (C8) and carrying out the integration yields for $A = 1$:

$$I_1 = \frac{1}{\pi \cdot (1-n)} \cdot \sin\left[(1-n) \cdot \arcsin\left(A_c\right)\right] - \frac{1}{\pi \cdot (1+n)} \cdot \sin\left[(1+n) \cdot \arcsin\left(A_c\right)\right] \tag{C9}$$

$$I_2 = \frac{2 \cdot A_c}{n \cdot \pi} \cdot \left[\cos\left(n \cdot \arcsin\left(A_c\right)\right) - \cos\left(n \cdot \{\pi - \arcsin\left(A_c\right)\}\right)\right] \tag{C10}$$

$$\begin{aligned} I_3 = {} & \frac{1}{\pi \cdot (1-n)} \cdot \left[\sin\{\pi \cdot (1-n)\} - \sin\left[(1-n) \cdot \{\pi - \arcsin\left(A_c\right)\}\right]\right] \\ & - \frac{1}{\pi \cdot (1+n)} \left[\sin\{\pi \cdot (1+n)\} - \sin\left[(1+n) \cdot \{\pi - \arcsin\left(A_c\right)\}\right]\right] \end{aligned} \tag{C11}$$

For $n = 1$, the above formulae contain sinc-functions and become:

$$I_1 = I_3 = \frac{1}{\pi} \cdot \arcsin\left(A_c\right) - \frac{1}{2 \cdot \pi} \cdot \sin\left[2 \cdot \arcsin\left(A_c\right)\right] \tag{C12}$$

$$I_2 = \frac{2 \cdot A_c}{\pi} \cdot \left[\cos\left(\arcsin\left(A_c\right)\right) - \cos\left(\pi - \arcsin\left(A_c\right)\right)\right] \tag{C13}$$

The behaviour of these expressions when A_c varies from 0-1 is displayed in figure 3.C1b and C1c. It follows that even for $A_c / A \rightarrow 1$ the amplitude of the harmonics has still a considerable value. This is understandable as the sine-function about $t = L_s$ is very shallow and therefore the duration of the level A_c remains rather large when $A_c / A \rightarrow 1$.

(C3) Derivation of the formula for Double Side Band modulation (DSB)

Removing the carrier-signal from eqn (14) leads to the formula of double sideband modulation:

$$\begin{aligned} y_1(t) = {} & y(t) - A \cdot \cos\left(\omega_C \cdot t\right) = +A \cdot m \cdot \cos\left(\omega_{AM} \cdot t\right) \cdot \cos\left(\omega_C \cdot t\right) = \\ & = \frac{A \cdot m}{2} \cdot \left[\cos\left(\{\omega_C + \omega_{AM}\} \cdot t\right) + \cos\left(\{\omega_C - \omega_{AM}\} \cdot t\right)\right] \end{aligned} \tag{C14}$$

(C4) Derivation of the formula for Single Side Band modulation (SSB)

Removing one of the sidebands from eqn (14) leads to a formula of single sideband modulation:

$$\begin{aligned} y_2(t) = {} & y(t) - \frac{A \cdot m}{2} \cdot \cos\left(\{\omega_C \pm \omega_{AM}\} \cdot t\right) = A \cdot \cos\left(\omega_C \cdot t\right) + \frac{A \cdot m}{2} \cdot \cos\left(\{\omega_C \quad \omega_{AM}\} \cdot t\right) = \\ & = A \cdot \cos\left(\omega_C \cdot t\right) + \frac{A \cdot m}{2} \cdot \cos\left(\omega_{AM} \cdot t\right) \cdot \cos\left(\omega_C \cdot t\right) \pm \frac{A \cdot m}{2} \cdot \sin\left(\omega_{AM} \cdot t\right) \cdot \sin\left(\omega_C \cdot t\right) \end{aligned} \tag{C15}$$

Removing also the carrier-signal from the above formula leads to single sideband modulation used in radio engineering:

$$y_t = A \sin\left(\omega\, t + \frac{m}{p} \sin\, pt\right) = A\left[\sin \omega\, t \cos(\frac{m}{p} \sin\, pt) + \cos \omega\, t \sin(\frac{m}{p} \sin\, pt)\right] \tag{C16}$$

(C5) Angular modulation: Calculating energy distribution in side bands using Bessel functions

Eqn. (17) describing angular modulator, can be rewritten in:

$$y_t = A\sin\left(\omega\ t + \frac{m}{p}\sin\ pt\right) = A\left[\sin\omega\ t\cos(\frac{m}{p}\sin\ pt) + \cos\omega\ t\sin(\frac{m}{p}\sin\ pt)\right] \qquad \text{(C17)}$$

Both the terms $\cos(\frac{m}{p}\sin\ pt)$ and $\sin(\frac{m}{p}\sin\ pt)$ can be expanded in a Bessel function series:

$$\cos(\frac{m}{p}\sin\ pt) = J_0\left(\frac{m}{p}\right) + 2\left[J_2\left(\frac{m}{p}\right)\cos 2\,pt + J_4\left(\frac{m}{p}\right)\cos 4\,pt + \quad\right] = \sum_{n=-\infty}^{\infty} J_{2n}\left(\frac{m}{p}\right)\cos 2npt$$

(C18)

and

$$\sin(\frac{m}{p}\sin\ pt) = 2\left[J_1\left(\frac{m}{p}\right)\sin\ pt + J_3\left(\frac{m}{p}\right)\sin 3\,pt + \quad\right] = \sum_{n=-\infty}^{\infty} J_{2n-1}\left(\frac{m}{p}\right)\sin(2n-1)\,pt\ . \qquad \text{(C19)}$$

These functions are Bessel functions of the first kind, where the index specifies the order. Substitution of (C18) and (C19) into eqn (C17), [with $2\cdot\sin P\cdot\cos Q = \sin(P+Q)+\sin(P-Q)$]), results in

$$\begin{aligned} y_t = A.[&J_0\left(\frac{m}{p}\right)\sin\omega\ t + J_1\left(\frac{m}{p}\right)\sin(\omega\ + \mathrm{p})t - J_1\left(\frac{m}{p}\right)\sin(\omega\ - \mathrm{p})t + \\ &+ J_2\left(\frac{m}{p}\right)\sin(\omega\ + 2\mathrm{p})t + J_2\left(\frac{m}{p}\right)\sin(\omega\ - 2\mathrm{p})t + \\ &+ J_3\left(\frac{m}{p}\right)\sin(\omega\ + 3\mathrm{p})t - J_3\left(\frac{m}{p}\right)\sin(\omega\ - 3\mathrm{p})t\quad] = A\sum_{n=-\infty}^{\infty} J_n\left(\frac{m}{p}\right)\sin(\omega\ + np)t \end{aligned} \qquad \text{(C20)}$$

The summation follows from the formula $J_{-n}(x) = (-1)^n J_n(x)$.

Parseval's theorem can be restated for angular modulations:

$$\left[J_0\left(\frac{m}{p}\right)\right]^2 + 2\left[J_1\left(\frac{m}{p}\right)\right]^2 + 2\left[J_2\left(\frac{m}{p}\right)\right]^2 + \ldots = \sum_{n=-\infty}^{\infty} J_n{}^2\left(\frac{m}{p}\right) = 1 \qquad \text{(C21)}$$

This rule implies that the power of the angular modulated carrier is independent on the actual modulation, which corresponds to the constant amplitude of the angular modulated carrier. The modulation redistributes energy from the carrier frequency to the many sidebands.

(C6) Progressive modulation and combinations of modulation

We used the following definition of progressive FM:

$$y(t) = A\cdot\cos\left(\left[1 + n\cdot y_{FM}\right]\cdot 2\cdot\pi\cdot\left(\frac{t}{T_C}\right)^N\right) \qquad \text{(C22)}$$

The expressions for AM [eqn (14)], FM [eqn (17)] and progressive FM [eqn (C22)] can be combined in many ways.

The time signal of the example used in figure 3.6e is given by the expression:

$$\begin{aligned} y(t) = & A_1 \cdot \left(1 + m_1 \cdot y_{AM1}\right) \cdot \cos\left(\omega_{C1} \cdot t\right) + \\ & A_2 \cdot \cos\left(\left[1 + n_1 \cdot y_{FM1}\right] \cdot \omega_{C2} \cdot t\right) + \\ & A_3 \cdot \cos\left(\left[1 + n_2 \cdot y_{FM2}\right] \cdot 2 \cdot \pi \cdot \left(\frac{t}{T_{C3}}\right)^N\right) + \\ & A_4 \cdot \left(1 + m_2 \cdot y_{AM2}\right) \cdot \cos\left(\left[1 + n_3 \cdot y_{FM3}\right] \cdot \omega_{C4} \cdot t\right) \end{aligned} \qquad \text{(C23)}$$

The signal is composed of: (1) an amplitude-modulated signal, resulting in a carrier- and two side frequencies, (2) a frequency-modulated signal with a constant modulation-index. (3) a frequency-modulated signal with increasing modulation-amplitude (progressive FM), (4) a combination of AM and progressive FM.

(C7) AM to PM conversions in nonlinear oscillators

We consider the steady state solution of eqn (18) and (19) of the form $Q = A \cdot \cos(\omega \cdot t + \varphi)$. The first and second derivatives of Q are:

$$\frac{dQ}{dt} = -\omega A \sin\left(\omega t + \varphi\right) \text{ and } \frac{d^2Q}{dt^2} = -\omega^2 A \cos\left(\omega t + \varphi\right).$$

$$Q^3 = A^3 \cos^3\left(\omega t + \varphi\right) = \frac{3}{4} A^3 \cos\left(\omega t + \varphi\right) + \frac{1}{4} A^3 \cos 3\left(\omega t + \varphi\right) \qquad \text{(C24)}$$

Substitution of the expression for Q in eqn (18) gives:

$$\left[\left(\omega_0^2 - \omega^2\right)\cos\left(\omega t + \varphi\right) - \omega\, \omega_0 d A \sin\left(\omega t + \varphi\right)\right] A +$$

$$\left[3\omega_0^2 \cos\left(\omega t + \varphi\right) + \omega_0^2 \cos 3\left(\omega t + \varphi\right)\right] \frac{\lambda A^3}{4} = B \cos \omega t$$

Due to the 3rd order nonlinearity a third harmonic is generated. We will concentrate only on the terms concerning the fundamental ω_0 to show the AM to PM conversion. Grouping equal powers of A gives:

$$\left[(\omega_0^2 - \omega^2)^2 + d^2 \omega_0^2 \omega^2\right] A^2 + \frac{9}{16} \omega_0^4 \lambda^2 A^6 + \frac{3}{2} (\omega_0^2 - \omega^2) \omega_0^2 \lambda A^4 = B^2 \qquad \text{(C25)}$$

This expression gives the amplitude as a function of the excitation. The solution of this polynomial of the 3rd degree in A^2 can be obtained numerically. The expression can be rewritten as $\omega = f_{A,B}$:

$$\omega_0^4 A^2 + \omega^4 A^2 - 2\omega_0^2 \omega^2 A^2 + d^2 \omega_0^2 \omega^2 A^2 + \frac{3}{2} \omega_0^4 \lambda A^4 - \frac{3}{2} \omega_0^2 \omega^2 \lambda A^4 + \frac{9}{16} \omega_0^4 \lambda^2 A^6 - B^2 = 0$$

$$\omega^4 - 2\omega_0^2 \left(1 - \frac{d^2}{2} + \frac{3}{4} \lambda A^2\right) \omega^2 + \omega_0^4 \left(1 + \frac{3}{4} \lambda A^2\right)^2 - \left(\frac{B}{A}\right)^2 = 0 \qquad \text{(C26)}$$

The solution for ω^2 is :

$$\omega_{12}^2 = \omega_0^2 \left[\left(1 - \frac{d^2}{2} + \frac{3}{4} \lambda A^2\right) \pm \sqrt{\left(\frac{B}{\omega_0^2 A}\right)^2 - \left(1 + \frac{3}{4} \lambda A^2\right)^2 + \left(1 - \frac{d^2}{2} + \frac{3}{4} \lambda A^2\right)^2}\right] \qquad \text{(C27)}$$

Discarding higher powers of λ leads to:

$$\omega^2_{12} = \omega_0^2\left[\left(1-\frac{d^2}{2}+\frac{3}{4}\lambda A^2\right)\pm\sqrt{\left(\frac{B}{\omega^2_0 A}\right)^2-d^2\left(1+\frac{3}{4}\lambda A^2\right)+\frac{d^4}{4}}\right] \tag{C28}$$

Only real solutions are relevant. Figure 3.7a shows ω^2/ω as function of A, with B is varied from 1 to 10, (λ = 0.01 and d = 0.1. Now the phase of the oscillation charge can be determined relative to the excitation (figure 3.7b).

$$(\omega^2_0 - \omega^2)bA - \omega_0\omega\, adA + \frac{3}{4}\lambda\, bA^3 = 0 = (\omega^2_0 - \omega^2)\sin\varphi\, A - \omega_0\omega\, \cos\varphi\, dA + \frac{3}{4}\lambda\, \sin\varphi\, A^3$$

$$\tan\varphi = \frac{\omega_0\omega\, d}{(\omega^2_0 - \omega^2)+\frac{3}{4}\lambda\, A^2} \tag{C29}$$

The phase of the charge oscillation is strongly dependent on the excitation amplitude, especially around the frequencies in the neighbourhood of the low amplitude resonance frequency. The AM to PM conversion is evident even in the simplest of all nonlinear differential equation. Other peculiar properties of this type of differential equation, such as amplitude instability regions, are beyond the scope of this article.

SECTION III

mechanical modelling
of the syrinx

chapter **4**

Vibration and sound in a mechanical model of the syrinx

Submitted as:
Elemans, C.P.H., Muller, M., Larsen, O.N. & van Leeuwen, J.L.
Vibration and sound in a mechanical model of the avian syrinx.

Abstract

The multidisciplinary approach of combining experimental data and mathematical modelling has greatly improved the understanding of neural control and peripheral motor dynamics of sound generation in birds. The vibratory behaviour of the labia or membranes in the avian vocal organ, the syrinx, determines to a large extent the nature of the produced sound. However, these complex movements are largely unknown due to the problems encountered with *in vivo* observations. Here, we present the first mechanical model of the syrinx that facilitates detailed study of membrane vibrations and allows altering material properties. We explored the conditions for sound production of the model. As inception we used a relatively simple non-oscine syrinx of the family Columbidae. Our model consists of a tube with a single membrane in its casing. The adduction of the membrane is controlled by the pressure in a simulated air sac relative to the driving pressure in the tube. The functional window for sound production was determined by the position of the membrane. Without complete closure, no membrane oscillations were induced and no sound was produced. The vibrations of the membrane showed limit cycle behaviour. The membrane vibrations were coupled to the resonance properties of the distal tube, but also membrane properties and tension altered the pitch of the sound. Our model is a gross simplification of the complex morphology found in birds, nevertheless the use of mechanical models greatly facilitates detailed study of the sound producing mechanisms that are hard to study *in vivo*.

Introduction

The multi-disciplinary approach of combining experimental data and mathematical modelling has greatly improved the understanding of neural control and peripheral motor dynamics of sound generation in birds (Fee et al., 1998; Fletcher, 1988; Gardner et al., 2001; Goller, 1998; Laje & Mindlin, 2002; Laje et al., 2002; Mindlin et al., 2003). To close the path that leads from the brain to the sound, it was necessary to formulate adequate mathematical models of the syrinx (Fee et al., 1998; Fletcher, 1988; Gardner et al., 2001; Laje & Mindlin, 2002; Laje et al., 2001). For a review of these models see Elemans et al. (2003). Some of the latest models focus on the control of sound production in songbirds and use modified oscillators to model labial movement. The virtue of these models is that they succeed in reducing the number of control parameters to the essential minimum. Furthermore, they provide a theoretical framework that could explain many *in vivo* observations. Mindlin et al. (2003) presented a model that simulated experimentally recorded songs when the input to the model was pressure and muscle activity data obtained from physiological measurements. By representing the avian vocal system as a simple nonlinear oscillator, however, the complex geometry and distribution of material properties are sacrificed for the focus on neural control. Different syringeal morphologies and thus sound producing solutions have evolved within birds (King, 1989). To explain the range of these different designs from a biomechanical and evolutionary point of view, we need to include more realistic geometries in quantitative syrinx models.

Ultimately, the complex vibratory behaviour of the labia in songbirds and membranes in non-songbirds determines to a large extend the nature of the radiated sound. The use of small endoscopes (Goller & Larsen, 1997a, 1997b; Larsen & Goller, 1999, 2002) identified the sound sources directly for the first time. Direct endoscopic observations showed that in two non-songbirds, i.e. the pigeon (*Columba livia*) and the cockatiel (*Nymphicus hollandicus*), sound was generated by oscillations of the paired lateral tympaniform membranes (LTM) (Goller & Larsen 1999). The membranes undergo large deflections, but mainly due to a limited light intensity, the temporal resolution of the used system was too low to resolve the high-frequency membrane vibrations (estimated fundamental frequency: 0.7 - 1 kHz) of the LTMs. Therefore, it was unclear whether there are higher modi of vibrations or if the LTMs collide or not. Larsen & Goller (1999) used a phototransisitor that measured light reflections from the LTMs as a measure of vibration amplitude. This technique suggested that the membranes vibrated at the same frequency as the generated sound.

Both techniques mentioned above are very invasive due to the use of fibre optics. This has the disadvantage that the birds have to be anaesthetized and vocalizations can only be induced with gas injections or intracranial brain stimulation. The techniques that are used successfully in spontaneously vocalising birds, such as pressure, flow and EMG measurements, can only be used for short periods, since the calibration changes rapidly due to clogging, mucous accumulation or tissue rejection by the bird.

At present, there is no quantitative information on the complex movement of the LTMs and the biomechanical parameters and mechanisms that control their oscillation. Due to the delicacy and the internal location of the syrinx, obtaining *in vivo* recordings at sufficiently high temporal resolution remains an experimental challenge. This is in contrast to laryngoscopic methods available for human phonation research, where the larynx is relatively easy to access and detailed studies on vocal chords movements are available (e.g. Seikel et al., 1999).

To overcome some of the difficulties experienced *in vivo*, we designed a simplified Artificial

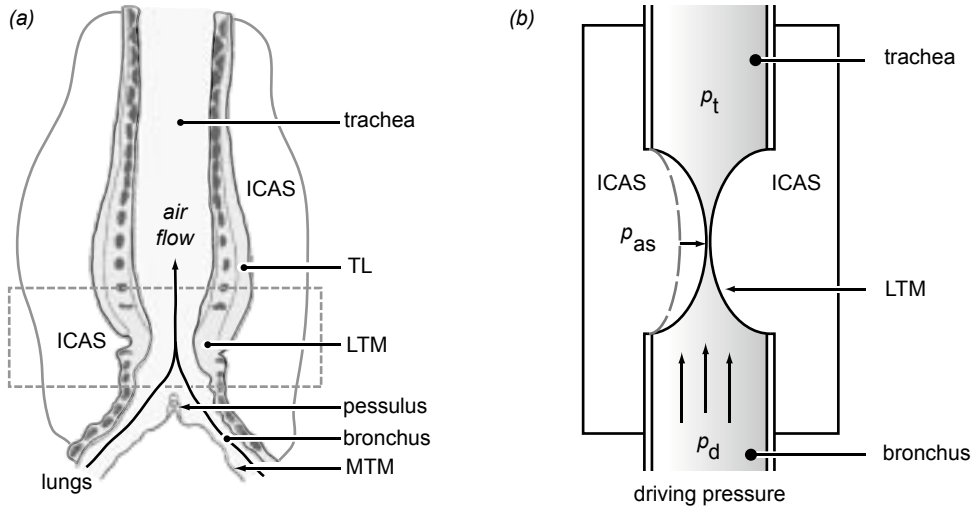

Figure 4.1 (a) A typical non-oscine syrinx; the tracheobronchial syrinx of *Streptopelia decaocto* modified from Ballintijn et al. (1995). ICAS, interclavicular air sac; LTM, lateral tympaniform membrane; MTM, medial tympaniform membrane; TL, *musculus tracheolateralis*. (b) Simplified representation of rectangle in (a). p_{as}, air sac pressure; p_d, bronchial or driving pressure; p_t, tracheal pressure.

Syrinx Model (SAM) of a 'typical' non-oscine syrinx. In addition to analytical and numerical modelling, real-life mechanical models facilitate the study of biological phenomena and provide insight into complex biomechanical problems e.g. flight mechanics (Ellington et al., 1996). Furthermore, mechanical models can be employed to test predictions by mathematical models, which has not been done with the mathematical models on song production in birds. To our knowledge, Brittain-Powell et al. (1997) presented the only mechanical model of the syrinx. This was a simple, but very illustrative model that consisted of straws. No detailed information of its mechanical properties was obtained.

In this paper, we present a mechanical model of the syrinx that allows for accurate measurements. In the first section, we provide a detailed description of the model. In the second section we focus on the parameters that control the amplitude and pitch of this artificial syrinx. The third section contains our conclusions and discussion.

Design and construction of the mechanical model: SAM

To allow for a more in depth study we deliberately made a step back from the biological complexity in terms of neuromuscular control and morphology. We ignored the syringeal muscles and larynx and did not engineer a complex morphology. The inception of our study was the non-oscine syrinx such as found in the family Columbidae (figure 4.1a). The syringeal morphology is relatively simple and membranes are employed to generate sound instead of the oscine labial masses, which are more difficult to engineer.

In pigeons (*Columba livia*), sound is thought to be produced by airflow-induced vibrations or

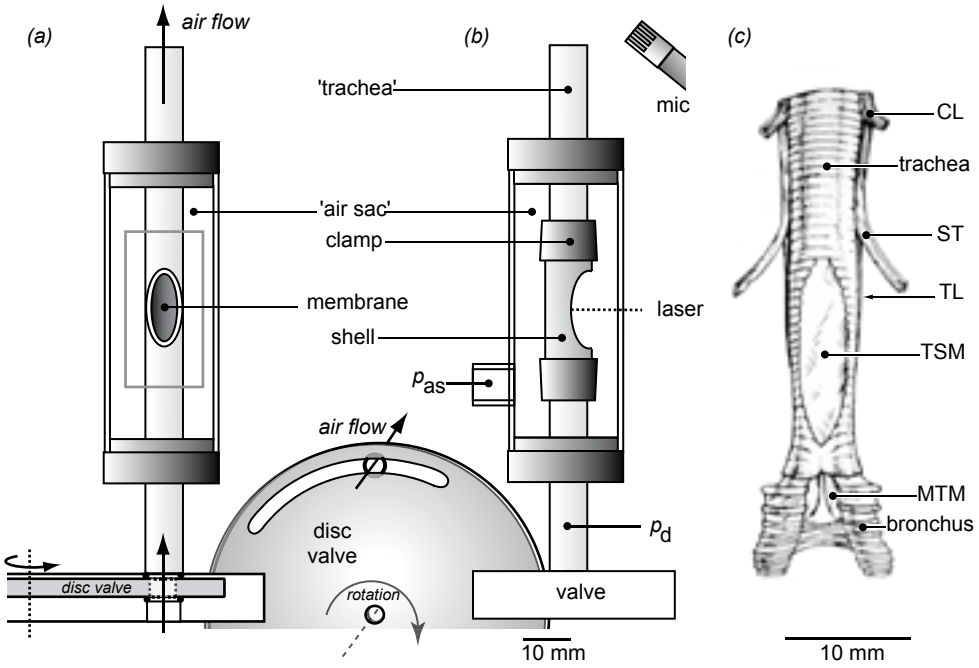

Figure 4.2 Schematic representation of the SAM with (a) frontal and (b) lateral view. In (b) the clamps and shells for mounting the membrane are shown. The rotating disc valve controls the driving pressure by closing and opening the tube inlet. The position of the two pressure transducers is indicated with p_d and p_{as}. mic, location of microphone. (c) Syrinx of a female whistling duck (*Dendrocygnus bicolor*, Anatidae, Anseriformes), ventral view. CT, *m. cleidotrachealis*; LT, *m. tracheolateralis*; MTM, medial tympaniform membrane; ST, *m. sternotrachealis*; TSM, tracheosyringeal membrane. Modified after King (1989).

collisions of the lateral tympaniform membranes (LTM) in the syrinx (Goller & Larsen, 1997a). The LTM's of *Columba livia* consist of collagenous tissue of about 100 μm thick (Goller & Larsen, 1997a). The airflow is generated by a pressure difference between upstream (i.e. bronchial or subsyringeal pressure) and downstream (i.e. tracheal or suprasyringeal pressure) of the LTMs (figure 4.1b). The syrinx is suspended in a lobe of the interclavicular air sac (ICAS) that is part of the complex respiratory system (figure 4.1). The respiratory muscles control the pressure in the air sacs of the respiratory system. Since all air sacs are interconnected, pressure has often been assumed the same in all air sacs, but very little is known about the 3D geometry of the air sac system and the pressure gradients during respiration (Fedde, 1987). However, the connections between the air sacs pose a resistance to flow and we suggest that during fast modulations phase delays between the pressure fluctuactions in various air sacs may be expected. Beckers et al. (2003a) demonstrated that the ICAS and bronchial pressure indeed show different patterns during cooing of ring doves (*Streptopelia risoria*), but the magnitude of the resulting pressure differential is unknown. An external force is thus applied to the LTM by the pressure differential between the ICAS and the bronchus.

The abovementioned essential elements for sound production are included in our mechanical model. Hereafter, we will refer to our model as SAM, an anagram for Artificial Syrinx Model. SAM consists of a 190 mm long aluminium tube (Young's modulus, E = 70 GPa) with an inner diameter

of 6 mm and outer diameter of 8 mm (figure 4.2a,b). One oval hole of 5.5 mm by 10.5 mm is milled in the casing of the tube. A latex membrane representing a single LTM was mounted over the hole. Such a simple 'one-membrane system' was found, for example, in the bronchial syrinx of owls (King, 1989), oilbirds and swiftlets (Suthers & Hector, 1982, 1985) and in the tracheal syrinx of the Whistling duck (*Dendrocygnus bicolor*; figure 4.2c). To simulate the interclavicular air sac, a portion of the tube including the membrane was enclosed in a polymethylmethacrylate (E = 3 GPa) cylindrical chamber (internal radius; 33.6 mm, internal length; 54.8 mm) in which the pressure could be regulated independently from the pressure in the tube. The folding of the LTM due to muscular contraction (Goller & Larsen, 1997a) could not be engineered. However, by increasing the pressure in the pressure chamber relative to the pressure in the tube, the membrane bulged into the lumen of the tube, forming a constriction resembling the LTM in the pigeons' syrinx. A rectangular window in the air sac allowed observations of membrane movements. All experiments were performed at room temperature in a semi-anechoic room at Wageningen University.

Methods

The driving pressure at the base of the tube was controlled with a valve that consisted of a motor driven rotating disc, in which a sickle shaped slit was milled (figure 4.2a,b). One rotation of the disc resulted in a periodical pressure pattern. The driving pressure (p_d) and the pressure in the simulated ICAS (p_{as}) were measured with Statham pressure transducers (Statham P23D6) at the points indicated with p_{as} and p_d in figure 4.2b. The signals from the Statham transducers were amplified (Dual channel electromanometer amplifier, Elema-Schönander type EMT 311. Full scale range 10 - 400 mm Hg, i.e. 1.3 - 53.3 kPa) and low-pass filtered (cut-off frequency 700 Hz). Prior to each measurement the complete system was calibrated with a water column. Pressure amplitudes mentioned in the texts are the pressures above atmospheric pressure.

Membrane velocity was measured with a Laser Doppler Vibrometer (LDV; Polytec, controller OFV 3001, Sensor head 353). The He-Ne laser beam (wavelength 633 nm) was reflected by a small piece of reflective tape (0.5 by 0.5 mm), which was glued to the membrane or to any other part of SAM. The inner surface of the aluminium tube was dyed black to reduce reflections from the laser beam. The velocity signal was positive (in Volts) if the marker was moving towards the LDV.

Sound was recorded with a 1/4-inch omni-directional condenser microphone (Brüel & Kjær, type 4939). The microphone signal was pre-amplified (Brüel & Kjær Preamplifier 2670), amplified and band-pass filtered (Brüel & Kjær, Nexus Dual channel, conditioning amplifier; high-pass filter 20Hz, 80dB/dec; low-pass 10 kHz, 40dB/dec). The front plate of the microphone was placed 3 cm from the tube outlet and directed to the tube-outlet from behind, at an angle of 45° with the tube (figure 4.2b) to avoid vortices coming out of the tube outlet.

Microphone, LDV and pressure transducers signals were digitized at 30 kHz using a 12-bit PCI-MIO16E-4 data-acquisition hardware architecture (National Instruments) on a Pentium III 700MHz Workstation. All signal acquisition and analysis software was custom developed in either LABVIEW 6.0 (National Instruments) or MATLAB 6.0 (The Mathworks).

Digitized signals of the microphone and vibrometer were filtered with a digital band-pass (resp. 20 Hz - 10 kHz and 20Hz - 5 kHz) fifth-order Butterworth filter implemented with zero phase-

shift. Digitized pressure signals from the Statham transducers (p_d and p_{as}) were filtered with a band-pass (20 - 700 Hz) third-order Butterworth filter with a zero phase-shift implementation. To construct spectrograms, 3500 pts discrete Fast Fourier Transforms (Hamming window) were calculated and slid over the digitized time signal with steps of 300 pts (See Chapter 3). The displacement of the laser spot on the membrane was calculated by integrating the velocity signal. The acceleration of the membrane was calculated by differentiating the velocity signal

Membranes; mounting and material properties

Latex membranes obtained from condoms were used to represent the LTM. Condoms provided ideal membrane material, because of the high quality and consistency demands in predestined use. Samples of 40 by 40 mm were rinsed with water and soap to remove lubricants. The membrane samples were mounted on SAM by two half-cylinder shells that fitted exactly on the oval hole (figure 4.2b). Pre-load in the samples was kept as close to zero as possible.

Tensile material properties of the membranes were determined using an ergometer (Aurora Scientific 300B) that is a force and length transducer. The membrane samples needed to be at least ten times longer than wide to ensure mono-axial testing. Six samples of 25 mm by 1 mm were cut either parallel or normal to the base of the condom, in order to investigate possible anisotropy in the latex. All samples were stored in sealed containers under moist conditions at room temperature. The latex samples were mounted in the test set-up with acrylate glue. With a slider the length of the samples could be increased by up to almost 200% of their resting length. Since latex is a rubber composite the elasticity properties are virtually time independent (Dr. C.W.J. Oomens, pers. comm.). Tensile tests were performed with sinusoidal length variations at a frequency of 10 Hz. This oscillation frequency was chosen to avoid lateral vibrations in the sample at the minimum longitudinal strain. After testing, the samples were carefully cut out of the set-up and stored at room temperature.

Stress and strain were calculated from the ergometer force and displacement signals, according to Vincent (1982). The nominal stress was defined as $\sigma_n = F / A_0$, where F is force (N), and A_0 is initial cross sectional area (m^2). The nominal strain was defined as $\varepsilon_n = (l - l_0) / l_0$, where l is the actual length (m) and l_0 the initial length of the sample (m) The initial length (l_0) was measured with a digital caliper. Initial cross-sectional area (A_0) was measured per sample using a Microphot-FXA microscope (Nikon) and ANALYSIS PRO 3.1 software.

In itself, rubber materials like latex, behave as linear springs (Vincent, 1982). Continuum mechanics theory, however, shows that during tensile tests, the nominal stress and strain curves for rubber are non-linear due to non-linear geometry and not due to non-linear material properties (Chadwick, 1999). To correct for this non-linear geometry in the results, we also used the so-called Neo-Hookean definitions of true stress (σ_t) and true strain (ε_t).The true stress was defined as:

$\sigma_t = F / A$, where F is force (N), and A is the actual cross sectional area (m^2). The true strain was defined as $\varepsilon_t = \ln (l / l_0)$.

The actual cross sectional area (A) for every discrete time-step was calculated by $A = V / l$, where V is the volume, and l the actual length of the sample. The volume V was assumed to be constant (Poisson-ratio = 0.5) for every sample, and calculated using the initial values ($V = A_0 \cdot l_0$). To calculate Young's modulus ($E = \sigma / \varepsilon$) at any given strain, a fourth-order polynomial was fitted through the loading curve of the data in a given strain range using the least squares method. The Young's modulus could be determined at any strain by calculating the derivative of these polynomials.

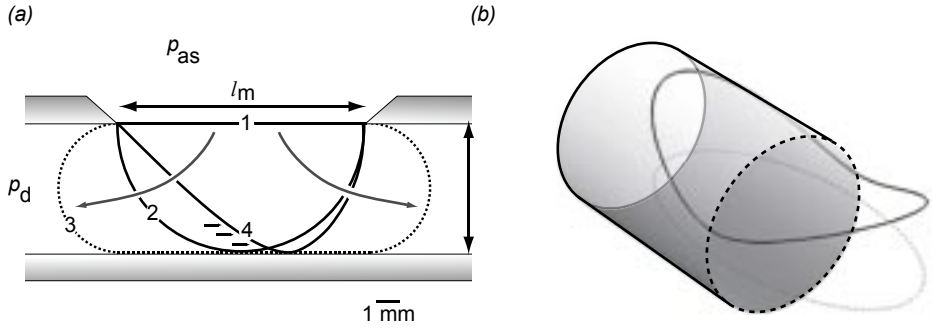

Figure 4.3 (a) Medial section through the SAM showing deflections in the membrane with increasing air sac pressure. Curve 1 represents the membrane at resting length (l_m). With increasing p_{as}, the membrane deflects more into the tube lumen (curve 2). Curve 3 represents the maximal length of the membrane during experiments. When air is flowing trough the tube (from left to right) the membrane deforms (curve 4). l_m = 10.55 mm; h_m = 5.60 mm. (b) To estimate the area of the membrane, an ellipse is projected on the tubes' casing.

Strain range and mass of the vibrating membrane in SAM

The relevant strain range occurring in the membrane during vocalizations in SAM was estimated from the tube dimensions (figure 4.3a). In the resting position with p_d and p_{as} at atmospheric pressure, the length at cross-section of the membrane l_m was 10.55 mm (curve 1 in figure 4.3a). At higher p_{as}, the membrane is forced into the lumen. When the membrane forms a circular arch with radius 5.2 mm (curve 2 in figure 4.3a), it almost touches the opposite side of the tube. The length of the sample is then 16.5 mm (ε_n = 0.55; ε_t = 0.19). At even higher p_{as}, the membrane is pressed against the opposite side of the tube and the membrane deflects side-wards (curve 3 in figure 4.3a), with l = 28.1 mm (ε_n = 1.67; ε_t = 0.43). The estimated strain range occurring in the SAM during the tests was between 0 - 1.67 (ε_n) or 0 - 0.43 (ε_t).

The mass (m_m) of the membrane free to vibrate in the mounted situation could not be measured directly. The total mass of the membrane was estimated from the specific density (ρ_s)of the material and area of the membrane that was enclosed by the clamps. The area was estimated by mathematically projecting an ellipse on the cylinders' casing (figure 4.3b). To determine the ρ_s per membrane type, four samples of 5 by 5 mm were randomly cut and weighed (Mettler Toledo AG204, accuracy ±0.1 mg). Their area was measured using a NIKON Microphot-FXA microscope and ANALYSIS PRO 3.1 software.

Testing protocols

To explore the behaviour of SAM, we performed three series of tests.

1) Sound was generated with a simple repetitive p_d pattern supplied by a disc valve with one slit (figure 4.2). At the onset of each 'vocalization' event, p_{as} was prescribed. The membrane vibrations,

pressure and sound were recorded. The signals were divided in bins of 10 ms. The mean p_d was calculated per bin. The RMS value and the fundamental frequency (f_0) were calculated for the sound and vibrometer signals. The spectral density of every bin was estimated using the multitaper method (Persival & Walden, 1993; Thompson, 1982). Bins were zero-padded to 8096 points to obtain a frequency resolution of 3.7 Hz.

2) To investigate the coupling between membrane vibrations and distal tube length, the length of the tube was increased systematically. Tube extensions of 1, 2, 5, 10, 20, 15, 20, 30, 40, 50 and 60 cm could be attached to the tube outlet of SAM. First, pressures p_{as} and p_d were ascribed to generate sound. Subsequently, extensions of increasing length were placed on the tube outlet. Driving pressure and sound were recorded for one second to calculate the mean p_{as}, p_d and fundamental frequency of the sound.

3) Both pressures p_{as} and p_d were altered systematically to explore the behaviour of SAM as a function of the pressure parameter space. First, both pressures were set to atmospheric pressure. A prescribed value of p_{as} was set and p_d was increased in discrete steps. The upper value of p_d was qualitatively judged to prevent rupture of the membrane and based on experience of previous rupture events. This procedure was repeated for different values of p_{as}. The sound, p_{as} and p_d were recorded for one second. The sound intensity (L_p = log(RMS/20 µPa)), the fundamental frequency (f_0), and the mean value of p_{as} ($\overline{p}_{as}$) and p_d ($\overline{p}_d$) were calculated for every recording. Sound intensity and fundamental frequency data were fitted on a 2D mesh of $\overline{p}_{as}$ and $\overline{p}_d$ (spacing 25 Pa) using triangle-based cubic interpolation (*griddata* algorithm Matlab). We omitted recordings with L_p lower than 50 dB (re 20 µPa) i.e. background noise level and with f_0 lower than 400 Hz since these were generally recordings of turbulent noise.

Results

SAM behaviour: (1): valve experiments

Traces of sound pressure, membrane velocity and driving pressure of typical results can be seen in figure 4.4. The SAM produced sound only when the pressure in the air sac, p_{as}, was set to a value high enough to result in complete closure of the tube by the membrane (p_{as} = 5.58 kPa above atmospheric for data presented in figure 4.4). We only observed sound production when the membrane closed off the tube completely before increasing p_d. The membrane never started vibration when it did not touch the other side of the tube initially. Sound was produced by raising the driving pressure (p_d) above a particular threshold. Modulation in p_d (figure 4.4c) resulted in modulation of the amplitude of sound pressure and membrane velocity (figure 4.4a,b). The first peak in p_d at the start of every 'syllable' (see arrow in figure 4.4c) is caused by the pressure head that emerged when the rotating disc valve opened. Spectrograms of sound and vibration signals show a harmonic stack with even and odd harmonics (figure 4.4d,e). Despite large changes in membrane velocity and sound pressure in the time domain, there seemed to be little effect of p_d on fundamental frequency.

Sound and membrane velocity as a function of driving pressure of four consecutive syllables can be seen in figure 4.5. The sound amplitude RMS has a linear relation with ascending driving pressure for half of the range (1.5 - 3.2 kPa). At p_d < 1.5 kPa, there is a nonlinear relation with RMS values (figure 4.5a). The membrane velocity shows a similar relation with p_d (figure 4.5b). The velocity levels off at about 1.1 m/s when p_d > 2.7 kPa. The patterns for fundamental frequency of

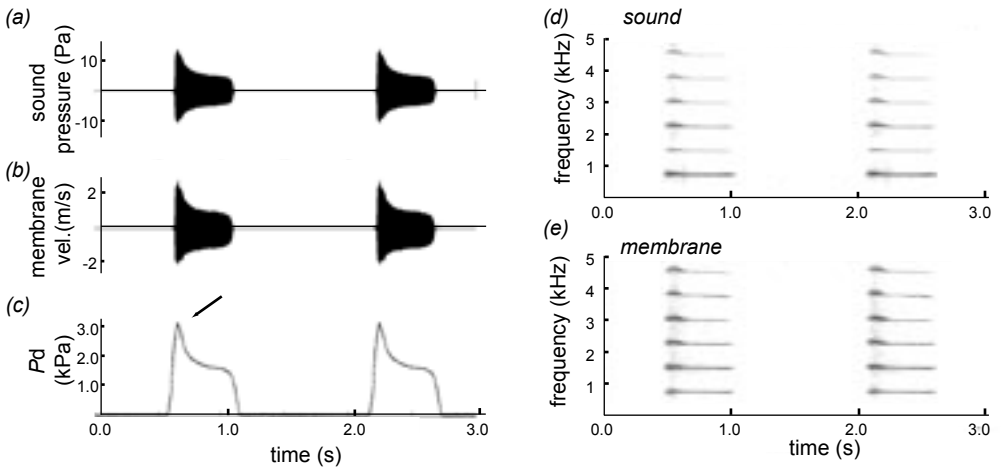

Figure 4.4 Typical results from a time series of (a) sound pressure, (b) membrane velocity, and (c) p_d. Arrow indicates the pressure head that emerges from the disc valve. Rotation frequency of airflow valve = 1.6 Hz. Mean p_{as} = 5.58 kPa. Spectograms of sound (d) and membrane velocity (e).

membrane vibrations and produced sound are nearly identical (figure 4.5c,d). The fundamental of both signals increased linearly from 750 to 800 Hz with increasing driving pressure from 1.4 kPa to 3.2 kPa. When p_d < 1.4 kPa, the fundamental deviates from the linear relationship and increases slightly (700-750 Hz) with decreasing p_d. However, the driving pressure does not cause large frequency modulation.

Interestingly, the relation between sound and driving pressure depended on the state of the membrane, emphasizing the non-linearity of this system. A gradual increase in p_d from atmospheric pressure, resulted in a sudden onset of the membrane vibration when p_d was above a threshold level (around 0.9 kPa). However, when the driving pressure decreased from 3.0 kPa to 2.5 kPa at the end of the syllable (see also figure 4.3), the membrane stops vibrating around p_d = 2.5 kPa even though p_d is much higher than the onset threshold. We will refer to this as the termination threshold. The SAM demonstrates hysteresis in its behaviour. During the recording in figure 4.5b, the p_{as} dropped slightly between consecutive syllables. This did not affect the phonation thresholds since the lines overlap, but the termination thresholds differed since four lines corresponding to the four consecutive syllables are clearly visible around 2.0-2.5 kPa.

To check whether the wall was resonating due to the produced sound, the vibration of several parts of the SAM were measured during sound production. At all investigated points on the tube and the pressure chamber, vibrations were below noise level of the LDV and could not be extracted even after averaging.

A detail of the onset of sound and membrane displacement is depicted in figure 4.6a,c. The maximal displacement of the membrane during ongoing signals was 0.25 mm. It should be noted that the velocity of the membrane is measured in line with the laser beam. One particular point on the membrane may in fact move in and out of the laser beam. But, since the position of the laser beam is fixed, a series of continuous points of the membrane reflect the laser beam. High speed filming did not provide enough detail for vibration analysis due to the small movements of the membrane at high speeds.

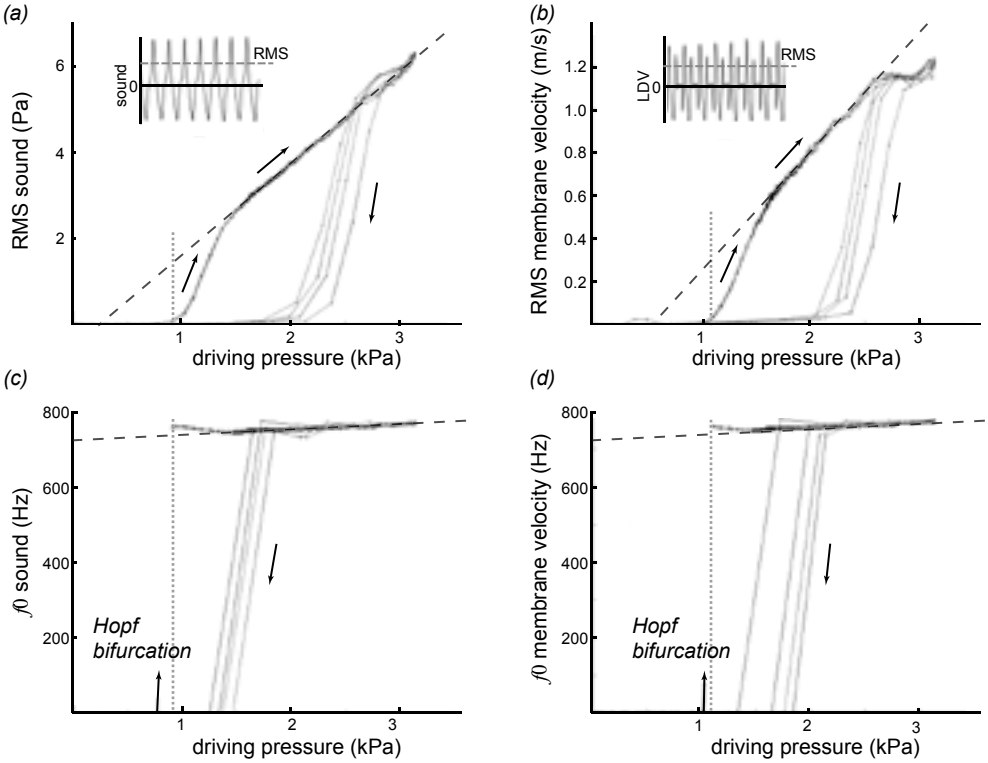

Figure 4.5 Sound and membrane parameters as a function of driving pressure. RMS values of (a) sound pressure and (b) membrane velocity. The arrows indicate the progression of time. The insets show one bin of the recorded signals with RMS values. Fundamental frequency of (c) sound and (d) membrane velocity. The state of the membrane changes instantly from no movement to oscillation at about 750 Hz. This is essentially a primary Hopf bifurcation of a nonlinear system.

The spectral density estimates of sound and membrane velocity (figure 4.6b,d) demonstrate odd and even harmonics of a fundamental of 758 Hz. In the sound spectrum, the fundamental is most dominant, whereas in the membrane velocity spectrum the 1st harmonic is most dominant.

Pressure proportional to force if the area on which the force is applied remains constant. The acceleration of a mass is also proportional to the force applied on it if the mass remains constant. Therefore we can study the phase relation between sound and membrane vibration, both proportional to force, by plotting the sound pressure vs. the membrane acceleration. The phase space of membrane acceleration and sound pressure (figure 4.7) of the onset of a syllable shows the complex relation between vibration and sound. The shape of the attractor seems proportional to excitation amplitude. The phase plot shows two crossings and almost three crossing that each represent a period doubling of the membrane acceleration with respect to the sound pressure.

Concluding, the driving pressure p_d controls the amplitude of the membrane vibrations and of the produced sound. The fundamental frequency is affected by p_d, but only over a very small range. The sound and membrane velocity spectra demonstrate both odd and even harmonics. The membrane movements form an attractor in acceleration-sound phase space.

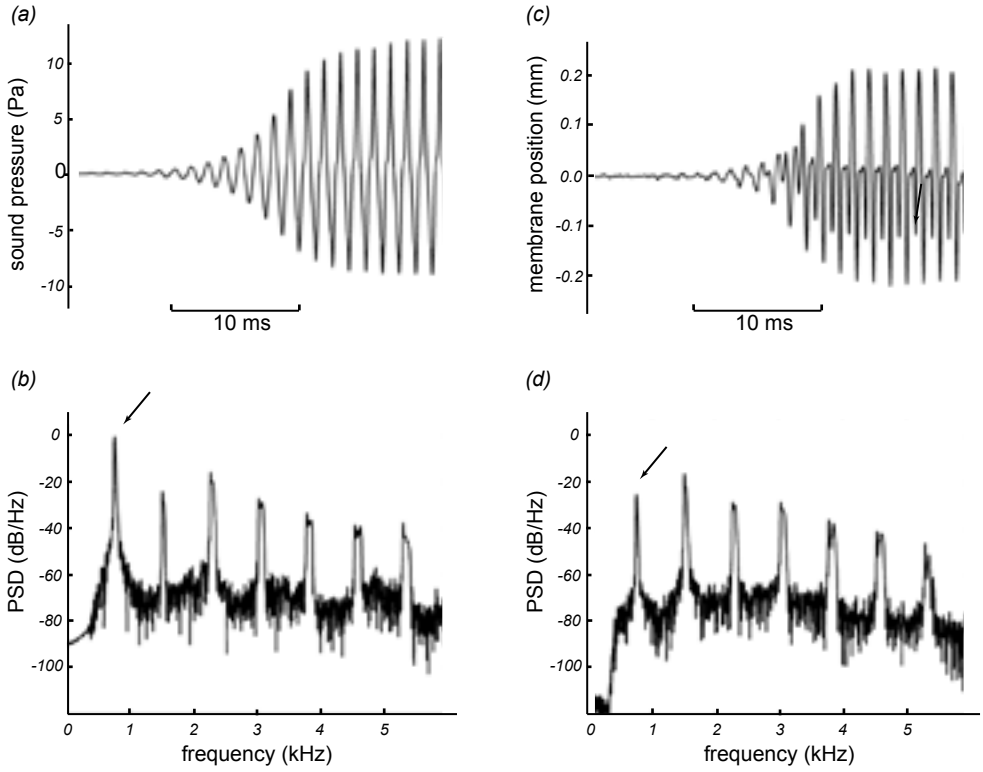

Figure 4.6 (a) Detail of sound wave and (c) membrane displacement. (b),(d) Spectrum estimates of above signals. Arrows indicate the fundamental frequency.

SAM behaviour (2): tube elongation

To investigate the relationship between sound and tube resonances, we systematically altered the length of the tube downstream (i.e. distal) to the membrane of the SAM. The resonance frequencies (H_n) of an open tube are located at the frequencies: $H_n = n(v/2L)$, where n =1,2,3..., v is the speed of sound (343 m/s at 20°C) and L the length of the tube [m]. The first resonance frequency H_0 is called the fundamental frequency and all odd and even harmonics are present. For a tube that is closed on one side we can write $H_n = n(v/4L)$, where n =1,3,5,7... and thus only the odd harmonics appear. From the centre of the membrane, the tube of SAM measured 97 mm, which corresponds to a H_1 of 1768 Hz and 884 Hz for an open and closed tube, respectively. The fundamental frequency of the generated sound in previous experiments was around 800 Hz (figure 4.4-4.6) and thus close to the lowest resonance frequencies of a tube closed on one end. However, the SAM produced both odd and even harmonics as predicted for an open tube (figure 4.4d,e & 4.6c,d).

The fundamental frequency of the sound (f_0) produced by SAM decreased with increasing tube length (L) and closely followed the H_1 for a closed tube (figure 4.8a). The difference between the measured f_0 and predicted H_1 of the tube decreased with increasing L. There was a linear relation-

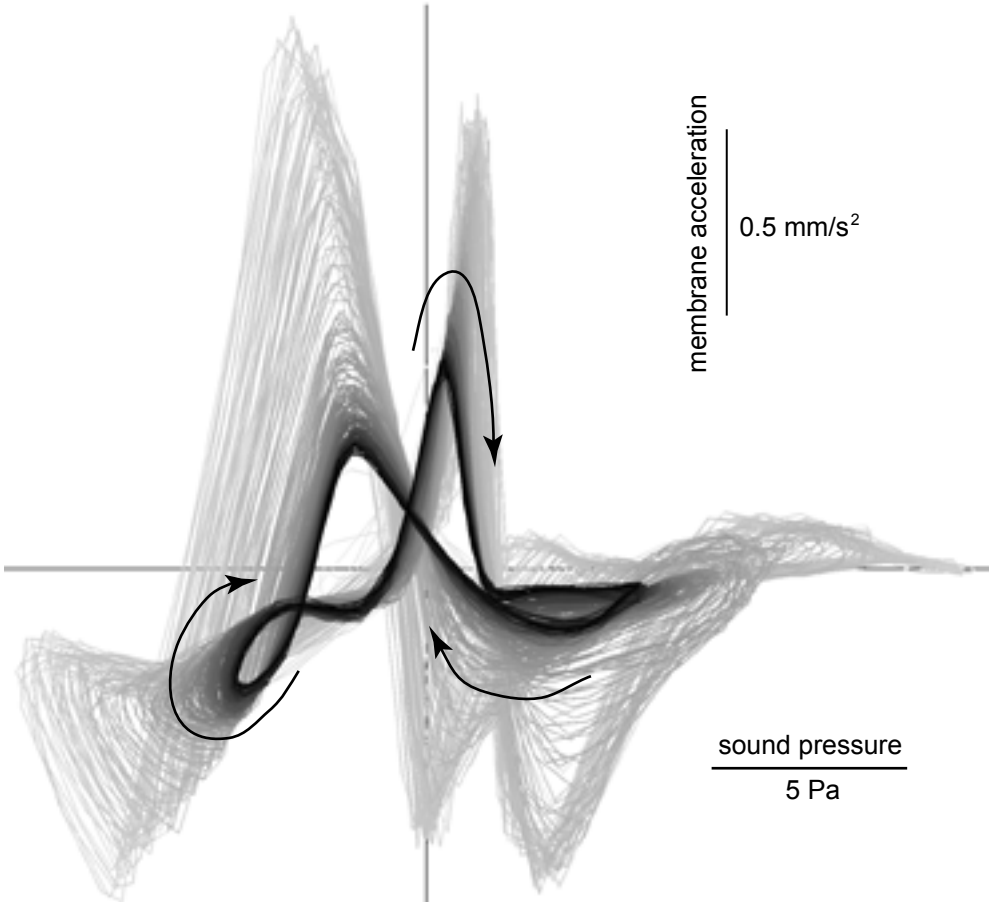

Figure 4.7 Typical behaviour of SAM in the phase space between membrane acceleration and sound pressure. The curve starts at the 0,0-coordinate and becomes progressively black with time. The shape of the attractor was similar for all tested runs.

ship between the reciprocal of the frequency difference and L (figure 4.8b). This discrepancy between observed and predicted values can be explained if we consider the column of oscillating air in the tube distal to the membrane. When at resonance, the air column moves back and forth in the tube and a small volume of air moves in and out of the tube at the tube outlet. This amount of air volume is dependent of the tube radius (r) and effectively increases the 'effective length' of the resonating air column. The pressure node is located out of the tube by a certain distance. Therefore, we need to add a so-called 'end correction' to the measured tube length to obtain the effective length of the air column. So instead of $f = v/4L$, we write $f = v/4\left(L + \Delta\right)$, where Δ is called the end-correction. We can rewrite this into $L + \Delta = \left(v/4\right)\left(1/f\right)$, with $\Delta = x \cdot r$. The factor x can be derived theoretically and is 0.61 for cylindrical tubes closed on one side (Rayleigh, 1945). In the plot L vs. $1/f$ (figure 4.8b), the slope (r^2= 0.997, p<0.001) will be equal to the speed of sound divided by four, and the intercept will be the negative of the end correction. The end correction is

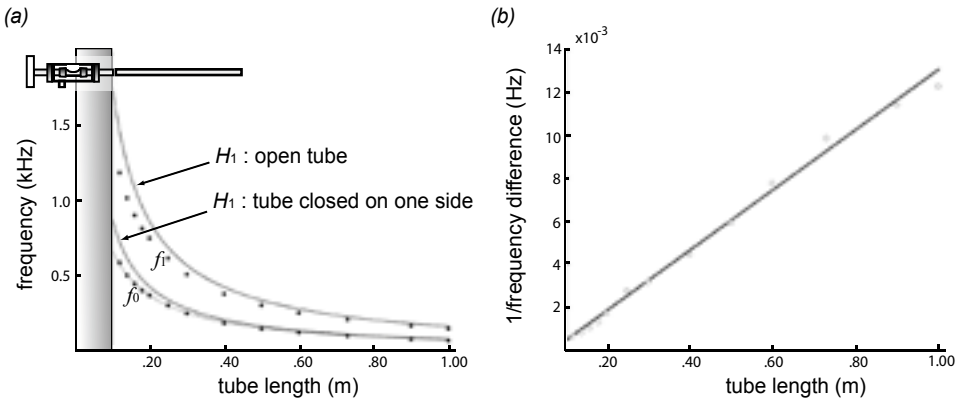

Figure 4.8 The effect of distal tube elongation on the frequency of the produced sound. (a) Shaded area is the minimal length of the tube. The fundamental and first harmonic are measured (dots). The two dotted lines show the lowest resonance frequency of a cylinder that is resp. open or closed on one side. (b) Frequency difference from the measured fundamental frequency (dots) and predicted lowest resonance frequency (line) of cylinder closed at one side due to 'end effect' (r^2=0.997, p<00.1). The effect decreased relatively with increasing tube length.

1.3 cm and x is 4.6. From the tube elongations, we can conclude that the frequency of the sound was coupled strongly to the resonance frequency of the tube.

SAM behaviour (3): pressure parameter space

We tested two membranes, M_1 and M_2, that differed in stiffness and mass (Table I). To close the tube of the SAM, a higher force was needed for M_2 than for M_1. Therefore the pressure needed to close the tube with M_2 was higher than for M_1. For both membranes, sound was produced only in a limited range of driving and air sac pressure (figure 4.9). With membrane M_1, sounds could be produced up to 112 dB (at p_{as} = 4.12 kPa and p_d = 1.88 kPa). The fundamental frequency varied from 717 to 913 Hz. At a particular value of pas (e.g. line a in figure 4.9b), the fundamental frequency of the sound increased with p_d from 755 to 850 Hz. This correlation was observed previously in figure 4.5. At a higher value of p_{as} (line b in figure 4.9b), the range of fundamental frequencies (to Hz) spanned was also 750 to 850 Hz, but in combination with a higher driving pressure. A fundamental of e.g. 800 Hz was generated at a range of combinations of p_{as} and p_d, that are roughly located at a pressure difference isoline between p_{as} and p_d (dotted line in figure 4.9b).

Similar patterns of sound intensity and fundamental frequency emerge for the stiffer membrane M_2. Sounds were produced up to 114 dB at p_{as} = 8.02 kPa and p_d = 2.90 kPa. The fundamental frequency of the sound ranged from 820 to 888 Hz and also exhibited correlation between frequency isolines and pressure differential between p_{as} and p_d.

Not every combination of p_{as} and p_d could be realized experimentally. At a low p_{as} it is not possible to get a high p_d since the air-resistance in the tube is low. At high p_d or p_{as} the membrane ruptured. We can conclude that the amplitude and fundamental frequency depend on both p_{as} and p_d.

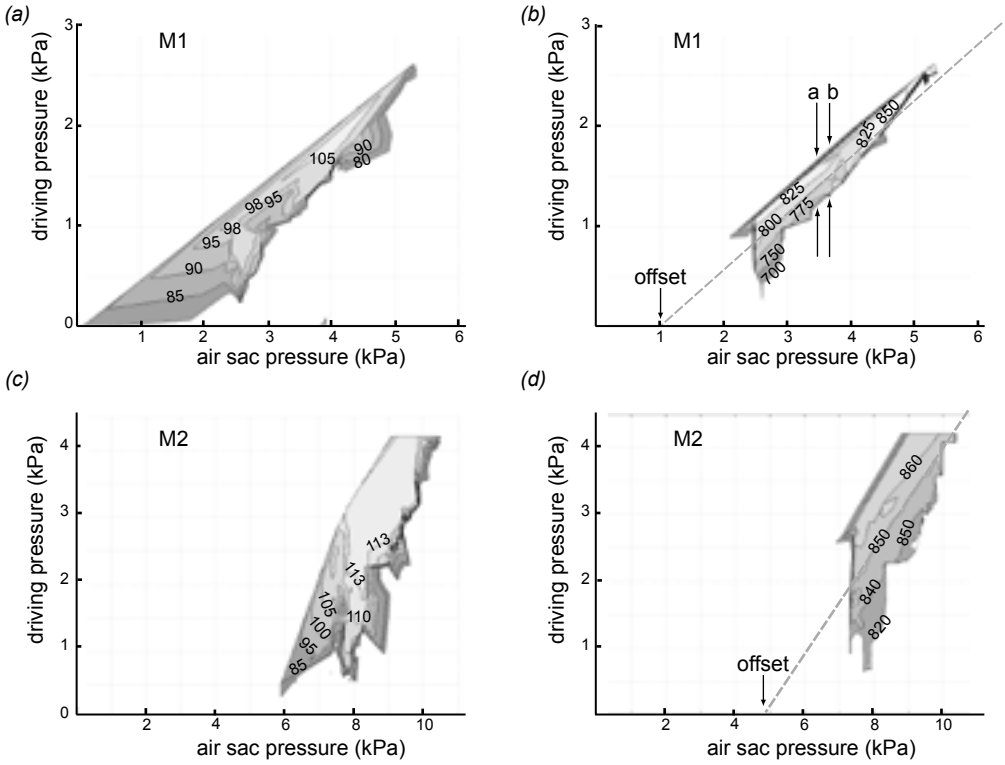

Figure 4.9 Interpolated contour plots of (a) sound intensity (L_p: in dB re 20 µPa (RMS values)) and (b) fundamental frequency in the p_{as} , p_d - parameter space of membrane M_1. Similar plots of RMS (c) and fundamental frequency (d) for the stiffer membrane M_2.

Table 4.I Membrane material properties (n=10).

type	*membrane density*	*membrane mass*	*Youngs modulus in MPa nominal strain (ε_n) range*			*Youngs modulus in MPa true tensile strain (ε_t) range*		
	(mg/mm²)	*(mg)*	*0.56*	-	*1.66*	*0.19*	-	*0.43*
M_1	6.32 10^{-2}± 2.0 10^{-3}	1.63± 0.05	0,730	-	0,576	5,98	-	16,75
M_2	1.04 10^{-1}± 5.0 10^{-3}	2.70± 0.13	0,769	-	0,841	6,66	-	22,53

Discussion

SAM behaviour

Our results strongly suggest that the amount of adduction of the membrane determines the functional window for sound generation in our SAM. As mentioned before, local forces acting on the membrane are the pressure differential over the membrane i.e. a force perpendicular to the membrane, and the local stress gradients in the membrane. The difference between p_{as} and p_{d} should be correlated with the local force, and also with the strain and material properties of the membrane. Therefore, the pressure in the pressure chamber needed to close the tube for a stiffer membrane is higher than for a more compliant membrane. If sound is produced either by vibrations of the membrane very close to the wall of the tube or by collisions with the wall, the position and thus the strain in the membrane determines the window for sound production. Therefore, with a stiffer membrane we expect sound to occur at higher air sac pressures. Our results support this hypothesis, since with the stiffer membrane M_2 sound was generated within a range of higher p_{as} values (7 to 11 kPa) compared to M_1 (6 to 10 kPa).

The pressure differential between p_{as} and p_{d} also affects the tension in the membrane. Tension in a vibrating membrane determines the oscillation frequency (Fletcher, 1988). The isolines in figure 4.9b and 9d indicate that also during oscillation the overall tension in the membrane affects the fundamental frequency of membrane vibration and produced sound.

We observed a strong coupling between fundamental frequency of the sound and the vibration of the membrane and we suggest that this strong coupling may be caused by reflections of sound waves on the smooth surface of the distal tube. The fundamental of sound and membrane vibrations is determined by the resonance properties of the distal tube and by the properties of the membrane. The end effect of 4.6 is much higher than the theoretically derived value. The presence of the room at the open end of the tube affects the resonance within the tube and shifts the fundamental. It is assumed that the open end acts to lengthen the tube, such that its acoustical length is really given by the total length plus the end correction . This end correction depends on the radius of the tube *r* and a constant *x*. This discrepancy between the theoretical derived value of *x* (0.61; Rayleigh, 1945; *http://hyperphysics.phy-astr.gsu.edu*) and our observed value (4.6) could be caused by the membrane. The mass of the vibrating system consists of the mass of the vibrating air and an 'effective' membrane mass. This added mass due to the membrane, would indeed increase the value of *x*. We did not investigate the effect of different membranes on the end-effects and on the parameter *x*.

The SAM behaves acoustically as if it is a tube closed on one end. The SAM is obviously not closed since air is blown through. We observed, however, both odd and even harmonics. This deviates from musical instruments that act as a closed tube. The complex 3D-movement of the membrane could not be quantified with this dataset, so it remains unclear which parts of the membrane contribute to the oscillations and if these parts collide with the wall or oscillate at close distance.

Are the SAM results representative for the findings of mathematical models?

Physical models are useful to test the different mathematical models present in the literature. The two mass-models published by Gardner et al. (2001) and Laje et al. (2002) are homologous to human sound production models and can simulate many features of bird song. Laje et al. (2002) showed that simple control loops in parameter space of a stiffness-parameter and a pressure-param-

eter result in complex 'song'. These models provide insight in the system but are far from the very complex biological reality. The parameters used in these models cannot be simply translated to real stiffness of the tissue and the real pressures in the bird's syrinx. We have not tested the predictive performance of published models.

Are the SAM results representative for the in vivo conditions?

The SAM deviates from real birds in several aspects. The pressures in the pressure chamber, representing the interclavicular air sac surrounding the syrinx, and the driving pressure, representing the bronchial pressure, are essentially different. We speculated that the difference in pressures is necessary to initiate LTM oscillations in real birds. To our knowledge, calibrated measurements have not yet been done on bronchial pressure and interclavicular airsac pressure simultaneously. Beckers et al. (2003a) measured ICAS pressure during cooing in ringdoves, and found that the pressure in the interclavicular airsac was related to the fundamental frequency of the sound produced. This suggests that the pressure in the ICAS increases tension in the LTM. We demonstrate that a quantitative insight into this system requires information on the pressure differential over the membrane instead of the absolute pressure in one of the cavities it borders.

The *in vivo* pressure differential over the LTM is presumably smaller than the pressures used in the SAM. These high differences would imply considerable dangers of membrane rupture to the bird. However, syringeal closure caused by inward bulging of the LTM 's can be maintained with a reduced air sac pressure by two factors. First, the evolved complex control and morphology of the system can reduce the pressure difference. In some non-oscines, evidence has been found that in preparation for phonation the syrinx is reconfigured in a so-called 'phonatory position' (Goller & Larsen, 1997a). Activation of the *musculus sternotrachealis* in pigeons "draws the trachea caudaad and [...] causes folding of the LTM into the tracheal lumen." (Goller & Larsen, 1997a). In the presented physical model this mechanism to fold the membranes into the lumen is omitted and only the pressure in the pressure chamber is used to accomplish this 'phonatory positioning'. Second, the mechanical properties of the tympaniform membranes in birds are not known. If the LTM's are more compliant than the membranes used in SAM, the pressure needed for them to bulge into the lumen is smaller. The largely unknown intrinsic material properties of the syrinx, such as ultra-structure of the tissues of which it is constructed, may help to guide movements of the syrinx. So, the combination of muscle control and specific ultra-structure will tend to decrease the pressure difference. Hence, a relatively low ICAS overpressure is sufficient to close the syrinx. The membranes used in the model consist of isotropic latex and their structure is far less complex than the LTM's. Only a few studies on the ultra-structure of the LTM and MTM are performed in non-oscines. The LTM of the mallard (*Anas platyrhinchos*) is a regionally differentiated structure with different layers of epithelium and fibres (Scala et al., 1990). Furthermore, the mechanical behaviour of LTM and MTM is likely to be anisotropic, i.e. different in mechanical properties with orientation and dynamics of the applied load. To start off simple, we decided to use isotropic material such as latex.

If changes in tissue properties affect sound production, these changes may be biologically relevant on different time scales: within the life of an individual bird and on an evolutionary time scale. The complex vocalization system of birds is a result of a long evolutionary process. The differences in structural design of the syrinx can obviously not emerge in one generation. Thus changes in inheritable tissue properties are reasonable to expect. This could then lead to changes in the

generated sound if allowed for by the song control system.

In future work, mechanical modelling could be used to test the suggestions and insights from mathematical models of bird song. Since mechanical models are often more close to the physical situation described by mathematical models they are the ideal candidates for testing. Furthermore, these experiments provide strong evidence that it is important to include mechanical properties of the membranes and complex deformations of the syrinx in quantitative considerations on sound production in the syrinx.

Acknowledgements

The investigations were (in part) supported by the Research council for Earth and Life Sciences (ALW) with financial aid from the Netherlands Organisation for Scientific Research (NWO). The authors wish to thank Evert Jansen, Eric Karuppannan, Mees Schimmel and Jan Theunissen (Mechanical Workshop/Wageningen University) for constructing and contributing in the development of SAM, condomshop 'Het Gulden Vlies' (Amsterdam) for making SAM whistle and Dr. C.W.J. Oomens for advises on the tensile tests.

SECTION IV

muscular control of vocal production

chapter 5

Biology of the ring dove (*Streptopelia risoria*)

Introduction

In this chapter, we shortly describe the biology of the ring dove or Barbary dove (*Streptopelia roseogrisea* forma *risoria* or *S. 'risoria'*, see figure 5.1) that is used as a model species to study the mechanical properties of the syringeal muscles in this section of the thesis. Most of the text is based on Cramps (1994) unless noted otherwise. The Barbary dove is the domesticated variant of the African collared dove ring dove or Pink headed Turtle dove (*Streptopelia roseogrisea*). In this thesis, we will use the name ring dove (*S. risoria*) except for the species description later in this chapter. It belongs to the family of Pigeons and doves, the Columbidae, which is the single exant family within the Order of the Columbiformes, that also includes the extinct dodos (Raphidae) and solitaires (Pezophapidae).

The Columbidae

The Columbidae are a well-defined, natural assemblage with no close relatives. They exhibit a considerable ecological diversification, but are mainly arboreal and frugivorous and graniforous. Some strictly terrestrial forms occur in the humid tropics and Australia. There are about 300 species in ca. 42 genera. Goodwin (1970) recognized 295 species, of which 2-3 are recently extinct. Bock & Farrand (1980) recognized 303 species. In the Western Palearctic, the main genera include (1) *Columba*, typical pigeons, 51 species; (2) *Streptopelia*, turtle-doves, 15 (Cramps, 1994) to 17 species (Johnson et al., 2001); (3) *Geotrygon*, American quail-doves, 13 species; (4) *Gallicolumbi*, old world quail-doves, 18 species; (5) *Treron*, green pigeons, 23 species; (6) *Ptilinopus*, fruit-doves, 49 species and (7) *Ducula*, imperial pigeons, 36 species. The names pigeon and dove are synonymous, but pigeon is popularly used for larger species and dove for smaller ones.

The members of the Columbidae have rigid flight feathers that cause the loud and characteristic clapping sound when the bird flies away. Their plumage is dense, with the feathers loosely set in a thin skin. Their crop is large, with 2 lobes. During the relevant stages or the breeding cycle, the crop produces a nutritious secretion (crop milk) from lining for the feeding of small young.

Figure 5.1 The ring dove *Streptopelia risoria* during experiment of chapter 6. See also front cover folding.

The Barbary dove *Streptopelia roseogrisea* forma *risoria* (Linnaeus, 1758)

The barbary dove (*Streptopelia roseogrisea* forma *risoria* or *S. 'risoria*') is the domesticated form of *S. roseogrisea*, that is locally established in feral state. For instance, it breeds on Tenerife, Canary Islands (Svensson et al., 2003). The wild nominate form *S. roseogrisea roseogrisea* occurs in the dry zone south of the Sahara (figure 5.2) from central Mauritania and northern Mali east to central northern Sudan and western Ethiopia, north to Tibesti (Chad).The extralimital form *S. roseogrisea arabica* occurs on the coast of the Red sea in western Arabia and from northern Somalia to Gebel Elba (North-eastern Sudan).

Field characteristics

Length, 27-30 cm; (Svensson et al, 2003) wing-span, 45-50 cm. *S. risoria* resembles *S. decaocto*, but is slightly smaller and has a shorter tail. Usually less intensely coloured than wild races, distinctly buffier, fading when worn to pale cream. The grey and vinous tones as found in *S. roseogrisea* are suppressed or absent. The wing pattern lacks the rim found in wild birds and sometimes appears more uniform than *S. decaocto*. The black ring in the neck is slightly broader and more rounded instead of a small streak compared to *S. roseogrisea* (Svensson et al, 2003). Separation from *S. roseogrisea* or *S. decaocto* in the field is never easy, requiring close observation and is best based on voice and circumstances of use.

Habitat

The habitat is inadequately described for both wild and domesticated forms. The wild form can be found in sub-desert at tropical low latitudes. In Somalia, it is extraordinarily plentiful along the coast, where it is found in every garden and at every watering place, and crowding every Tamarisk tree (*Tamarix*) near overflow from wells. Often, they are too tame to be driven away. They are ca-

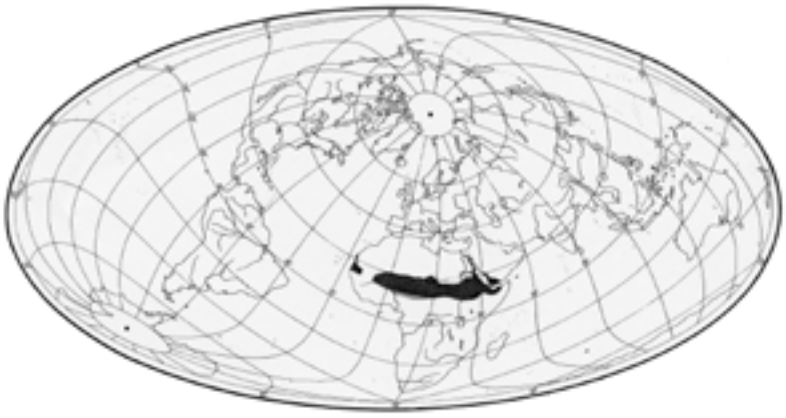

Figure 5.2 Geographical distribution of *S. roseogrisea*, the wild variant of the ring dove, in the Western palearctic.

pable of surviving for long periods in the interior of Somalia without access to water. They prefer open dry Acacia thorn-bush and avoid forest (Archer & Godman, 1937), but are found in desert mountain terrain at Tibesti, Chad (Moreau, 1966). They may nest ca. 20 km from nearest watering place (Morel, 1975).

Food

S. risoria feeds on seeds of grasses and other plants. Occasionally, they take spilled grain (Goodwin, 1970). In the southern Sahara, they eat mainly seeds of the euphorbia *Chrozophora* (Bates, 1943). They are suspected to go without water for considerable periods and found in arid areas away from water (Lynes, 1925). Berries can supplement their water requirements (Bates, 1927).

Voice

Streptopelia coos are divided into at least three context-dependent vocalisations based on accompanying vocalisations; the perch-coo, bow-coo and nest-coo (de Kort, 2001). The perch-coo is the most conspicuous and most frequently used of the three. Perch-coos are usually produced from high perches within the territory and function as territorial signal. They play an important role in male-male competition (ten Cate et al., 2002) and possibly in female attraction (Slabbekoorn, 1998).

The coo of *S. risoria* consists of two syllables separated by a pause (see chapter 6 and 7). The second syllable starts with a trill (Slabbekoorn & ten Cate, 1999). In phonatic terms: the voice is a soft 'ku-kruuu' or 'koo-krr-oo', with characteristically rolled 'r' in central syllable that is totally lacking in *S. decaocto*. During excitement they use a jeering 'hek-kek-kek' suggesting a trisyllablic laugh that is given just after landing on the ground or perch. Next to males, the females also vocalise, probably to stimulate follicular growth (Cheng, 1992).

The ring dove is an excellent model organisms to study vocal production and control: it has a relatively simple vocalizations and their syrinx has a relatively simple morphology (King, 1989; Warner, 1972). The vocalizations of the *Streptopelia* genus was studied in all fields relevant to sound production, such as neurobiology (Ling et al, 1997), immunology (Rodriguez & Lea,

1994), choreography (Fusani et al., 1997), reproductive biology (ten Cate & Taborsky, 1992; ten Cate et al., 1993; Lehrman, 1965), flight mechanics (Tobalske et al, 2003), development (Nottebohm & Nottebohm, 1971), genetics (Lade and Thorpe, 1964), neuro-endocrinology (Cheng, 1998), behavioral ecology (de Kort et al., 2001; ten Cate, 1992) and perception (Beckers et al., 2001, 2003b).

chapter **6**

Superfast muscles control sound in bird song

Published in revised form:
Elemans, C.P.H., Spierts, I.L.Y, Müller, U.K., van Leeuwen, J.L. and Goller, F. (2004) Superfast muscles control dove's trill. *Nature* **431**, 146.

Many birdsongs contain sound elements that require extremely fast control (Greenewalt, 1968; Goller & Suthers, 1996b; Podos, 1996). The trill of the ring dove (*Streptopelia risoria*) is a sequence of short sound elements that may be as short as 10 ms. If their generation is under active control, fast muscle contractions are required that approach the performance limits of vertebrate muscles (Fine et al., 2001; Rome et al., 1996; Rome et al., 1999; Young & Rome, 2001). Here we show that the vocal muscles of ring doves are superfast muscles. Simultaneous *in vivo* recordings of sound and muscle activity show that the syringeal muscles gate and frequency-modulate individual sound elements of the trill. *In vitro* force measurements confirm the superfast twitch characteristics of the syringeal muscles. Co-contraction of the antagonistic syringeal muscle pairs affords the bird rapid and accurate control (Harris & Wolpert, 1998). Superfast muscle can no longer be considered a rare adaptation of a few highly derived acoustic organs such as in the toadfish (Fine et al., 2001) and rattlesnake (Rome et al., 1996), but is probably the main muscle type controlling birdsong.

Doves generate a relatively simple, highly stereotyped song, the familiar coo. We recorded perch coos of six adult male ring doves. The coos contain two syllables (figure 6.1). The second syllable starts with a trill. The pitch during each trill element varies between 0.5 and 0.8 kHz, and the individual trill elements are generated at repetition rates of up to 40 Hz (figure 6.1b). To control these fast modulations, the sound-generating structures must be switched on and off rapidly, and their vibrations must change quickly to alter pitch. Typical vertebrate muscles are too slow for such vocal control (Young & Rome, 2001). We propose that doves control the pitch, i.e. frequency, and the gating, i.e. on- and offset, of the vibrations directly at the membranes, using highly specialised syringeal muscles.

When doves coo, flow excites membranes (Fletcher, 1988) deep in their trachea to vibrate (figure 6.1a) (Goller & Larsen, 1997; Larsen & Goller, 1999). Flow is driven by the pressure gradient along the trachea generated by respiratory muscles. Membrane vibrations also depend on the tension of the membranes (Fee et al., 1998; Fee, 2002), which can be modified by activating syringeal muscles (Gardner et al., 2001; Laje & Mindlin, 2002). The paired tracheolateralis muscles (TL) run along the trachea and insert directly on the membranes (figure 6.1a). The paired sternotrachealis muscles (ST) run through the interclavicular air sac and insert on the sternum (King, 1989; Warner, 1972). The two muscle pairs act as antagonists (Goller & Larsen, 1997a): the TL puts abductive force on the membranes, causing the membranes to move out of the tracheal lumen, whereas the ST indirectly pulls the tracheal rings T1 and T2 closer together, causing the membranes to slacken and to adduct. In doves, the pressure difference between air sac and bronchi might also affect membrane tension (Beckers et al., 2003a).

The acoustic output of birdsong corresponds to activity of syringeal muscles (Gaunt et al., 1982; Vicario, 1991; Goller & Suthers, 1996b), but it is not known how directly the muscles control phonation. If, for a given air pressure pattern, doves rely solely on the nonlinear mechanical behaviour (Fee et al., 1998; Fee, 2002) of their membranes to generate the varying pattern of pitch and gating, then muscle activity will not correlate with the sound pattern. Doves might also use their syringeal muscles (Beckers et al., 2003a; Gaunt et al., 1982) to control phonation. The muscles might generate different sound sequences by altering the initial position and tension of the membranes. In this case, muscle activity should correlate strongly with the on- and offset of phonation, but not with the gating and pitch of the sound elements. The syringeal muscles might also alter the tension of the membranes continually during the coo to control the gating and pitch of individual

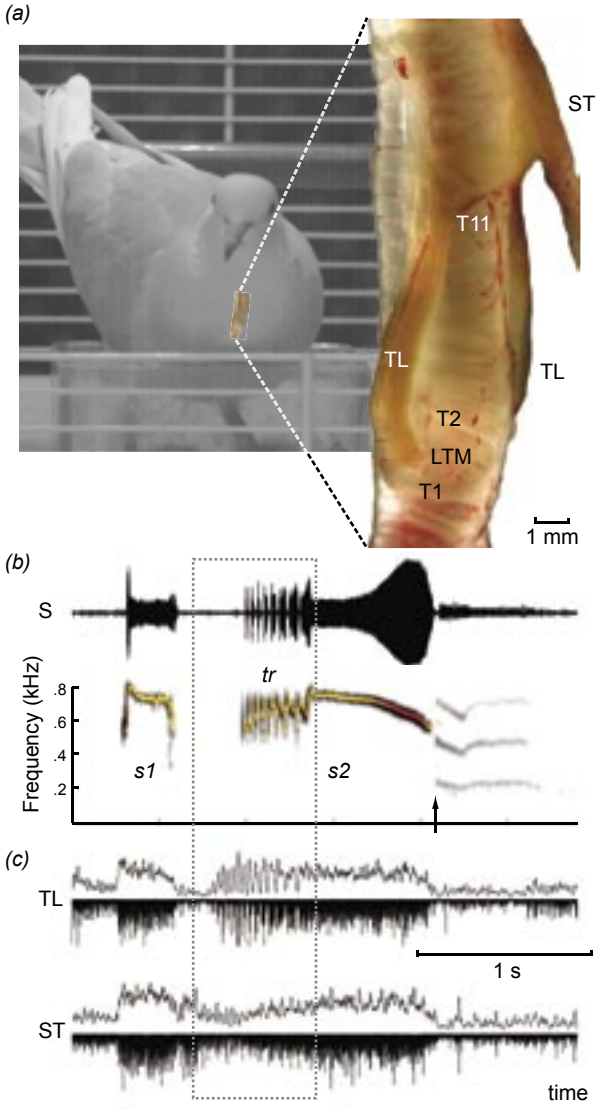

Figure 6.1 Muscle activation patterns during song in the ring dove (*Streptopelia risoria* L.). (a) Syrinx morphology with paired extrinsic syringeal muscles; *m. tracheolateralis* (TL) and *m. sternotrachealis* (ST). The lateral tympaniform membranes (LTM) are suspended between tracheal rings T1 and T2. T11 was used to define TL resting length. (b) Sound oscillogram (top) and spectrogram (bottom) of the stereotyped coo that consists of two syllables (*s1*, *s2*), followed by an inspiratory note (arrow). Syllable *s2* starts with a trill (*tr*). (c) Electromyographic recording of TL and ST. (EMG signal: upward, integrated; downward, rectified). Signals inside box are enlarged in figure 6.2.

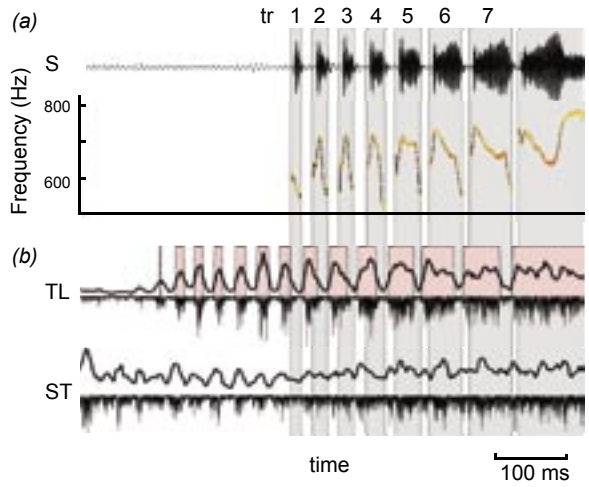

Figure 6.2 Sound modulation correlates with muscle activation patterns during the trill. (a) Sound oscillogram (top) and spectrogram (bottom). (b) TL and ST activity. TL activation (red boxes) precedes the corresponding trill elements (grey boxes). Asterisk indicates TL burst associated with the first trill pulse (tr 1). ST activity shows no obvious temporal pattern.

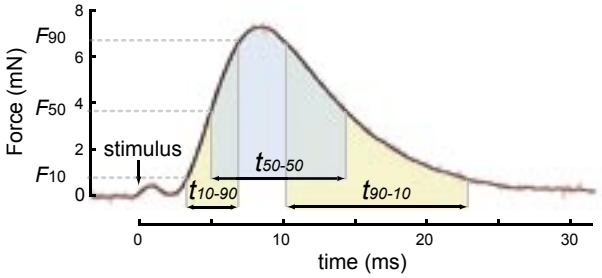

Figure 6.3 Single twitch contraction of TL preparation. F_{10}, F_{50} and F_{90} were defined as 10%, 50% and 90% of the maximum force F_{max}. $t_{10\text{-}90}$, time to ascend from F_{10} to F_{90}, $t_{90\text{-}10}$, time to descent from F_{90} to F_{10}. $t_{50\text{-}50}$, half-twitch time.

sound elements. In that case, muscle activity should correlate with individual sound elements.

We measured EMG activity of the TL and ST in spontaneously cooing doves. Doves use both muscles simultaneously to control their song (figure 6.1c). The ST is active during the entire coo. Its activity attenuates during the silent interval between syllables. However, ST activity does not modulate in correspondence with individual sound elements within the trill (figure 6.2). TL activity, on the other hand, correlates highly (r=0.87±0.08; n=5) with the voiced periods of the trill (figure 6.2b). Its correlation with the silent periods (binary signals: r=0.55±0.14; n=5) remains strong due to the periodic nature of the signal, but it is significantly weaker (p<0.05 Wilcoxon Signed Rank test; Zar,1998). Clearly, the TL muscles directly promote sound: they do not disable,

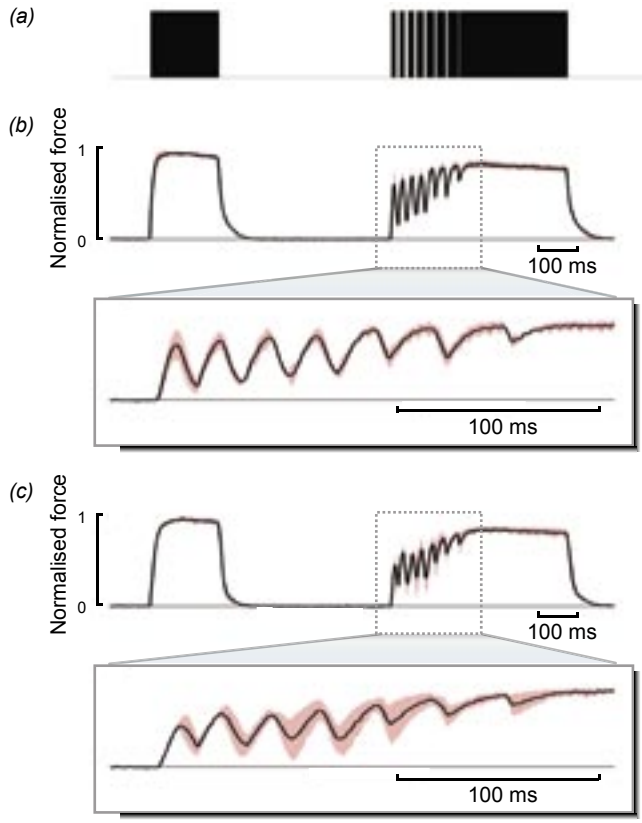

Figure 6.4 Force modulation in syringeal muscles. (a) Stimulation pattern based on averaged vocalization. (b) Normalised traces of force development during a whole coo and detail of the trill of *m. tracheolateralis* (TL) and (c) the antagonistic *m. sternotrachealis* (ST). [(mean(black trace)±SD(pink trace), *n*=4].

but facilitate the vibration of the membranes. These muscles not only gate the on-and offset of sound elements; the EMG amplitude pattern of the TL also correlates with pitch during the trill (r=0.88±0.07; n=5) and even the entire coo (r=0.82±0.08; n=5). Apparently, TL activity alters membrane tension to control both gating and pitch. Onset of TL activation precedes onset of sound generation during the trill by 14.8±1.1 ms (n=5). This delay between EMG and sound signal reflects the combined effect of (1) delay between muscle activation and force development and (2) delay between force development and mechanical effect on the membranes.

The TL muscles alter not only the initial condition of the membranes, but control membrane vibrations throughout the sound pulse. To modulate the brief sound elements of a trill (≥ 9 ms), the TL is required to modulate its force rapidly. The TL must also contract aerobically to power cooing sessions that can last for many minutes. Such extreme demands on performance are within the realm of superfast muscles, the fastest muscles known in vertebrates (Fine et al., 2001; Rome et al., 1996; Rome et al., 1999; Young & Rome, 2001).

To demonstrate that the syringeal muscles are synchronous and capable of rapid cyclic force modulation, we measured isometric force generation of excised muscles (n=7). Single-pulse stimulation of the left TL (5.4±0.8 mg) and left ST (5.7±1.4 mg) resulted in single twitches with twitch halftimes ($t_{50\text{-}50}$; figure 3) of 9.2±0.8 ms and 10.3±1.7 ms for TL and ST, respectively, at 39°C. Within each twitch, force rapidly developed ($t_{10\text{-}90}$; TL, 3.5±0.4 ms and ST, 4.7±1.2 ms) and decreased ($t_{90\text{-}10}$; TL, 10.6±1.7 ms and ST, 10.4±2.2 ms). These benchmark values reveal that the TL is indeed a superfast muscle that can deliver the very fast force modulation required to directly control individual sound elements. Surprisingly, the ST also has superfast-muscle properties, which was not evident from the EMG recordings. Stimulus frequencies to obtain tetanic contraction were 200-275 Hz for TL, and 200-400 Hz for ST. Occasionally, stimulation at 275 Hz still resulted in a serrated tetanic response. The maximal twitch force (F_{max}) and the maximal isometric stress (MIS= F_{max} /A) of both muscles were low (TL: F_{max} = 5.4±2.9 mN, MIS= 8.0±4.8 kN/m^2; ST: F_{max} = 7.3±5.4 mN, MIS=20.6±15.7 kN/m^2), but typical for superfast muscles, which trade force for speed (Rome et al., 1999).

We also subjected both syringeal muscles to a playback of the *in vivo* TL activation pattern (figure 6.4a) to test their modulation capacities. During the simulated trill, both TL (figure 6.4b) and ST (figure 6.4c) are clearly capable of modulating force. As the silent intervals in the playback signal shorten from 12 to 3.5 ms, the latter no longer provides enough time for complete relaxation, causing the depth of this modulation to decrease. Since the precise role of the ST in sound production is unclear (Goller & Larsen, 1997), its fast contraction characteristics suggest that the ST is also involved in fine-tuning membrane position.

We have demonstrated that the syringeal muscles control gating and pitch of phonation in ring doves. Our *in vivo* measurements show that contracting the TL accompanies voiced rather than silent periods. Our results suggest that the muscles exert control directly at the syringeal membranes by altering membrane position, which in turn alters membrane tension. The TL pulls the syringeal membranes apart allowing them to vibrate in the flow, which supports indirect observations that the syrinx is closed (partially) in between the trills (Beckers et al., 2003a). The proposed control mode implies that membrane position determines gating, and membrane tension determines pitch. It also implies that the syringeal muscles of ring doves cannot control gating and pitch independently. Our *in vitro* experiments demonstrate that both syringeal muscles possess the superfast properties that are necessary to control individual sound elements during the trill. The co-activation of both the TL and the ST affords the bird very fast and accurate position control of the syringeal membranes, akin to saccadic eye and rapid arm movements (Harris & Wolpert, 1998).

Birds modulate their song extremely rapidly (Suthers & Hector, 1982, 1985) at frequencies greater than 100 Hz (Goller & Suthers, 1996b). While intrinsic nonlinear properties of the syrinx (Fee et al., 1998; Fee, 2002) add complexity to the level of motor control, only muscle control can explain fast but gradual modulations that underlie the amazing intra-specific variability and flexibility of phonation (Greenewalt, 1968). The stereotyped coos of doves are considered simple vocalisations among birds. Nevertheless, our measurements show that even doves control their song with superfast muscles that perform in the same league with the fastest currently known vertebrate muscles (Fine et al., 2001; Rome et al., 1996; Rome et al., 1999; Young & Rome, 2001). Considering their "vocal gymnastics" (Goller, 1998) songbirds have probably evolved muscles that out-perform the syringeal muscles of doves. We expect that superfast muscles are widespread in avian vocal control.

Methods

In vivo recordings

Sound and electromyographic (EMG) activity of TL and ST were recorded of six spontaneously vocalizing male ring doves (Salt Lake City, Utah, USA). Teflon-coated copper wire electrodes (65 (m diameter) with 1 mm tips of Nickel wire (25 µm diameter) were inserted about 2 mm apart in the muscle body to avoid the movement artefacts that we encountered in our initial measurements with the electrodes placed closely together (Gaunt et al., 1982). Separated electrodes provided signals from several motor-units at low impedance. The electrodes were glued to the fascia with cyanoacrylate tissue adhesive, routed out of the interclavicular airsac and led subcutaneously to a backpack (Goller & Suthers, 1996a). Spontaneous vocalizations started 1-2 days after surgery. The caged bird was placed in the centre of a cubic-meter box, open at the front, with sound-insulating foam to suppress reflections. Sound was recorded at 20-30 cm from the cage using two microphones (Audiotechnica AT835b and a 1/4" Brüel & Kjær omni-directional condenser microphone model 4939 for calibrations). We obtained signals from two healthy, spontaneously vocalising males. We analysed five coos of one dove, in which both EMG and sound recordings showed distinct pulses in the trill of syllable *s2*. The other dove showed similar EMG patterns, but the sound amplitude of the *s2* syllable was too weak to analyse individual pulses in the trill. Experiments followed federal regulations and approval for animal experimentation.

In vitro muscle performance

Seven ring doves (Rotterdam, The Netherlands) were anaesthetised and euthanised using CO_2/O_2. Whole-muscle preparations of the left TL (n=7) and ST (n=7) were dissected within 1 hour, whilst continuously flushing the muscles with oxygenated Ringers solution (Askew & Marsh, 2001). Finished preparations were stored up to five hours at room temperature on Sylgard-covered Petri dishes in oxygenated Ringers solutions. Muscle preparations were mounted on both ends in a test chamber filled with oxygenated Ringers' solution at 39±0.2°C. One end of the muscle was mounted to the arm of a dual-mode servo system (Aurora Scientific model 300b). After a rest period of 60 minutes, several tests were conducted at 2-minute intervals to optimise length and twitch parameters to achieve maximal isometric force (Askew & Marsh, 2001). Optimal TL length was 7.29±0.76 mm, measured from insertion on LTM to tracheal ring T11 (figure 6.1a), optimal ST length was 14.60±0.73 mm. Optimal tetanic stimulation was defined as the stimulus frequency at which the highest isometric stress was measured that did not decline during 100 ms of stimulation. Maximal isometric stress (MIS) was calculated as F_{max}/A_{cr} of the muscle, where the cross-sectional area A_{cr} was estimated from the resting length and weight of the muscle fibres (assuming a density of 1060 kg/m^3; Méndez & Keys, 1960). After testing, non-contractile and dead material was removed before weighing the preparations (Mettler Toledo type AG204; ±0.1mg). Muscle fibres were stimulated with external-field platinum wire electrodes. Twitch stimulations were applied using MuscleWork Software developed for Labview 6.0 (National Instruments), kindly provided by R.J. Josephson and J. Malamud. We used Matlab 6.5 (The Mathworks) to analyse our data and to construct the playback signal in figure 6.4a by averaging the time signature of ten coos recorded (Brüel & Kjær condenser microphone, model 4939) from one animal in a semi-anechoic room at Wageningen University, The Netherlands. The animal testing committee of Wageningen University approved all experiments.

Acknowlegdements

The investigations were (in part) supported by the Research council for Earth and Life Sciences (ALW) with financial aid from the Netherlands Organisation for Scientific Research (NWO) and a NIH grant to FG. The authors thank R.K. Josephson & J. Malamud for the use of their MuscleWork software, A. Janssen & M. Hendriks for technical assistance and O. Berg, O.N. Larsen & M. Muller for critical comments on the manuscript.

chapter **7**

Mechanical poperties of the syringeal muscles in ring doves

Submitted in revised form:
Elemans, C.P.H., Spierts, I.L.Y, Hendriks, M., Schipper, H., Taverne-Thiele, A. & van Leeuwen, J.L.
Mechanical properties of syringeal muscles in Ring doves (*Streptopelia risoria*).

Abstract

The dynamic vocalizations of most birds are controlled by muscle activity at the level of the sound generators in the syrinx. However, the force exerted by muscles can differ significantly from its electrical activation as measured with EMG. Here, we present the first data on the *in vitro* mechanical properties of the syringeal muscles of the ring dove (*Streptopelia risoria*) and the implications for the *in vivo* performance. Both the tracheolateralis and sternotrachealis muscle exhibit superfast muscle properties and the overall relationships between net work and power output versus cycle frequency resembles that of the fastest known vertebrate muscle, the toadfish swimbladder muscle. We observed large quantities of mitochondria, sarcoplasmatic reticulum and two T-tubuli per sarcomere in both muscles, typical for muscle fibres that are superfast and need a long endurance. The capabilities of the syringeal muscles strongly support the notion that they act as antagonists for the positioning of the sound producing structures, the lateral tympaniform membranes. The highest power output is generated at 20 Hz cycle frequency for both muscles, close to the trill rate of 25 Hz in the main vocalisation of doves, the coo. Furthermore, the contraction amplitude where the power output is highest is the same (0.75 mm) for both muscles. We suggest that the syringeal muscles are the main frequency modulating mechanisms in ring doves, since we were able to estimate that the stress on the LTM exerted by the muscles is at least ten times higher than the stress caused by pressure differences in the respiratory system during 76% of the coo. Since muscles are adapted to the function they perform, the *in vitro* performance of muscles provides strong evidence for *in vivo* functioning and can be used to calibrate force modulation in state-of-the-art physical models of sound production in birds. At present, besides electrical activation, the behaviour of syringeal muscles during spontaneous song is unknown and poses the next challenge for the quantitative understanding of vocal control.

Introduction

The dynamic vocalizations of most birds are controlled by muscle activity at the level of the sound generators in the syrinx (Vicario, 1991; Goller & Suthers, 1996a, 1996b; Suthers, 1998; Suthers et al., 1999; Elemans et al., 2004). The sound sources are labia (song birds) or membranes (non-songbirds) that exhibit flow-induced vibrations (Fletcher, 1989; Fee et al., 1998; Fee, 2002; Larsen & Goller, 1999). Respiratory muscles power the flow needed for vocal production and gas exchange (Fedde, 1987). By altering position and tension of the labia, the syringeal muscles control pitch and gating of the sound elements (Gardner et al., 2001; Goller & Larsen, 1997, 2002; Laje et al., 2002; Mindlin et al., 2003).

Direct observations of the mechanical action by syringeal muscles have fed hypotheses on their function (Goller & Larsen, 1997a, 1997b, 2002; Larsen & Goller, 1999, 2002). In the Passerines, i.e. songbirds, six or more pairs of intrinsic syringeal muscles have lateralised control over the position and tension of an external or internal labium. The principal muscles that control gating and modulate pitch are identified in the brown thrasher (*Toxostoma rufum*), but the mechanisms causing the labia to move in and out of the bronchial lumen are poorly understood (Chamberlain, 1968; Goller & Larsen, 1997b; Suthers et al., 1999). In the non-Passerines, i.e. non-songbirds, control over position of the syrinx and associated syringeal membranes seems less complicated. Most non-Passerines possess only two pairs of extrinsic muscles that control shape and position of the syrinx and occasionally interact with syringeal membranes (Elemans et al., 2004; Goller & Larsen, 1997a; King, 1968; Warner, 1972; Suthers & Hector, 1982, 1985).

However, at present, the imputed roles of most syringeal muscles rely on EMG measurements (e.g. Goller & Suthers, 1995, 1996a, 1996b; Vicario, 1991). EMG reflects the electrical activity of a muscle and has the advantage that it can be used in freely singing birds, whereas endoscopes can be used only in anaesthetised birds. However, EMG activity is related to the exerted force in a complex manner: force and power output of muscles can differ significantly for different stimulation and contraction regimes. This is well-documented in locomotory muscles, whose performance strongly depends on strain regime, repetition of movement and phase of stimulation (e.g. Askew & Marsh, 2001; Josephson, 1985). Force development of a muscle during repetitive movements, as can be expected to occur in modulated vocalizations such as trills, cannot be simply derived from its electrical activity. Beside EMG, there is no information of muscle behaviour during singing in birds. The mechanical output strongly depends on muscle design. Muscles are adapted to the functions that they must perform and therefore much can be learned about the function of a muscle by looking at its contractile performance (Rome et al., 1988). To understand the function of syringeal muscles during vocalisation, we need to know their mechanical properties next to their electrical activity.

Here, we study the mechanical properties of the syringeal muscles of the ring dove (*Streptopelia risoria*). Ring doves have relatively simple vocalizations, and their syrinx has a relatively simple morphology (King, 1989; Warner, 1972). Next to males, the females also vocalise, probably to stimulate follicular growth (Cheng, 1992, 2003). The coo of *Streptopelia risoria* consists of two syllables separated by a pause. The second syllable starts with a trill (Slabbekoorn et al, 1999).

The mechanisms underlying sound production and modulation in pigeons and doves are still being debated (Abs, 1980; Baptista & Abs, 1983; Ballintijn & ten Cate, 1998; Beckers et al., 2003a; Elemans et al., 2004; Gaunt et al., 1982; Goller & Larsen, 1997a; Wundelrich, 1884; Warner,

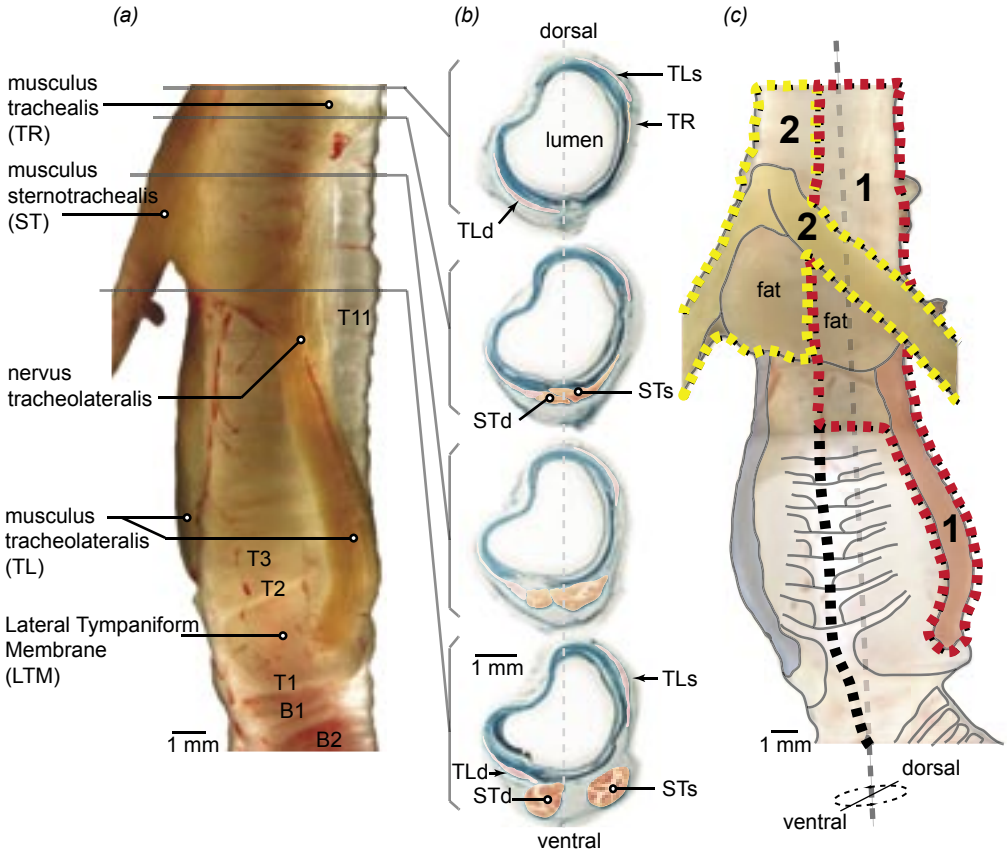

Figure 7.1 (a) Morphology of the fresh syrinx of a male ring dove (*Streptopelia risoria*). The TL clearly inserts on the LTM, but since the muscle fibres blend in with fibres of the *m. trachealis* (TR) more rostral around T18, the origo of the TL cannot be determined exactly *in vivo*. Both ST's run parallel and together in several layers of fascia from their origo around T17-T19. The muscle fibres of the left ST overlap the fibres of the right ST. Around T12, the two muscles split, run through the ICAS separately and insert bilaterally on two protuberances of the sternum. The ST's run symmetrically around the midline of the body. The syrinx is tilted considerably with respect to the body. (b) Sections through the trachea and upper-syrinx using Masson's trichrome staining. Muscle fibres of the TL and TR can only be distinguished by following the sarcolemma in subsequent sections. (c) Dotted lines are dissection lines for whole muscle preparations; 1, left TL; 2, both ST's. B1-2; Bronchial rings, LTM; Lateral tympaniform membrane, T1^{-1}1; tracheal rings, TLd; right and, TLs; left TL, TR; musculus trachealis, STd; right and, STs; left ST.

1972). Larsen & Goller (1999) showed that in the pigeon (*Columba livia*) vibrations of the paired lateral tympaniform membranes (LTMs) produce sound. This mechanism is also likely to hold for ring doves which have a very similar syringeal morphology (figure 7.1a). The two paired extrinsic muscles, the *m. tracheolateralis* (TL) and *m. sternotrachealis* (ST) affect the position of the LTM (Gaunt et al., 1982; Warner, 1972; Goller & Larsen, 1997a). The TL applies abductive force directly on the LTM, and the ST adducts the LTM indirectly by pulling the syrinx caudad (Goller & Larsen, 1997a). As such, they seem to function as antagonists, but ST activity was not essential for

sound production (Smith, 1977; Goller & Larsen, 1997a). Elemans et al. (2004), however, showed that both the TL and the ST have superfast properties that were found only in highly derived acoustic organs (Fine et al., 2001; Rome et al., 1996, 1999; Tavolga, 1964). This implies that not only the TL, but also the ST serves a crucial function in fine-tuning the vocalisation.

Here, we investigate whether the two syringeal muscles in ring doves are capable of being antagonists. We provide the first measurements on work and power output of syringeal muscles and examine the strain and shortening regimes in which the muscles perform best.

Muscles that contract at high speeds, as found in ring doves by Elemans et al. (2004), face a trade-off between force and speed (Young & Rome, 2001). The contractile elements, the sarcoplasmatic reticulum (SR) that regulates myofibrillar calcium concentration, and the mitochondria that supply ATP, compete for space at the ultra-structural level. Fast muscles that are active continuously for long periods need many mitochondria and SR to fuel and regulate contraction. This leaves less space for contractile elements, which results in a lower force and power output of the muscle fibres. This trade-off was found in the rattlesnake tail shaker muscle and in the swimbladder muscles in various fish families (Fine et al., 2001; Parmentier et al., 2003; Rome et al., 1999). The syringeal muscles, however, are not active continuously during a coo (Elemans et al, 2004; Gaunt et al, 1982; Slabbekoorn et al, 1999): there are pauses in between coos that might be essential to drain metabolites. Nevertheless, cooing sessions can last for 10 minutes or longer (CPHE pers. obs.), so large quantities of mitochondria can be expected. We also studied whether the ultra-structure of the syringeal muscles is in accordance with the requirements for superfast aerobic muscles.

Material and Methods

Animals

Nine adult ring doves (*Streptopelia risoria*, m=156±8.7 g, n=9) were obtained from a local vendor (Rotterdam, The Netherlands), maintained at a 12:12h light-dark period at 'de Haar' animal facilities (Wageningen University) and provided with food and water ad lib. Doves were anaesthetised with CO_2/O_2 and decapitated. We avoided the use of barbiturates since the effects on muscle performance are unknown. Rectal temperature was recorded (Lutron TM-906A thermometer, ZETA engineering ±0.1°C) when the animals were anaesthetised.

Sound recordings

Individual coos of all animals were recorded (Brüel & Kjær; condenser microphone 4939; preamplifier 2670; amplifier Nexus dual channel) in a semi-anechoic room. Trill repetition rate was measured as the reciprocal of the time between the middle of successive trill elements.

Histological preparations

To assess the exact origo and insertion sites of the TL and ST, the syrinxes of two male adult ringdoves were sectioned and stained with Masson's trichrome staining (Kiernan, 1990). The muscle fascia were identified in consecutive sections (Nikon Microphot-FXA) and photographed (Olympus DP50). Toto images of the syrinx were made with a stereomicroscope (Zeiss SV11). High magnification images of muscle fibres and sarcomeres were obtained with a Transmission Electron Microscope (Philips EM208S, The Netherlands). Multiple images were combined to generate a high-resolution overview using 2D cross-correlation algorithms (AnalySIS pro).

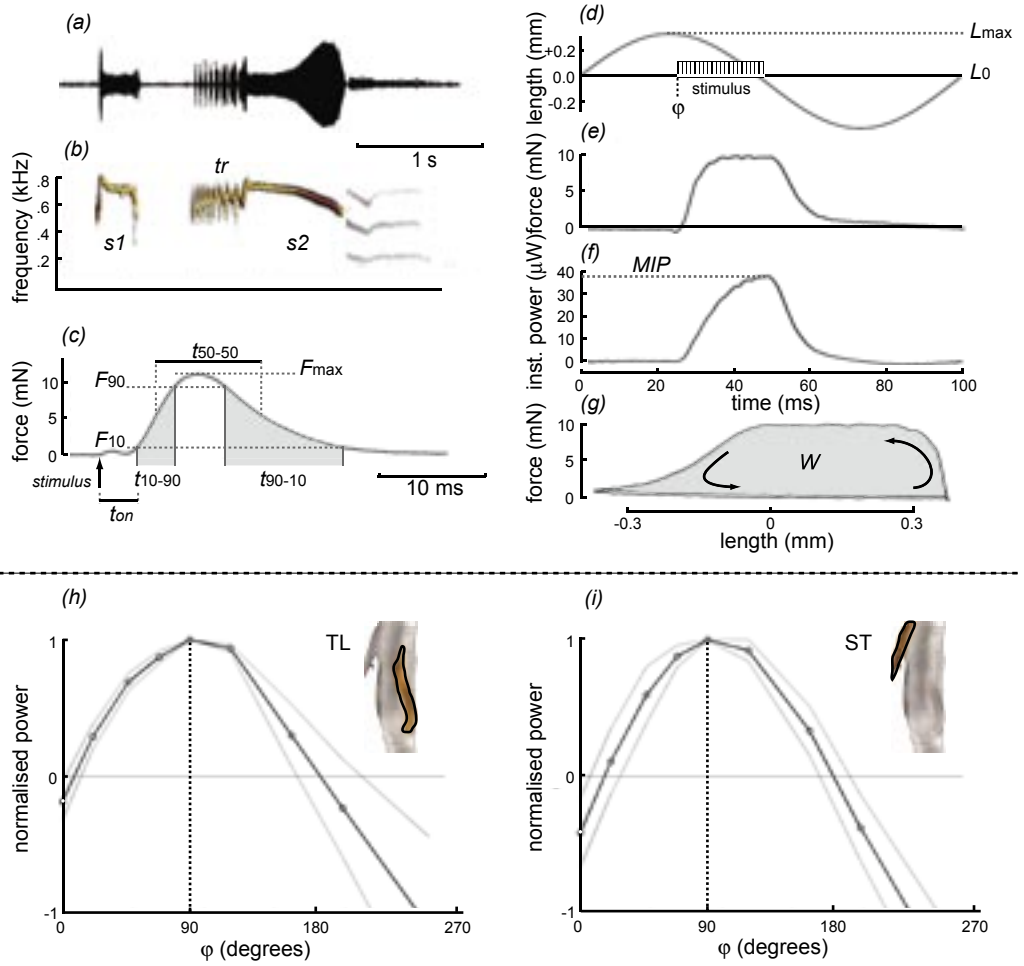

Figure 7.2 Measurements on muscle performance. (a) Oscillogram and (b) spectrogram of the perch coo of the ring dove. The song contains two syllables (*s1*, *s2*) of which the latter starts with a trill (tr). (c) Twitch characteristics of a single pulse muscle stimulation. (d) Muscle preparations were subjected to a sinusoidal length change with cycle frequency f and strain amplitude Lmax. The stimulus pulse train started at phase ((degrees) in the cycle and lasted for 25% of the cycle. (e) Force development during cycle. (f) Instantaneous power during cycle. (g) Workloop with shaded area W represents work. Graphs (d)-(g) are presented as mean (solid lines)±S.D. (dotted lines). Since the SD are low, the lines are difficult to discern. (h) Normalised power as a result of stimulation at different phases in the shortening-lengthening cycle for TL and (i) for ST, at cycle frequency 10 Hz and strain 5%.

In vitro power output

The work loop technique was used to determine the mechanical power output of both syringeal muscles *in vitro*. The TL and ST were isolated from the syrinx and subjected to an array of length changes, cycle frequencies and activity patterns.

The syringeal muscles were dissected as whole muscle preparations. We dissected the syrinx including TL and ST and part of the trachea and fixed this on Sylgard (silicone elastomere, Dow Corning Corp. Midlands, USA) covered Petri dishes with oxygenated Ringer's solution for birds (recipe cf. Askew & Marsh, 2001). At all times during dissection, we continuously irrigated the muscles with oxygenated Ringer's solution at room temperature. To isolate the left TL, the syrinx was cut medially from the fusion point of the bronchi along the trachea (black dotted line in figure 7.1c). The exact origo of the TL muscle fibers could not be determined *in vivo*, because the fibers seemingly merged with fibers of the m. trachealis that runs along the trachea rostrad to the larynx. Based on observations on histological sections, the trachea was cut at the 20th tracheal ring (T20) to avoid damage to TL fibers (prep 1 in figure 7.1c). The TL was fixed in a Sylgard covered Petri dish and carefully pared down from the insertion on the membrane to about T9. Some collagenous tissue from the LTM was left to mount the preparation in the test set-up. TL length was measured from the insertion in the LTM to T11. The paired ST's could not be separated at their insertion site around T17-T19 without the risk of severe damage. Therefore, the ST's were left unseparated at their insertion with a part of the trachea attached (prep 2 in figure 7.1c). At the origo sides, small bony protuberances of the sternum were left (typically under 1 mm).

The preparations were transferred to a small chamber with circulating oxygenated Ringers' solution. The Ringers temperature was maintained at 39±0.1°C, which was slightly lower than the average body temperature (41.3±0.5°C [n=9]) by heating a reservoir of Ringers' solution au bain Marie (water bath: LKB Bromma 2219, Lehman Scientific, USA). Both muscles measured about 1 mm in diameter. The tracheal rings of the preparations were secured to the base of the experimental chamber using insect pins. At the free end, the preparations were attached to a needle glued to the arm of an ergometer transducer (Dual-mode Servo series 300b, Aurora Scientific Inc., Canada). The TL was attached to the arm by pinning the collagenous LTM on a hook. To connect the left ST, the small piece of sternum was mounted on the needle of the transducer. The right ST was mounted away from the transducer arm and could not affect the measured force during contraction. The position and length of the muscle was varied using three micro-manipulators. Muscle length was initially set to about 0.95% of the measured *in vivo* length. Flexible platinum wire electrodes ran parallel along the full length on opposite sides of the muscle. Stimuli were applied with a pulse generator (TGP110, Thurlby-Thandar Instruments LTD., UK). After mounting, the preparations were left to recover for about 60 minutes. After experiments, all non-contractile and dead tissue was removed from the preparation and the mass (m) of the fibers was measured (Mettler Toledo ±0.1 mg).

The ergometer measured force and length and was controlled using the application Muscle Work (kindly provided by Dr. R.K. Josephson and Dr. J.J. Malamud) developed in Labview 6.0 (National Instruments). Signals were digitized at a sample frequency of 7.5 kHz using a 12 bits A/D converter (National Instruments PCI-MIO^{-1}6E4) with a built-in amplifier. Analysis software was written in-house in Matlab 6.0 (The Mathworks Inc.).

First, series of isometric twitches and 100 ms tetanic contractions were performed to measure the twitch dynamics and isometric stress of the preparations. We used similar time parameters as

previous authors (e.g. Askew and Marsh, 2001; Rome et al., 1996; Young & Rome, 2001) to characterize the twitch (figure 7.2c). Maximum isometric stress (MIS) was:

$$\text{MIS} = \sigma_{max} = F_{max} / A_0 \quad [\text{N/m}^2] \qquad (1)$$

where F_{max} is the maximal force output and A_0 is the cross-sectional area. The area was assumed constant and defined as: $A_0 = m / (\rho \cdot L_0)$, where m is the mass of the preparation and ρ is the muscle density of 1060 kg/m^3 (Méndez and Keys, 1960).

Muscles were subjected to a series of five sinusoidal strain cycles with frequency f and amplitude L_{max} about L_0 (figure 7.2d). The 2nd to 4th cycle were analysed to avoid on- and offset transients. Lagrangian strain amplitude was expressed as $\varepsilon = \Delta L / L_0$, with maximal amplitude ε_m. A run consisted of a series with stimulation (i.e. active series), followed by a series without stimulation (i.e. passive series). The measured force, length and stimulus signals of a run were aligned in time by cross-correlation of the strain signals of the two series. To estimate the force pattern solely caused by the contractile elements in the muscles, we subtracted the aligned force signals of the passive set from those of the active set (figure 7.2e). This procedure also reduced deviation in force measurements due to inertial forces at high cycle frequencies. The instantaneous power was $P_{inst} = F \cdot \frac{dL}{dt}$ [W]. The maximal instantaneous power (MIP) was measured for all runs (figure 7.2f). Mean power per cycle was defined as the area of the work loop (figure 7.2g): $W = \oint F \cdot dL$ [J]. Mean power was calculated as the product of mean net work over three cycles and cycle frequency: $\overline{P} = \overline{W} \cdot f$ [W]. To find optimal power, first the stimulation was started at various phases (φ = 0, 22.5, 45, 67.5, 90, 120, 162, 198 and 260°) that lasted 25% (equals 90°) of the cycle (figure 7.2d). Further experiments were carried out over a range of cycle frequencies (TL: 5, 10, 15, 20, 25, 30, 40 and 50 Hz; ST: 1, 2, 5, 10, 20, 30, 40 and 50 Hz) and strain amplitudes (TL:1, 2, 5, 10 and 15% [and 20% for two preparations]; ST:1, 2, 5, 10, 15, 20 and 25%) with a stimulus onset at 90° during 25% of the cycle (figure 7.2d). Preparations were allowed to rest for two minutes between isometric contractions and three minutes between series of workloops. Every 30 minutes, a twitch contraction and a run of work loops (f = 10 Hz and (ε_m = 5%) was performed to monitor changes in performance. All experiments were approved by the Committee of Experimental Animal Use of Wageningen University.

Statistics

All values presented are means ± s.d. Comparisons between two groups were made with Students *t*-test. A value of $p < 0.05$ (two-tailed) was considered significant.

Results

Trill rates and morphology

The coo of *Streptopelia risoria* consists of two syllables separated by a pause (figure 7.2a,b). Fundamental frequency of the coo ranged between 400-800 Hz. Syllable *s1* was 188±43 ms long, *s2* 1,117±249 ms separated by pause p of 296±79 ms (*n*=9). A coo lasted for 1,601±257 ms and was followed by a respiratory note. These measurements correspond well with Slabbekoorn et al. (1999). *S2* started with a trill that consisted of short sound elements. The repetition rate typically decreased over the trill since the elements increased in length. The mean trill repetition rate was 24.2±3.0 Hz (*n*=9).

The syrinx was rotated to the left with respect to the medial body axis. The TL muscle fibres insert in the collagenous Lateral Tympaniform Membranes (LTM) and the muscle is slightly flattened (figure 7.1a,b). More rostrad, the TL muscle flattens into a sickle shape on sagital cross-section. The TL attached around tracheal ring T19-20 and was distinct from the musculus trachealis (TR). In one specimen, we found several fibres inserting at T2-4, however the vast majority inserts in the LTM. We suggest that the TL can move freely in collagenous fascia during shortening. The ST's have a very peculiar position for a vertebrate muscle: from the insertion on the trachea around T17-19, both ST's run parallel and are partially (3-4 mm out of 14-16 mm) suspended in the air-filled cavity of the interclavicular air sac. They originate on small protuberances on the ipsilateral side of the sternum close to the attachment of the pectoralis muscles. The insertion of the ST's is about 1 mm to the right of the midline of the syrinx. However, due to the axial rotation of the syrinx, the ST's run in the midline of the body and parallel to the syrinx.

Mechanical output; isometric properties

The TL (*n*=7) and ST (*n*=7) measured 7.56±0.38 mm and 14.60±0.73 mm, and weighted 5.4±0.8 mg and 5.7±1.4 mg, respectively. One of the ST preparations showed 50% decline in reference experiments; it was only used for isometric results. Single-pulse stimulation resulted in single twitches. For twitch characteristics see figure 7.1c. Muscles reacted (t_{on}) in 3.21±0.41 ms and 3.22±1.44 ms after stimulation for TL and ST, respectively. Within each twitch, force rapidly developed ($t_{10\text{-}90}$; TL, 3.5±0.4 ms and ST, 4.7±1.2 ms) and decreased more slowly ($t_{90\text{-}10}$; TL, 10.6±1.7 ms and ST, 10.4±2.2 ms). Twitch halftime ($t_{50\text{-}50}$) was 9.2±0.8 ms and 10.3±1.7 ms for TL and ST, respectively. MIS for twitch contractions was 8.0±4.8 kPa and 20.6±15.7 kPa for TL and ST, respectively. Smooth tetanic contractions were achieved at pulse train frequencies of 250±29 Hz and 250±72 Hz for TL and ST, respectively. MIS during tetanic stimulation was about twice the MIS for a twitch: 18.1±7.2 kPa and 48.5±34.7 kPa.

Mechanical output; non-isometric properties

The preparations showed the highest power output when stimulated at 90° of the cycle (figure 7.2h,i). Net work and power output varied with cycle frequency and strain (figure 7.3). Work per cycle was highest at low cycle frequencies and high strain rates. Mean work per cycle for TL (figure 7.3a) was highest on the edge of the investigated parameter space at 5 Hz and 20% strain (1.18±0.34 Jkg^{-1} [*n*=2]) and for ST (figure 7.3d) at 2 Hz and 20% strain (1.63±2.04 Jkg^{-1} [*n*=7]). Work per cycle decreased considerably with increasing frequency. However, the TL was still capable of generating positive work at 40 Hz and 5% strain and at 50 Hz and 2% strain (figure 7.3a).

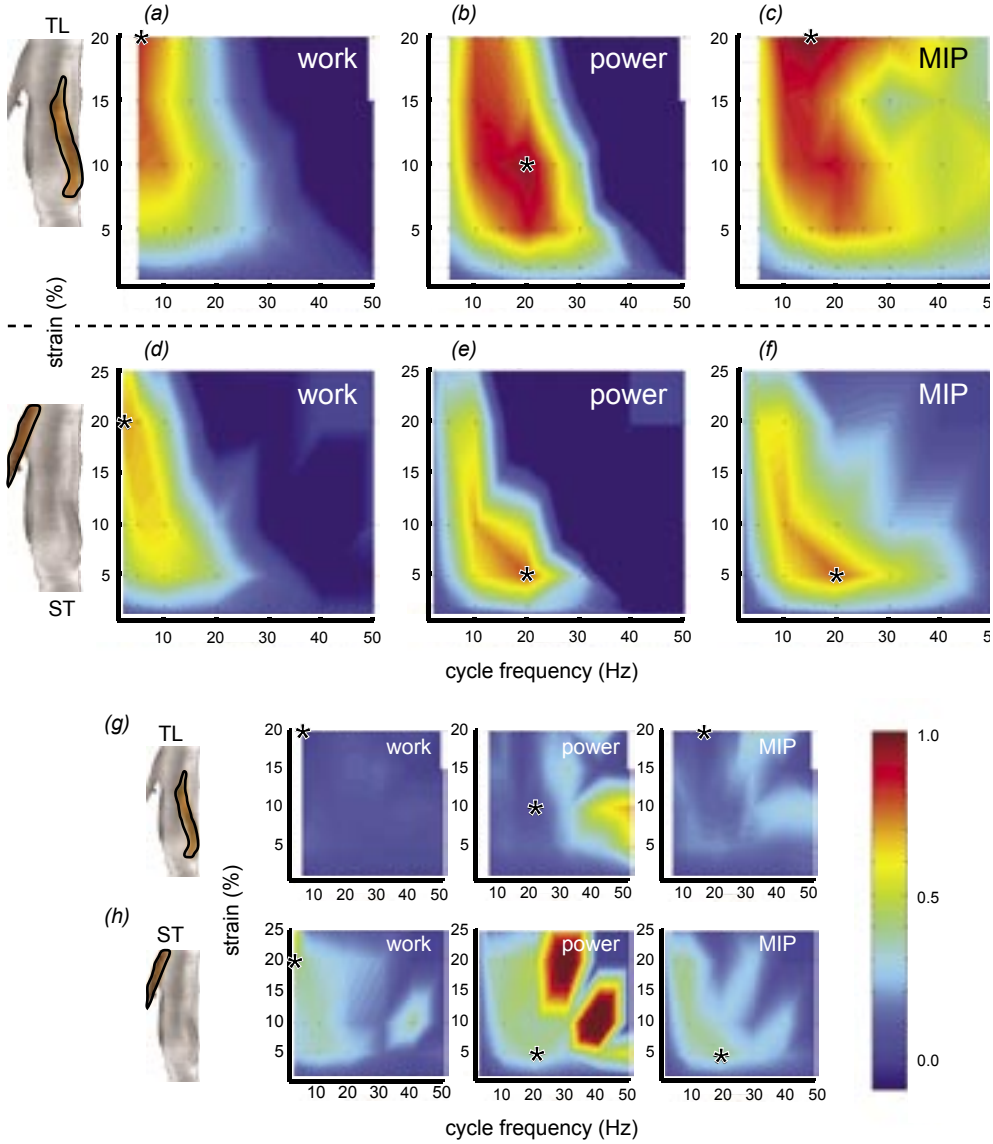

Figure 7.3 Work loop results. Normalised contour plots of (a) mean work, (b) mean power and (c) mean maximal instantaneous power (MIP) for TL of all preparations. (d)-(f) Mean values for ST preparations. (g) Plots of corresponding standard deviation for TL and (h) ST preparations. All values are normalised per preparation. The asterisks show maxima. See back cover folding for colour image.

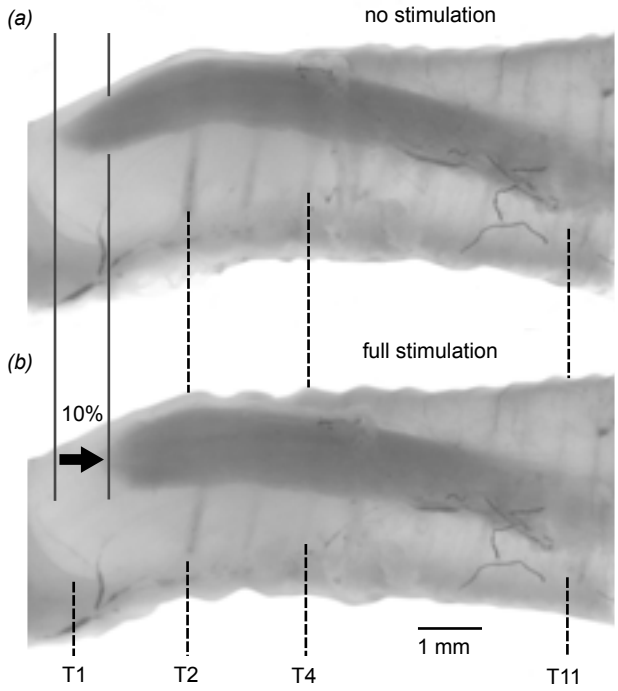

Figure 7.4 Shortening of intact TL on fresh syrinx. *In situ* length of TL when either (a) not stimulated and (b) under full stimulation. The length change is about 10%.

Work output of the TL was more sensitive to cycle frequency than to strain amplitude. The ST still produced positive work per cycle at frequencies up to 30 Hz and 5% strain (figure 7.3d).

Both TL and ST generated positive power output over a broad range of cycle frequencies and strains (figure 7.3b,e). The highest mean power output of TL was produced at 20 Hz and 10% strain (normalised: 0.964±0.072, raw: 7.15±4.04 Wkg^{-1} [n=7]). Interestingly, an in situ preparation with the TL still attached to a freshly excised syrinx showed about 10% shortening under full stimulation (figure 7.4). Similar to work per cycle, the power output was not very sensitive to strain in the investigated range and remained high up to 20% strain.

The mean power output for the ST (figure 7.3e) was highest at 20 Hz and 5% strain (normalised: 0.792±0.394, raw: 11.62±8.85 Wkg^{-1} [n=6]). The power output of both the ST and TL peaked at 20 Hz (figure 7.3b,e), which was very close to the mean trill repetition rate of 24.2±3.0 Hz (n=9), but significantly different (p=0.03). For both TL and ST, the standard deviations of power outputs (middle panels in figure 7.3g,h) were high, but only in the regions where the power was negative (cf. figure 7.3b,e).

The maximum instantaneous power of TL (figure 7.3c) peaked at 15 Hz and 20% strain (normalised: 0.996±0.006, raw: 58.48±16.86 Wkg^{-1} , n=2). At the maximum of power output for TL (at 20 Hz and 5% strain), the normalised and raw MIP was 0.964±0.07 and 31.00±16.86 Wkg^{-1} (n=6), respectively. Both the MIP (figure 7.3e) and mean power output (figure 7.3f) of ST peaked at 20 Hz and 5% strain (normalised: 0.778±0.387, raw: 49.61±39.23 Wkg^{-1} [n=6]).

Muscle fibre structure

The TL consisted of many serially connected, tapered, muscle fibres of 300-1200 µm (figure 7.5a). The fibres contain great quantities of mitochondria that were organised in bands parallel with the fibre direction (figure 7.5b,c). The ST fibres also contain large amounts of mitochondria (figure 7.6d-f). Based on mitochondrial and myofibillar packing there are probably several unidentified fibre types present in TL and ST. The ST is a cylindrical muscle, and the nervus sternotrachealis runs in the middle, surrounded by fat (figure 7.5d). The myofibrils of the TL and ST are surrounded by a well-developed sacroplasmatic reticulum (figure 7.6a,c), and the T system has two tubular systems per sarcomere situated at the overlap of actine and myosine filaments (arrows in figure 7.6b,d). The ST exhibited less SR around the myofibrils than the TL (compare figure 7.6b with 6d).

Discussion

Syringeal muscles of ring doves are capable of very fast contractions and generate positive work and power up to cycle frequencies of 50 Hz. They are not likely to be optimised for power but for fast contractions that enable accurate and fast control over position of the Lateral Tympaniform Membranes (LTM's). The respiratory muscles power the flow that induces vibrations of these membranes. Syringeal muscles therefore do not necessarily need high specific mechanical power output, but the capacities to quickly alter the LTM position or tension.

The isometric contraction speeds of both syringeal muscles are close to the fastest vertebrate muscles. The twitch half times of both TL and ST are about 10 ms. This is close to the twitch half times of the toadfish swim bladder muscles (9.5 ms at 16°C and 5.8 at 25°C) and the rattle snake tail shaker muscles (8.5 at 35°C, Rome et al., 1999) Muscle designs are mutually exclusive: fast muscles with high endurance generate low power, fast muscles for burst activities generate high power (Young & Rome, 2001). The observed large quantities of mitochondria and SR in the TL and ST muscle fibres, limits the space for contractile elements. Therefore, the maximum force and power generated by these muscle fibres decreases. The maximal isometric stress (MIS) during tetanic contraction of 18.1±7.2 kPa and 48.5±34.7 kPa for TL and ST is about ten times lower than the 200-400 kPa for normal skeletal muscles. The MIS reported for other superfast muscles is comparable with our findings; the oyster toadfish swimbladder muscle produces a MIS of 15 kPa (at 15°C, Young & Rome, 2001).

The overall performance in net work and power as function of cycle frequency is very similar to the performance of the toadfish swimbladder muscle (Young & Rome, 2001). The TL produced the highest work at low frequencies of 5 Hz such as most skeletal muscles, regardless of strain amplitude. The ST produced higher work at 10 Hz and 10 % strain and shows a similar pattern as the swimbladder muscle that also produced highest work (1 Jkg^{-1}) at 10 Hz but at unknown strain (figure 2 in Young & Rome, 2001).

The power output is highest at 20 Hz for both syringeal muscles, which corresponds to findings in the swimbladder muscle in Young & Rome (2001). The syringeal muscles can generate constant force for more than 300 ms when undergoing tetanic contraction (Elemans et al., 2004). This is in contrast with the swimbladder muscle, which reduces force considerably (only 10-20% of the maximum force) already after tens of milliseconds during tetanic stimulation (Rome et al., 1999;

Young & Rome, 2001). Therefore, the power output of the syringeal muscles is about twice compared to the swimbladder muscles, during a repetition of sinusoidal strain cycles.

The syringeal muscles of ring doves and the swim bladder muscles of the toadfish differ most in the maximum cycle frequency where positive net work and power is generated: 110 Hz for the swimbladder, 50 Hz for the TL and 40 Hz for the ST. However, we estimate the *in vivo* strain in syringeal muscles to be 10-20%, which is high compared to strain regions where the rattlesnake tailshaker and the swimbladder muscles of the toad fish operate. The tail shaker operates at very low strains of 2-4% (Moon et al., 2003). The strain for the swimbladder is not mentioned in Young & Rome (2001). We did not test the performance of the syringeal muscles at strains below 1%, but the maximal frequency where positive work is still produced can be expected to increase considerably.

The modulations of frequency and gating that are found in songbirds are much faster than the trill of ring doves. For instance, the tracheobronchealis muscle in brown thrashers modulates flow at 125 Hz (Goller & Suthers, 1996b). The songbirds possibly harbour some of the fastest muscles known to vertebrates, if their modulations are indeed under active control.

The measured power output of the syringeal muscle does not represent optimal performance, as we did not optimise all settings during the work loop experiments. We made a small underestimation of the power output of our muscles at low frequencies due to a relative short stimulation (25% of the cycle, i.e. a low duty factor). Also, the *in vivo* strain is unlikely to be a pure sine wave and asymmetrical strain regimes result in a higher power output (Askew & Marsh, 2001). Frog calling muscle generated 60% more power at asymmetrical strain regimes (Girghenrath & Marsh, 1999). At present, there is no information how the syringeal muscles shorten or lengthen during song production. The TL and ST might control the LTM position with smooth cyclic contractions, but also might gate sound with short jerks on the LTM.

Implications for in vivo function: TL and ST can be antagonists

Our results clearly show that the two syringeal muscles are capable to act as fully functional antagonists with respect to LTM positioning. (1) First, the force directions of both muscles are aligned, since the ST and TL run in parallel in the intact body. To clarify the anatomy, the ST is often depicted as two muscles that run almost perpendicular to the medial axis of the syrinx (figure 7.1c; e.g. King, 1989), which provides an incorrect representation of the *in vivo* position. Due to the axial rotation of the syrinx with respect to the midline of the body (figure 7.1b), the insertion of the ST's runs in the medial plane of the body. The ST generates about twice the force of the TL. This extra force is necessary to pull down the whole syrinx, whereas the TL applies force directly on the LTM. (2) Second, the contraction amplitudes of the two muscles, at which the power output is highest, are not significantly different (p <0.001). The TL has the highest power output at a strain of 10%, which corresponds to a contraction amplitude of 0.76±0.04 mm, and the ST at a strain of 5%, which corresponds to a contraction amplitude of 0.73±0.04 mm. With these contraction amplitudes, the syringeal muscles can vary the LTM position over a range that fully opens or closes the syringeal aperture. If we assume that contraction amplitude in a TL equals lateral excursion of one LTM, the LTM can be controlled within 1.50 mm or 0.75 mm around its resting position. This implies that the difference in syringeal aperture of an opened and closed syrinx can be accurately controlled within a range of 3 mm, since the LTMs are paired. By stretching a freshly excised syrinx, its syringeal aperture can be changed roughly from 0 to 2 mm. The range of muscular control

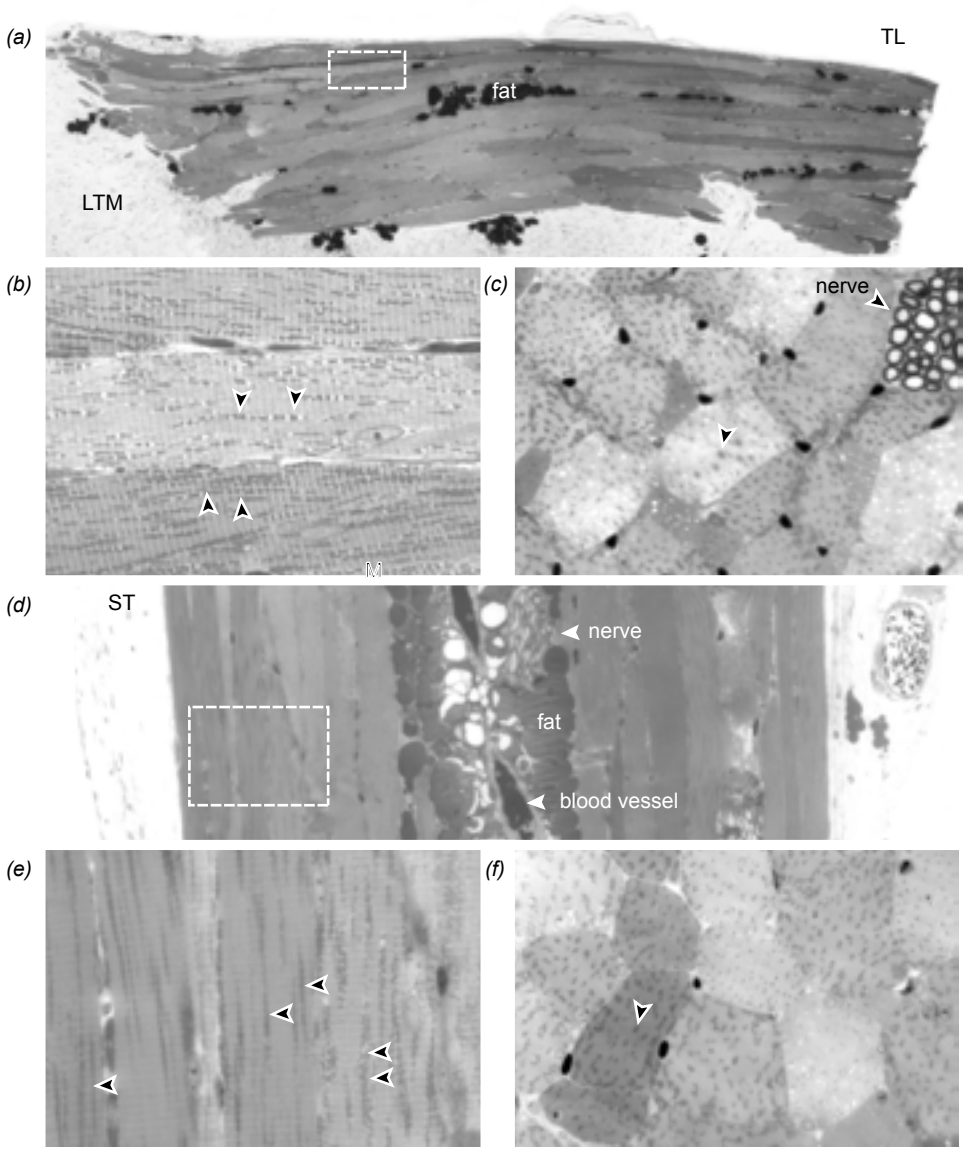

Figure 7.5 Large amount of mitochondria present in both syringeal muscles. (a) TL insertion in the LTM. (b) Large amounts of mitochondria (arrows) are arranged in bands, detail of (a). (c) Cross-section thought the TL. Dark spots (arrow) are arrays of mitochondria. A nerve with myelinated axons is visible. (d) Section thought the ST about 6 mm from the insertion at the trachea. In the middle the nervus sternotrachealis and surrounding fat is visible. (e) Detail of (d). Also here, large amount of mitochondria (arrows) are arranged in bands. (f) Cross-section though the ST.

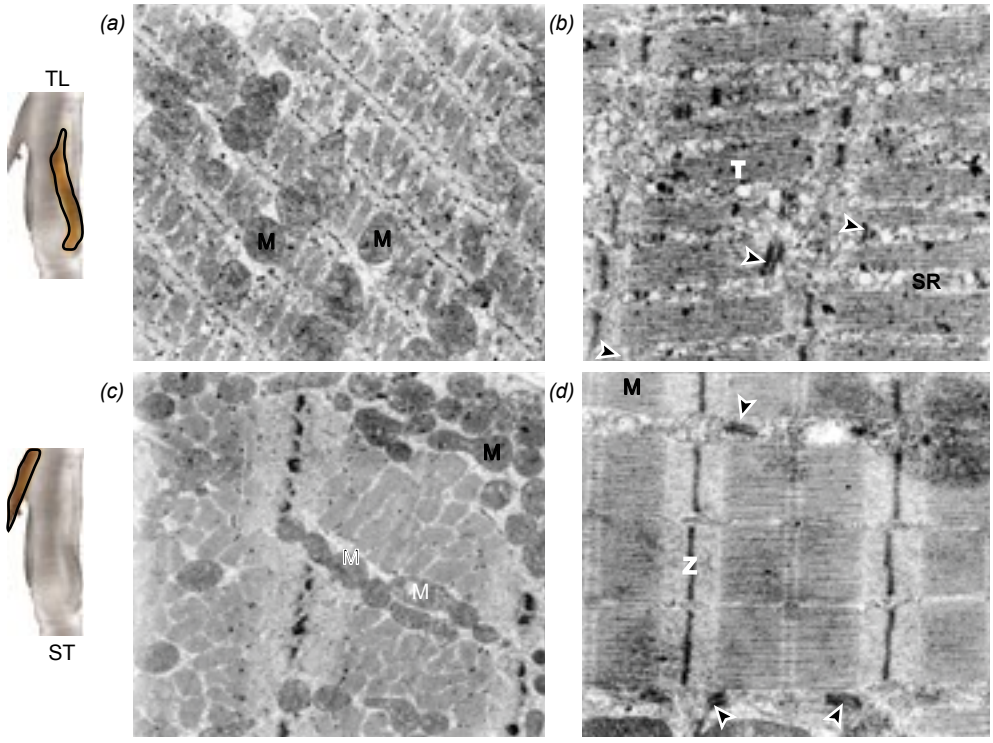

Figure 7.6 Sarcomeres of the syringal muscles. EM images of section through TL (a),(b) and ST (c),(d). m, mitochondrium; SR, Sarcoplastatic reticulum; T, T-tubulus system; Z, z-line.

overlaps this passive LTM movement. (3) Third, both muscles provide highest power at the same frequency of 20 Hz. This is very close to the mean trill rate of 25 Hz.

We show that both syringeal muscles of ring doves have very similar contractile properties. These capacities support earlier direct observations that the TL and ST have an antagonistic mechanical effect (Goller & Larsen, 1997a). At presence, the role of the ST during phonation is unclear (Goller & Larsen, 1997a; Smith, 1977). Phonation was still possible with completely severed ST's in several species of songbirds and non-songbirds (Smith, 1977). Also gas-induced phonation in anesthetised pigeons resulted in phonation (Goller & Larsen, 1997a). The very special contractile properties of the ST, however, strongly suggest that the ST has a very important function during sound production. The TL and ST potentially have an equally important role in fine-tuning the LTM position. Herewith, they control the complex vibration of the LTM's and thus the nature of the produced sound. In humans, small changes in vocal fold behaviour such as the ratio opened/closed per oscillation cycle, already have dramatic effects on the perception on the quality of the voice (Henrich et al., 2003). Therefore, small effects on LTM positioning may have significant effects on the quality of sound for a conspecific mate. As such, we suggest that both syringeal muscles have a crucial function in the quality of the produced song.

Implications for in vivo function: Frequency modulation in ring doves.

The pitch of the produced sound in ring doves is most likely determined by the tension in the LTM (Fletcher, 1988; Gardner et al., 2001; Laje et al., 2002; Mindlin et al., 2003). The tension in the LTM is determined by a complex interplay of syringeal muscle activity, pressure in the air sac system and body posture that affects the positioning of the syrinx. Elemans et al. (2004) suggested that the TL controls the position and tension of the LTM and as such controls pitch and gating during phonation in ring doves. LTM tension can also be affected by a pressure differential between the interclavicular air sac (ICAS) and bronchial lumen (See Chapter 4 in this thesis; Beckers et al., 2003a; Fletcher, 1988). Depending on activation state of the muscles, the bronchial and ICAS pressure forces obviously affect membrane tension and thus correlations can be expected.

With our results, we can estimate the relative contributions of the stress that is applied on the LTM by either muscular contraction or by the pressure differential between ICAS and bronchial lumen. In ring doves, the maximal pressure during cooing is about 3.5 kPa (cf. figure 5 in Gaunt et al., 1982), which corresponds to our personal observations (CPHE and Franz Goller, unpub. results). This pressure is also the maximal pressure difference that can occur between bronchus and ICAS pressure during a coo and equals a pressure difference over the LTM of 3.5 kPa. Although very little is known about the geometry and connections between the various air sacs (Duncker, 1972), it is very unlikely that pressure differences of such magnitude can exist within the air sacs of a singing bird. From figure 2 in Beckers et al. (2003a), we can roughly estimate the maximal difference between ICAS and bronchial pressure (that presumably equals the pressure in the cranial thoracic air sac). If we assume that both traces have their maximum at 3.5 kPa, the maximal pressure difference during the whole coo is 1 kPa at the end of *s2*. However, the pressure difference is less than 0.5 kPa for 76% of the coo (not shown).

Our results show that the locally applied stress on the LTM due to TL contraction is in the order of 20 kPa (tetanic contraction) and likely to be more *in vivo*. The surface of the LTM is about 4 times larger than the cross-section of the TL (Figure 7.1 and 4). If we assume that the stress due to TL contraction is applied evenly across the LTM, the resultant stress on the LTM is about 5.0 kPa. Therefore, the TL modulates a stress that is about ten times higher than the stress due to a pressure differential over the membrane during 76% of the coo. This strongly supports the earlier findings that syringeal muscles are the primary candidates for frequency modulation in ring dove song by altering tension and position control of the LTM (Elemans et al., 2004). Nevertheless, the correlation between ICAS pressure patterns and pitch during song observed by Beckers et al. (2003a) can be explained. This correlation was reported for the last part of *s2*, when the frequency slowly decreases (figure 7.2b). In this part of the coo, the EMG activity of both TL and ST is rather constant (Elemans et al., 2004 and Chapter 6). This implies that the resultant stress exerted on the LTM by TL and ST is rather constant. When the state of muscle activation is balanced, every small change in body posture, bronchial pressure or ICAS pressure alters the pressure force over the LTM, which in turn alters its tension and thus pitch of the coo. If the ICAS pressure decreases relative to the bronchial pressure, the pressure difference decreases and thus the tension in the membrane, which in turn lowers the pitch.

The syrinx is a very complex structure that generates intricate sounds. Hypotheses of the functions of separate parts of the vocal system are mostly based on indirect observations. Virtually nothing is known about the muscle length changes, the properties of the LTM and its behaviour

in vivo. Also the connections between the air sacs that might cause different pressure patterns in different parts of the respiratory system of birds (Beckers et al., 2003a, Boggs et al., 2001) are still unidentified (Duncker, 1972). The syringeal muscles control many aspects of phonation and appear to be highly specialised muscles that have evolved separately from other fast muscles. We present the first data on syringeal muscle performance and structure. The mechanical performance of syringeal muscles helps to identify the function of syringeal muscles to control sound production. Furthermore, estimates of force production by syringeal muscles can calibrate state-of-the-art models that bridge the gap between vocal learning, neuromuscular control and sound production (Mindlin et al., 2003). Syringeal muscles thrive in a dynamic environment: their activity must be synchronised with heartbeats, respiratory functions (Hartley, 1990) and other complex movements as a result of body posture (Cooper & Goller, 2004; Todt and Fiebelkorn, 1980; Williams, 2001). To be conclusive about the functional repertoire of syringeal muscles, we ultimately need *in vivo* length measurements of the muscles in combination with EMG. These measurements pose one of the next challenges in vocal studies.

Acknowledgements

The authors thank Ole Næsbye Larsen, Mees Muller and Ulrike Müller for critical comments on the manuscript. The investigations were (in part) supported by the Research council for Earth and Life Sciences (ALW) with financial aid from the Netherlands Organisation for Scientific Research (NWO).

Appendix A; Abbreviations and units

Morphological parameters

B_i	bronchial ring number *i*
CTAS	cranial thoracic air sac
EMG	electromyogram
FM	frequency modulation
LTM	lateral tympaniform membrane
ICAS	interclavicular air sac
MIP	maximal instantaneous power
MIS	maximal isometric stress
MTM	medial tympaniform membrane
SR	sacroplasmatic reticulum
ST	musculus sternotrachealis
T_i	tracheal ring number *i*
TL	musculus tracheolateralis
TR	musculus trachealis

Physical parameters

f	cycle frequency	[Hz]
F	force	[N]
l	length	[m]
P	power	[W]
W	work	[J]
ε	Lagrangian strain	[%]
ρ	density	[kgm^{-3}]
σ	stress	[kNm^{-2} = kPa]

SECTION V

General discussion

chapter **8**

General discussion

The aim of this thesis was to improve the understanding of sound production and vocal control of birds. To circumvent problems encountered with obtaining and interpreting *in vivo* observations, such as the uncertainties of transducer conditions and placement and the often-low sample sizes due to complicated surgical procedures, we presented three distinct approaches to study sound production and vocal control in birds

Sound analysis: from sound to the sound generator.

In section II, we explore the spectral structure of sound signals by theoretical signal analysis. We used spectrograms to study the clues we can extract about the mechanical origin of the sound signals. To use of spectrograms as a time-frequency representation of sound is widespread in biology for decades (Greenewalt, 1968; Stein, 1968). We demonstrate that most features we see in spectrograms can be obtained by simple modifications of sine waves. An overview of types of modulations of sound signals, such as amplitude modulation and angular (i.e. frequency and phase) modulation, is presented. Although most of the methods are commonly used in engineering, they are not readily accessible to biologists and we aim to provide a self-containing chapter that also includes the basis of Fourier analysis theory. Chapter 3 can be readily used as a tutorial that reviews the basics of signal analysis and sound modulation in animals for people new to the field of sound production.

To calculate the distribution of energy in the harmonics stack of a clipped sound signal, we solved the Fourier expansion of a clipped sine wave analytically. With relatively simple and well-studied differential equations, the conversion from amplitude modulation to frequency modulation and the generation of nonlinear effects can be generated. It is not possible, however, to a priori interpret the mechanical origin of features found in spectrograms without extensive knowledge of these underlying mechanical events.

Mechanical modelling of the syrinx

In chapter 4, we present the first mechanical model of the syrinx. This artificial syrinx model (SAM) enables detailed study of the behaviour of the vibrating membranes that generate the sound waves. We show that both frequency and amplitude of the generated sound depend on three important parameters; driving pressure, air sac pressure and the material properties of the membranes.

We found that the membrane oscillations are the sound source in our model, which are strongly coupled to the tube resonances. The acoustic feedback of distal structures affects the amount of coupling between source and resonator. The strong coupling in our SAM is probably due to the reflective properties of the smooth surface and the stiffness of the aluminium tube. Many songbirds produce songs with weak coupling between syringeal vibrations and vocal tract (Nowicki, 1987) and in only one example interaction between the bilateral sound sources were demonstrated (Nowicki & Capranica, 1986a, 1986b). The behaviour of the syringeal membrane vibrations is also affected by acoustic feedback. This phenomenon probably plays an important role in the produc-

tion of complex sounds (Goller et al, 2003; Laje et al., 2001).

In the construction of our mechanical model, the pressure in the air sac surrounding the syrinx, i.e. the interclavicular air sac, and in the bronchi can be varied independently. The morphology of the air sac system was described for 155 species by Duncker (1972) and, as already pointed out by Lighthill (1975), it is difficult and time consuming to collect experimental data. Without pressure differences in the respiratory system there is no flow and thus no gas exchange, therefore the presence of pressure gradients is essential for the functioning of the respiratory system. Currently, not much is known about pressure distributions in the respiratory system of birds during vocalisation. The occurrence of different pressure patterns in the air sacs during song was not yet reported during the construction of our model, but indeed demonstrated later by Beckers et al. (2003a) to occur in ring doves (*Streptopelia risoria*). We do not know the magnitude of pressure differences between air sacs and their importance in vocalisation, but the study by Beckers et al. (2003a) indicates that our original assumption to separate bronchial and air sac pressure is valid.

An important condition that had to be met to produce sound with SAM, was the position of the membrane. The membrane needed to close of the tube completely, otherwise no vibration was induced. Control of membrane position was achieved by the pressure difference between the pressure in the tube and in the air sac. Therefore, our model essentially requires the pressure difference between air sac and bronchus to produce sound.

The use of mechanical models to study sound production is novel to the field of ornithology. Numerous mechanical models have been developed of the mammalian vocal folds (e.g. Deverge et al., 2003; Lous et al., 1998), larynx and hemilarynx (e.g. Alipour & Montquin, 2000) to study human sound and speech production. Mechanical modelling provides an excellent opportunity to test the mathematical models of the syrinx (Fee et al., 1998; Fletcher, 1988; Gardner et al., 2001; Laje et al., 2001; Mindlin et al., 2003). Similar to the available mathematical models, our mechanical model is a gross simplification of syringeal morphology and syringeal control. The real-time control over pressure, flow and membrane tension could be engineered in the future, but it is of higher priority to compare the behaviour of our mechanical model with the performance of the available mathematical models.

Muscular control of vocal production in ring doves

In Section IV, we focussed on the muscular control during the song of ring doves and discovered that this mode of control is extremely fast. The syringeal muscles control gating and frequency in the song of ring doves, and are among the fastest vertebrate muscles known (Elemans et al., 2004, chapter 6 and 7). Other very fast changes of frequency (<5 ms) can be the result of nonlinear mechanical properties of the syrinx, as found in Zebrafinches (Fee et al., 1998; Fee, 2002). These changes are almost instantaneous and are the results of different modes of vibration. The occurrence of sudden frequency changes and subharmonics in song are the fingerprints of nonlinear dynamics that can also be observed in the song of ring doves (Figure 8.1).

The control of sound parameters during song is thought to consist of slow changes in bronchial pressure and motor gestures controlling tension and position of the syringeal labia of songbirds (Laje et al., 2002) or membranes (Fletcher, 1988). Fast frequency jumps were accounted by intrinsic nonlinear effects. However, we found that the syringeal muscles in ring doves are capable of

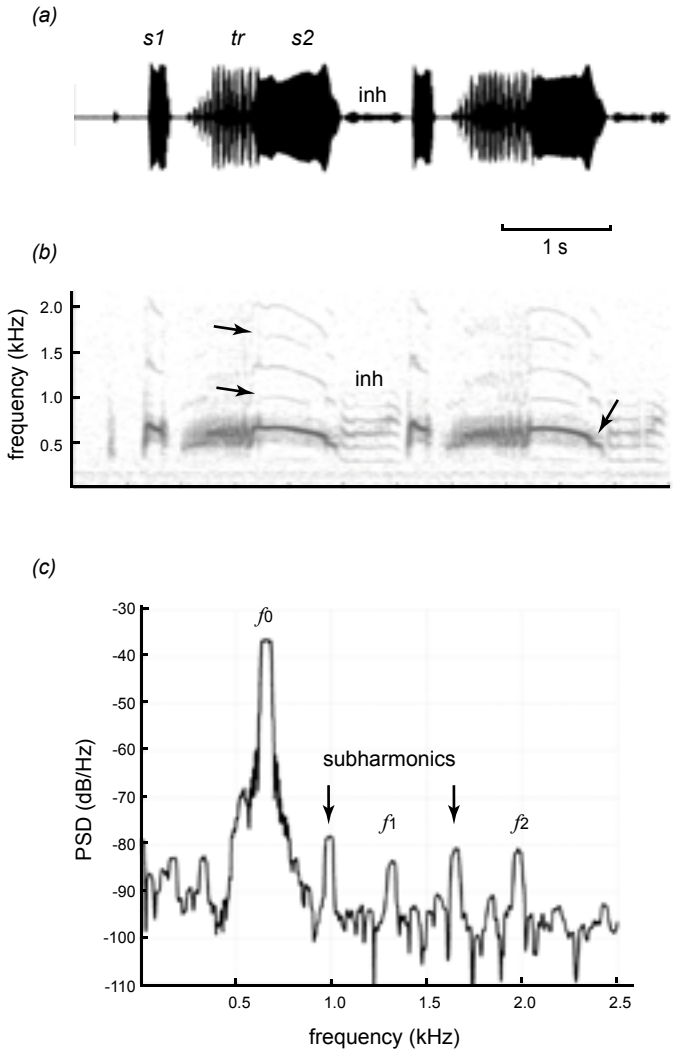

Figure 8.1 Signatures of nonlinear dynamics in ring dove song. (a) sound amplitude and (b) spectrographic representation of the coo of a ring dove. The arrows indicate subharmonics and sudden frequency jumps. inh: respiratory note during inhalation. (c) Spectral density estimate using the multi-taper method. The harmonics f_1 and f_2, and the subharmonics are more than 50 dB less powerful than the fundamental.

modulating force within several milliseconds (Elemans et al., 2004). Active control by superfast syringeal muscles allows for very fast and accurate control of syringeal configuration. We expect that highly specialised fast muscle types are ubiquitous in the vocal control system in both songbirds and non-songbirds. The evolution of superfast muscular control in combination with nonlinear intrinsic material properties of the syrinx provides birds with a nearly unlimited number of possibilities to generate different and complex syllables.

Sound production in ring doves

Analogous to observation in pigeons (Goller & Larsen, 1997a) large amplitude oscillations of, or collisions between the Lateral Tympaniform Membranes (LTM) are most likely essential for sound production in ring doves. As we showed in chapter 3 and 4, collisions generate strong harmonics in the spectrum, but these are not observed in the vocalisations of adult ring doves. Young specimens, however, exhibit considerable acoustic energy in the harmonics that disappear after several months (CPHE, pers obs), which indicates that learning, possibly in combination with morphological changes is involved in reducing the amount of energy in the harmonics.

The coos of ring dove are classified as so-called tonal song, i.e. song where the sound intensity of the first harmonic is reduced by more than 20 dB compared to the fundamental (Greenewalt, 1968). There are theoretical difficulties in explaining how a vibration based system can generate tonal sounds (Casey & Gaunt, 1985; Gaunt & Gaunt, 1985, Fletcher, 1988, 1989) and this led the idea that tonal sound was produced by vortex generated whole-tone whistles (Gaunt et al, 1982; Nottebohm, 1976). It should be noted that even musical instruments that produce vortex induced sounds, such as recorders and flutes, exhibit multiple and strong harmonics (e.g. Dequand, 2000). However, no experimental evidence was found to supported this 'whistle hypothesis' in several bird groups (Ballintijn & ten Cate, 1998; Hersh, 1966; Nowicki, 1987; Brittain-Powell et al., 1997). Direct observations strongly support a vibration-, or collision-based mechanism (Goller & Larsen, 1997a, 1997b, 2002; Larsen & Goller, 1999, 2002) - as found in humans - that results in multiple harmonics.

Several mechanisms can account for the suppression of higher harmonics and we have to take the whole system into account. First, the walls of the trachea and oesophagus consist of soft tissues that both reflect and dissipate sound energy. The material properties of these proximal structures and the opening of the beak (Fletcher & Tarnapolski, 1998) are likely to affect the acoustic feedback to the membranes (Laje et al., 2001) and thus the amount of coupling between syringeal vibrations and resonant structures. Adults keep their beak (Beckers, 2003b; CPHE pers. obs.) and nares (Gaunt et al., 1982) closed during cooing. During inspiration after the last syllable of the coo (*s2*), the beak is open. The sound that is produced during inspiration is rich in harmonics. The area from which the sound radiates during singing is unknown, but since the beak is closed, it is most likely that sound radiates thought the crop. The cumulative sound absorbing properties of the walls of the crop, oesophagus and trachea can greatly reduce the amount of energy in the higher harmonics.

Second, we speculate that the vibratory behaviour of the vocal folds also affects the amount of energy in the overtones. Small changes in vibrations can alter the asymmetry of the oscillation, e.g. the duration of closure relative to opening per cycle, which affects the amount of energy in the harmonics. Therefore, accurate control over membrane position and tension as provided by the syringeal muscles could reduce energy in overtones of the vibrations.

The relative importance of these suggestions can only be tested by constructing mathematical models that also include acoustic feedback. To explain the complex features of song, such as the control over harmonic content and complex sounds, we need a more profound insight in the interactions between membrane vibrations and vocal tract. In songbirds, this is even more challenging due to additional acoustic interaction between the left and right side of the syrinx (Suthers, 1990).

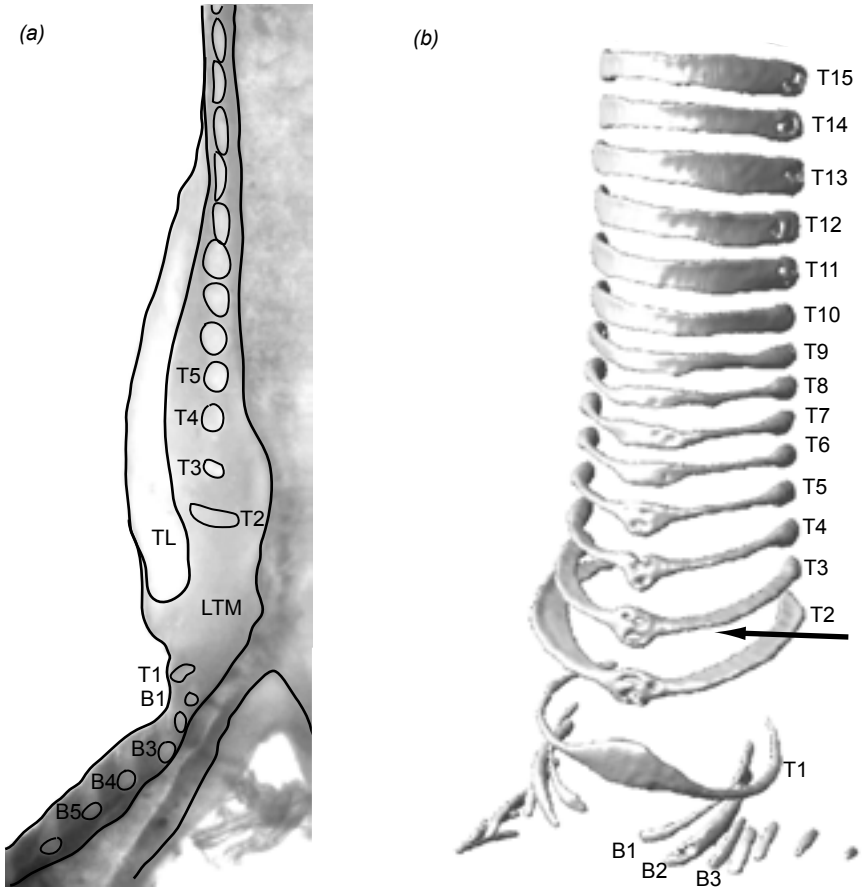

Figure 8.2 (a) Mass distribution of lateral tympaniform membrane in cross-section. (b) Bony elements of the ring dove syrinx. (based on micro-CT scan; courtesy by Dr. S. Kranenbarg). The arrow indicates the direction in which the flattened rings T2-T4, provide resistance to bending due to the large second moment of area. B1-B5, bronchial rings; LTM, Lateral tympaniform membrane; T1-T5, tracheal rings; TL, tracheolateralis muscle.

Frequency and amplitude control in ring doves

We showed in chapter 6 that the activation of the tracheolateralis muscle (TL) correlates with both frequency modulation and gating in the coo *in vivo*. Furthermore, we have demonstrated in chapter 6 and 7 that both syringeal muscles are also capable of the extremely fast contractions necessary to modulate the exerted force on the Lateral Tympaniform Membranes (LTM). As argued in chapter 4, 6 and 7, the tension in the LTM probably determines the frequency of the produced sound. Tension is affected by at least three forces: 1) the force exerted by the syringeal muscles, 2) the pressure difference between bronchus and the interclavicular air sac (as present in our mechanical model and reported by Beckers et al., 2003a), and 3) forces resulting from changes in body posture (e.g. Boggs et al., 2001). Especially during the elaborate display of the bow coo in ring doves, the latter might have some effect, but we did not investigate this.

To control membrane tension, the syringeal muscles are the prime candidates as argued in chapter 7. We do not know whether the pressure difference between air sac and bronchus is under direct control. Even so, due to the compressive and elastic properties of air, this mode of control is likely to be much slower compared to the direct effect of the muscles.

For the first time, we presented a quantitative consideration on the forces exerted on the LTM. The force applied on the LTM by the syringeal muscles is at least ten times higher than the maximal tension applied by the pressure difference between bronchus and ICAS as argued in the discussion of chapter 7.

The exact mechanism that causes the frequency modulation is not yet certain. We need more information on the structure of the LTM. The thickness of the LTM is reported to be 100 (m in pigeons (Goller & Larsen, 1997a). A morphological study on a close relative of the ring dove, the collared dove (S. decaocto), did not provide data on LTM thickness (Ballintijn et al. 1995). Personal observations (CPHE) on a fresh syrinx indicated that the thickness of the LTM is around 0.5 -1.5 mm in ring doves (Figure 8.2a). Therefore, it is certainly not a membrane in the histological sense, i.e. a few cell layers, and one can also question whether it will behave as a membrane from a physical point of view.

When the paired tracheolateralis muscles contract, they exert force on the LTM and additionally tend to push the tracheal rings T2-T4 into the tracheal lumen. The tracheal rings have to withstand this bending force. In one specimen, we observed that T2-T4 are flattened (figure 8.2b), which increases the second moment of area of these rings in the principal direction indicated in figure 8.2b. This provides a large bending resistance in this direction. Therefore, we can assume that the T2 does not deform considerably into the tracheal lumen when the tracheolateralis muscles contract. The T2 is also unlikely to rotate because the tracheal rings are connected ventrally by cartilaginous, partly ossified tissue.

We hypothesise that two main principles can account for the frequency modulation:

1) If we assume that force applied by the TL is spread equally across the LTM (as already suggested in chapter 7), the overall tension increases throughout the LTM. An increase of tension in a membrane increases its resonance frequency (Fletcher, 1988), and consequently the oscillation frequency and thus the frequency of the produced sound. If we consider the LTM to be a single lumped mass-spring system, the natural oscillation frequency is , where k is the spring stiffness and m is the mass. To accomplish the 7-fold frequency increase observed in Zebrafinches, the vibrating

membrane would need a 50-fold increase in tension (Fee, 2002). This is unlikely and therefore this mechanism is not plausible for frequency modulation over a large range (Fee, 2002). However, the observed two-fold increase in frequency in ring doves (400-800 Hz) requires only a fourfold tension increase in the LTM. Such an increase is feasible, but still has to be tested.

2) Another mechanism for frequency modulation consists of the capability of the TL's to redistribute the mass of the LTM during oscillation and thus decrease its effective vibrating mass (figure 8.3). This would increase the resonance- and oscillation frequencies proposed for zebra finches by Fee (2002). This mechanism might explain why we did not observe large activity fluctuations in the ST activity during song. The ST is not capable of redistributing the mass of the LTM directly, but is more likely to have an overall effect on the LTM.

From our measurements, we cannot conclude which of the two hypotheses about the mechanisms that control frequency modulation agrees best with the vibratory behaviour of tissues in the syrinx *in vivo*. In the ring dove, frequency control due to pressure differences can only play a minor role because the force generated by these pressure differences is very small compared to the force generated by the syringeal muscles as argued in chapter 7.

To approximate the LTM as thin membranes does not seem suitable for a model approach. In fact, the LTM of ring doves more closely resembles the labial masses of song birds. This observation implies that the mathematical model by Fletcher (1988), which is based on vibration of a thin membrane (See Chapter 2), is unsuitable for sound production in ring doves. The visco-elastic material properties of the syringeal tissues are unknown in any bird. Morphological descriptions omit this information essential to sound production. There are some histological records on the medial tympaniform membranes in the collared dove (*Streptopelia decaocto*; Ballintijn et al., 1995) and the mallard (*Anas platyrhinchos*; Scala et al., 1990). However, these structures are not the essential sound generators (Goller & Larsen, 1997a, 199b), and at presence their role is unknown.

Concluding, we emphasize that amplitude and frequency modulation in ring doves is not controlled by separate mechanisms. Altering position of the LTM also alters its tension and effective mass, and this action thus affects both gating and oscillation frequency. There is, however, some degree of seperate control of frequency due to the seperate effect of TL and ST activity. We venture to speculate that complete separate control of amplitude and frequency is yet another key invention that occurred during the evolution of sound production in birds that has ultimately led to the evolution of the songbird syrinx.

It is not mere amplitude or frequency that characterises the quality of sound. The quality of song, i.e. the attractiveness for a conspecific mate, is more likely to be determined by many more, yet unknown, properties of sound that are also species-specific. If the temporal patterns of the trill are more important for the attractiveness than the capacity of frequency modulation, sexual selection pushes for faster syringeal muscles. Superfast frequency modulation might be a simple consequence of syringeal architecture. Information is coded in the relative strength of overtones as found in e.g. Zebrafinches (Sturdy et al., 1999; Tchernichovski & Mitra, 2002) and blackbirds (Dabelsteen & Pedersen, 1993). Even specific groups of neurons sensitive to harmonics have been identified in Zebrafinches (e.g. Margoliash & Fortune, 1992). If the harmonic content of sound is also important in mate selection in ring doves and this could be regulated by very accurate control of LTM vibration, it would require the special contractile properties we discovered in both syringeal muscles. This would also explain why the ST has such fast mechanical properties. The evolutionary driving force for the surprising contractile properties of the ST might be the fine-tuning of the quality of sound, and not merely the control of frequency or amplitude.

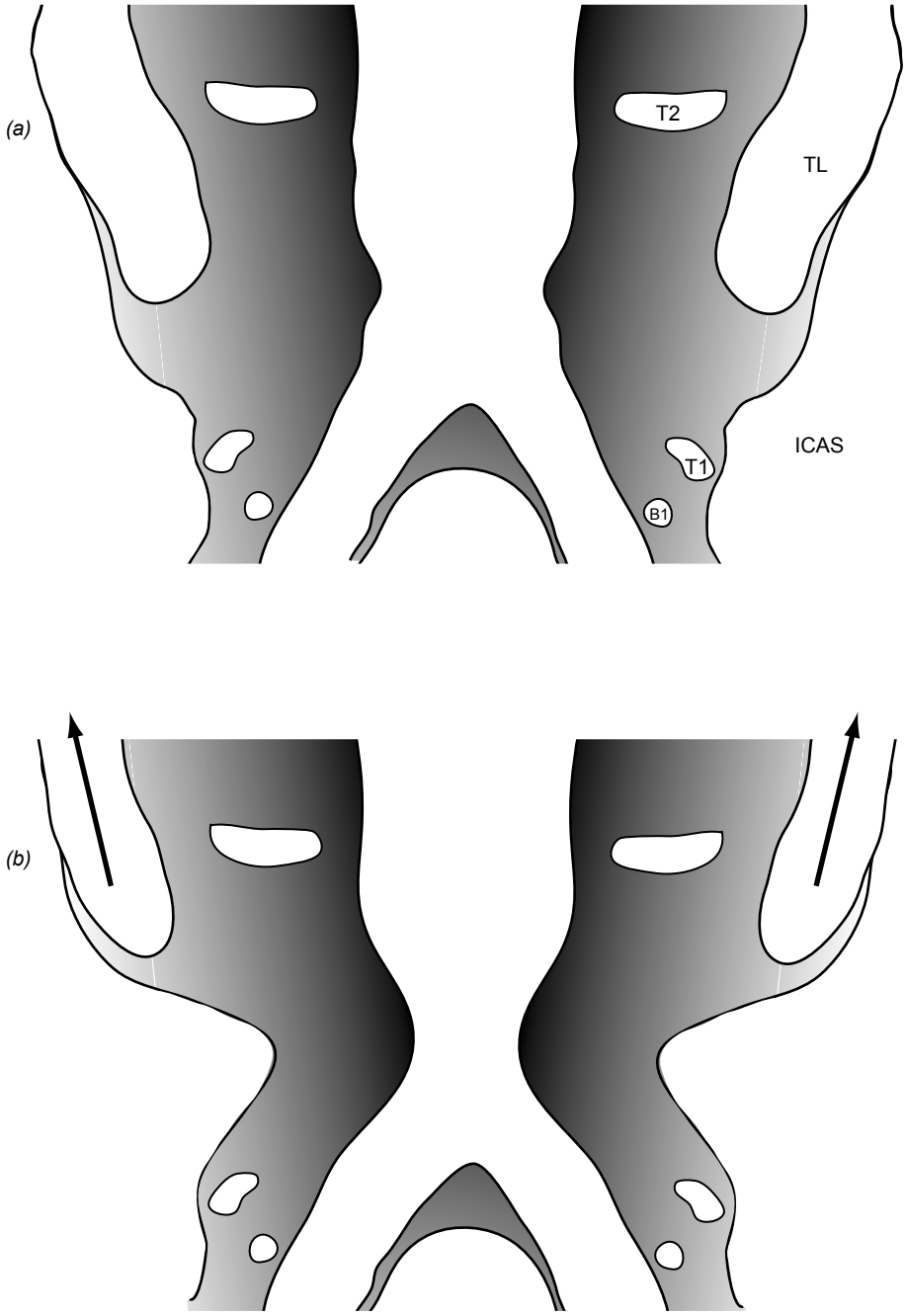

Figure 8.3 Schematic representation of the effect of TL contraction on the mass redistribution and tension in the LTM during phonation. (a) TL relaxed, (b) TL contracted.

Perspectives on the science of bird vocalisation

Only a few studies exist that provide a physical framework to explain a large amount of the scattered observations on the physiology of vocal production. The mathematical models of the mechanical events that occur in the syrinx are an indispensable complement towards the study of motor control of birdsong (Suthers & Margoliash, 2002). Although one can be content with a simple one-, or two-mass model that reproduces many observed phenomena (Mindlin et al., 2003), these simple mathematical models cannot account for the incredible variety in syringeal morphologies we observe. Their virtue is that they represent a first step towards quantitative integration of morphology and control; from brain to behaviour.

Insights in mechanisms of vocal control in birds are of broader interest than to the scientific community alone. The tremendous diversity of syringeal morphology is bound to incorporate aberrant mechanisms of e.g. frequency modulation that can inspire to physicians to construct prosthetics, which provide a more natural voice to laryngectomised patients in the future.

The experiments that knocked out parts of the vocal system showed partial insight, but we can now move towards quantitative integration. Mathematical modelling is a first step towards such integration. To answer the major questions on the functional and evolutionary morphology of the vocal system, we need to develop a new generation of models that account for the architectural complexity, spatial variation in material properties and control function of the syringeal muscles. Such models could subsequently be integrated with neural control models in an attempt to understand of the role in the avian brain in vocalisation.

Acknowledgements

Ole Næsbye Larsen, Mees Muller and Ulrike Müller are greatly acknowledged for their critical comments on this chapter, and Sander Kranenbarg for the micro-CT scan of the syrinx.

Nederlandse samenvatting

Communicatie is cruciaal voor het overleven van organismen. Veel dieren maken gebruik van geluid om te kunnen communiceren en hiervan zijn de vogels zijn zonder twijfel de meest virtuoze zangers. Vogels kunnen de meest uiteenlopende geluiden maken om te kunnen communiceren, maar zijn ook in staat tot het nabootsen van geluiden (o.a. mobiele telefoons, kettingzagen). Vogelzang is een zeer belangrijk modelsysteem geworden voor aangeleerde communicatie zoals menselijke spraak, maar ook voor gedrag, de evolutie van signalen en soortsvorming.

Al sinds de 17e eeuw is bekend dat vogels geluid maken met een uniek orgaan dat andere gewervelde dieren niet bezitten, de syrinx. De syrinx zit ter hoogte van de splitsing van de luchtpijp naar de longen, diep verborgen in het lijf onder de enorme vliegspieren. De syrinx is moeilijk te bereiken om metingen te verrichten en er is verbazingwekkend weinig bekend hoe geluidsopwekking in de syrinx werkt. Er is pas enkele jaren geleden aangetoond dat trillende membranen of lippen in de syrinx geluid opwekken, waarschijnlijk op een vergelijkbare manier zoals dit bij mensen gebeurd in het strottenhoofd. De complexe stromingsgeïnduceerde bewegingen van deze structuren bepalen voor een belangrijk deel de eigenschappen van het geproduceerde geluid in andere vertebraten, maar directe observaties zijn in vogels nog niet gelukt in een zingend dier. Verder blijkt uit fysiologische metingen dat eigenschappen van het geluid zoals toonhoogte (frequentie) en volume waarschijnlijk gecontroleerd worden met behulp van spieren in de syrinx die de spanning en positie van de syrinx membranen beïnvloeden. De functie van de verschillende aanwezige spieren is onbekend.

Om de fysische mechanismen te onderzoeken die ten grondslag liggen aan de geluidsproductie van vogels, hebben wij drie benaderingen gebruikt die nieuw zijn voor het vakgebied.

Ten eerste hebben we bekeken in hoeverre het geluidsignaal hints kan bevatten ten aanzien van de mechanische gebeurtenissen die ten grondslag liggen aan geluidsproductie. Een spectrogram is een frequentie-tijd representatie van een signaal welke veel gebruikt wordt in de ornithologie om vogelzang te visualiseren. Het vertalen van een structuur in een spectrogram naar een potentiële mechanische gebeurtenis, vereist allereerst kennis van de algoritmen om het spectrogram te maken. Vervolgens hebben we met een aantal simpele analytische signaal beschrijvingen de algemeen voorkomende structuren in spectrogrammen gesynthetiseerd. Hierdoor is het mogelijk om wiskundige artefacten te onderscheiden van echte eigenschappen van het signaal, welke we koppelen aan mechanische gebeurtenissen. Met dergelijke analytische beschrijvingen kunnen we een willekeurig signaal opbouwen en dit demonstreren we door de analyse van de schreeuw van de lammergier. Verder bestuderen we de mechanische gebeurtenissen in een zeer simpel mechanisch model, bestaande uit een oscillerend riet van een doedelzak om het spectrogram te koppelen aan de mechanische gebeurtenissen.

We concluderen dat het vertalen van het spectrogram naar de mechanische gebeurtenissen die eraan ten grondslag liggen alleen mogelijk is indien er aanvullende observaties van deze gebeurtenissen gedaan kunnen worden. Het is niet mogelijk om op basis van alleen een spectrogram deze ondubbelzinnige te interpreteren.

Ten tweede hebben we een mechanisch model of artificiële syrinx gebouwd waaraan, in tegenstelling tot vogels, zeer nauwkeurige observaties verricht kunnen worden aan de complexe mem-

braanvibraties en geluidsproductie. Ons model is gebaseerd op de syrinx van een duif vanwege de relatief simpele morfologie en bestaat uit een buis met een enkele membraan in de wand. Geluid ontstond door botsingen tussen de oscillerende membraan en de buiswand. De oscillaties van de membraan waren sterk gekoppeld aan de resonantie eigenschappen van de buis stroomafwaarts en tevens afhankelijk ook de materiaal eigenschappen van de membranen. Het is noodzakelijk deze bevindingen kwantitatief te toetsen aan de bestaande wiskundige modellen.

Ten derde hebben we de functionaliteit en de mechanische eigenschappen van de syrinx spieren bestudeerd. Hiervoor hebben we de Barbarijnse tortelduif of lachduif (*Streptopelia risoria*) als model gebruikt. We hebben met spieractiviteit metingen in zingende duiven aangetoond dat de spieren zowel frequentie en het aan/uit zetten van membraanvibraties controleren. Deze spieren bleken net zo snel te zijn als de snelst contraherende spieren die momenteel bekend zijn. Hierdoor zijn duiven en waarschijnlijk ook alle zangvogels in staat tot zeer nauwkeurige en snelle sturing van de geluidsproductie.

Verder ondersteunde observaties op celniveau de speciale contractiele eigenschappen van de spieren. Door uitgebreide metingen aan het vermogen van twee syrinx spieren konden we voor het eerste een kwantitatieve analyse maken van de biomechanische effecten tijdens zang. De resultaten tonen aan dat beide spieren functionele antagonisten zijn in het positioneren van de syrinx membranen en het veranderen van de spanning in de membraan. We tonen aan dat deze spieren voor duiven het belangrijkste mechanisme vormen om de frequentie van hun zang te bepalen.

Bibliography

Abramowitz, M. & Stegun, I.A. (1970) *Handbook of Mathematical Functions.* (Eds.) Dover Publications, New York.

Abs, M. (1980) Zur Bioakustik des Stimmsbruchs bei Vogeln. *Zool. Jb. Physiol.* **84**, 289-382.

Alipour, F. & Montquin, D. (2000) Airflow patterns in hemilarynx model. *J. Acoust. Soc. Am.* **108**, 2530.

Archer, G.F. & Godman, E.M. (1937) *The birds of British Somaliland and the Gulf of Aden.* Edinburgh.

Arnold, V.I., Aframovich, V.S., Il'yashenko, Y.S. & Shil'nikov, L.P. (1999) *Bifurcation Theory and catastrophe Theory.* Springer, Berlin.

Askew, G. & Marsh, R.L. (2001) The mechanical power output of the pectoralis muscle of blue-breasted quail (*Coturnix chinensis*): the *in vivo* length cycle and its implications for muscle performance. *J. Exp. Biol.* **204**, 3587-3600.

Attenborough, D. (1998) *The life of birds.* Princeton University Press, USA.

Baptista, L.F. & Abs, M. (1983) Vocalisations. In: *Psychology and Behaviour of the pigeon.* (Ed: M. Abs), 309-325. London, Acad. Press.

Baines, A. (1973) Bagpipes. In: *Occasional papers on Technology, 9*. Edited by T.K. Penniman and B.M. Blackwood. Oxford University Press.

Ballintijn, M.R., ten Cate, C., Nuijens, F.W. & Berkhoudt, H. (1995) The syrinx of the collared dove (*Streptopelia decaocto*): structure, inter-induvidual variation and development. *Neth. J. Zool.* **45**: 455-479.

Ballintijn, M.R. & ten Cate, C. (1998) Sound production in the collared dove: a test of the 'whistle' hypothesis. *J. Exp. Biol.* **201**, 1637-1649.

Bates, G.L. (1927) Notes on some birds of Cameroon and teh lake Chad regio: their status and breeding times. *Ibis* **12**, 3, 1-64.

Bates, G.L. (1934) Birds of the southern Sahara and adjoining countries in French West Africa. *Ibis* **13**, 61-79.

Beckers, G.J.L. & ten Cate, C. (2001) Perceptual relevance of species-specific differences in acoustic signal structure in Streptopelia doves. *Animal Behaviour*, **62**, 511-518.

Beckers, G.J.L., Suthers, R.A. & ten Cate, C. (2003a) Mechanisms of frequency and amplitude modulation in ring dove song. *J. Exp. Biol.* **206**, 1833-1843.

Beckers, G.J.L., Goossens, M.A. & ten Cate, C. (2003b) Perceptual salience of acoustic differences between conspecific and allospecific vocalisations in African colllared doves. *Animal Behaviour* **65**, 605-614.

Beecher, M.D. (1988) Spectrographic analysis of animal vocalizations: implications of the 'uncertainty principle'. *Bioacoustics* **1**, 187 - 208.

Berry, D.A., Herzel, H., Titze, I.R. & Story, B. (1996) Bifurcations in excised larynx experiments. *J. Voice* **10**, 129-138.

Bertram, C.D. & Pedley, T.J. (1982) A mathematical model of unsteady collapsible tube *Behaviour*. *J. Biomech.*, **15**, 39 - 50.

Bock, W.J. & Farrand, , J. (1980) The number of species and genera of recent birds: a contribution to comparative systematics. *Am. Mus. Novit.* **2703.**

Boggs, D.F., Baudinette, R.V., Frappell. P.B. & Butler, P.J. (2001) The influence of locomotion on air-sac pressure in little penguins. *J. Exp. Biol.* **204**, 3581-3586.

Brackenbury, J.H. (1979) Aeroacoustics of the vocal organs of birds. *J. Theor. Biol.*, **81**, 341 - 349.

Bradbury, J.W. & Vehrencamp, S.L. (1998) *Principles of Animal Communication.* Canada: Sinauer Ass. Inc.

Brainaird, M.S & Doupe, A.J. (2000) Auditory feedback in learning and maintenance of *Behaviour*. *Nature Reviews* **1**, 31-40.

Brittan-Powell, E.F., Dooling, R.J., Larsen, O.N. & Heaton, J.T. (1997) Mechanisms of vocal production in budgerigars (*Melopsittacus undulatus*). *J. Acoust. Soc. Am.* **101**, 578-589.

Casey, R.M. & Gaunt, A.S. (1985) Theoretical models of the avian syrinx. *J. Theor. Biol.*, **116**, 45-64.

Catchpole,C.K. & Slater, P.J.B. (1995) *Bird song: Biological themes and variations.* Cambridge. Camb. Univ. Press.

Chadwick, P. (1999) *Continuum mechanics: Consise theory and problems*. 2nd ed. Dover Pub.

Chamberlain, D.R., Gross, W.B., Cornell, G.W. & Mosby, H.S. (1968) Syringeal anatomy in the common crow. *Auk* **85,** 244-252.

Cheng, M.F. (1992) For whom does the female dove coo? A case for the role of vocal self-stimulation. *Animal Behaviour* **43**, 1035-1044.

Cheng, M. F., Peng, J.P. & Johnson, P. (1998) Hypothalmic neurons preferentially respond to female nest coo stimulation: demonstration of direct acoustical stimulation of luteinizing hormone realease. *J. NeuroSci.* **18**, 5477-5489.

Chiel H. J. & Beer R. D. (1997) The brain has a body: adaptive behavior emerges from interactions of nervous systems, body and environment. *Trends Neurosci.* **20**, 553-557.

Clark, C.W., Marler, P. & Beeman, K. (1987) Quantitative analysis of animal phonology: an application to swamp sparrow song. *Ethology* **76**, 101 - 115.

Cooley, J. W. & Tukey, J. W. (1965) An algorithm for the machine calculation of complex fourier series. *Math. Computation*, **19**, 297-301.

Cooper, B.G. & Goller, F. (2004) Multimodal signals: enhancement and constraints of song motor patterns by visual display. *Science* **303**, 544-546.

Cortopassi, K.A. & Bradbury, J.W. (2000) The comparison of harmonically rich sounds using spectrographic cross-correlation and principal coordinates analysis. *Bioacoustics* **11**, 89-127.

Cramp, S. (ed) (1994) *Handbook of the birds of the Middle East and North Africa. The Birds of the Western Palearctic, Volume IV ; Terns to Woodpeckers.* Oxford Univ. Press. New York.

Cuvier, G. (1802) Ueber den unteren Larynx der Vogel. *Reils. Archiv. Physiol.* **5,** 67-96.

Dabelsteen, T. & Pedersen, S.B. (1993) Song features essential for species discrimination and *Behaviour* assessment by male blackbirds (*Turdus merula*). *Behaviour* **121**, 259-287.

Danielson, G.C. & Lanczos, C. (1942) Some improvements in practical Fourier analysis and their application to X-ray scattering from liquids. *J. Franklin Inst.* **233**, 365.

Darden, S.K., Pedersen, S.B. & Dabelsteen, T. (2003) Methods of frequency analysis of a complex mammalian vocalisation. *Bioacoustics* **13**, 247-263.

de Boor, C. A. (1978) *Practical Guide to Splines.* Springer-Verlag.

de Kort, S. R. & ten Cate, C. (2001). Response to interspecific vocalizations is affected by degree of phylogenetic relatedness in *Streptopelia* doves. *Animal Behaviour* **61**, 239-247.

Dequand, S. (2000) *Duct aeroacoustics: from technolgical applications to the flute.* PhD thesis Eindhoven University, The Netherlands.

Doupe, A.J. & Kuhl, P.K. (1999) Birdsong and human speechcommon themes and mechanisms. *Ann. Rev. Neurosci.* **22,** 567-631.

de Vries, M.P. (2000) *A new voice for the voiceless: design and in-vitro testing of a voice-producing element*. Ph.D thesis. University Groningen, The Netherlands.

de Vries, M.P., Hamburg, M.C., Schutte, H.K., Verkerke, G.J. & Veldman, A.E.P. (2003) Numerical simulation of self-sustained oscillation of a voice-producing element based on Navier-Stokes equations and the finite element method. *J. Acoust. Soc. Am.* **113**, 2077-2083.

Deverge, M., Pelorson, X., Vilain, C., Lagrée, P.Y., Chentouf, F., Willems, J. & Hirschberg, A. (2003) Influence of the collision on the flow through in-vitro rigid models of the vocal folds. *J. Acoust. Soc. Am.* **114**, 3354-3362.

Dowling, A.P. & Ffocws Williams, J.E. (1983) *Sound and sources of sound.* Ellis Howood Lim. Chichester.

Duffing, G. (1918) *Erzwungene Schwingungen bei veränderlicher Eigenfrequenz*. Vieweg. Braunschweig.

Duncker, H.R. (1972) *Respiration physiology*. **14**, 44-63.

Elemans, C.P.H., Larsen, O.N., Hoffmann, M. R. & Leeuwen, J.L. van (2003) Quantitative modelling of the biomechanics of the avian syrinx. *Animal Biology* **53**, 183-193.

Elemans, C.P.H., Spierts, I.L.Y., Müller, U.K., van Leeuwen, J.L. & Goller, F. (2004) Superfast muscles control dove's trill. *Nature* **431**, 146.

Elemans, C.P.H., Muller, M. & Heeck, K. (subm) Spectrogram analysis of mechanical events in sound production of animals.

Elemans, C.P.H., Muller, M., Larsen, O.N. & van Leeuwen, J.L. (subm) Vibration and sound in a mechanical model of the avian syrinx.

Elemans, C.P.H., Spierts, I.L.Y, Hendriks, M., Schipper, H., Taverne-Thiele, A. & van Leeuwen, J.L. (sum) Mechanical properties of syringeal muscles in Ring doves (*Streptopelia risoria*).

Ellington, C.P., van den Berg, C., Willmottt, A.P. & Thoman, A.L.R. (1996) Leading edge vortex in insect flight. *Nature* **384,** 626-630.

Fabre, B. & Hirschberg, A. (2000) Physical modelling of Flue instruments: A review of lumped models. *Acta Acustica* **86**, 599-611.

Fedde, (1987) Respiratoty muscles. In: *Bird Respiration vol I*, (ed T.J.Seller), 3-37. Boca Raton, Florida, CRC press.

Fee, M.S. (2002) Measurement of the linear and nonlinear mechanical properties of the oscine syrinx: implications for function. *J. Comp. Physiol. A*, **188**, 829 - 839.

Fee, M.S., Shraiman, B., Pesaran, B. & Mitra, P.P. (1998) The role of nonlinear dynamics of the syrinx in the vocalisations of a songbird. *Nature* **395**, 67 - 71.

Feynman, R.P., Leighton, R.B. & Sands, M. (1963) *The Feynman lectures on physics. Mainly mechanics, radiation, and heat.* 6th ed. Addison-wesley Publishing comp. Massachusetts, USA.

Ffocws Williams, J.E. & Lovely, D.J. (1975) Sound radiation into uniformly flowing fluid by compact surface vibration. *J. Fluid. Mech.* **71**, 689-700.

Fine, M.L., Malloy, K.L., King, C.B., Mitchell, S.L. & Cameron, T.M. (2001) Movement and sound generation by the toadfish swimbladder. *J. Comp. Physiol.* A **187**, 371-379.

Fitch, W.T., Neubauer, J. & Herzel, H. (2002) Calls out of chaos: the adaptive significance of nonlinear phenomena in mammalian vocal production. *Animal Behaviour* **63**, 407-418.

Flanagan, J. L. (1972) *Speech analysis, synthesis and perception.* Springer Verlag, New York.

Fletcher, N.H. (1988) Bird song - a quantitative acoustic model. *J. Theor. Biol.*, **135**, 455-481.

Fletcher, N.H. (1989) Acoustics of bird song - some unresolved problems. *Comm. Theor. Biol.*, **1**, 237-251.

Fletcher, N.H. (2000) A class of chaotic bird calls? *J. Acoust. Soc. Am.* **108**, 821-826.

Fletcher, N.H. & Tarnapolsky, A. (1998) Acoustics of the avian vocal tract. *J. Acoust. Soc. Am.* **105**, 35-49.

Frommolt, K.-H. (1999) Sidebands - facts and artefacts. *Bioacoustics* **10**, 219-224.

Fry, C.L. (1998) *A Source-filter Model of Birdsong Production.* Ph.D. thesis, University of California

San Diego)

Fusani, L., Hutchison, R. E. & Hutchison, J. B. (1997). Vocal-postural co-ordination of a sexually dimorphic display in a monomorphic species: the barbary dove. *Behaviour* **134**,321 -335.

Gardner, T., Cecchi, G., Magnasco, M., Laje, R. & Mindlin, G.B. (2001) Simple motor gestures for birdsongs. *Phys. Rev. Lett.* **87**, 208101 - 208105.

Gaunt, A.S. & Gaunt, S.L.L. (1985) Syringeal structure and avian phonation. *Curr. Ornith.* **2**, 213 - 245.

Gaunt, A.S., Gaunt, S.L.L. & Casey, R.M. (1982) Syringeal mechanisms reassessed: evidence from *Streptopelia*. *Auk* **99**, 474-494.

Girghenrath, M. & Marsh, R.L. (1999) Power of sound producing muscles in the gray tree frogs *Hyla versicolor* and *Hyla chrysoscelis*. *J. Exp. Biol.* **202**, 3225-3237.

Gittes, F. & Schmidt, C.F. (1998) Signals and Noise in micromechanical meaurements. *Meth. Cell Biol*. **55**, 129 - 156.

Goller, F. (1998) Vocal gymnastics and the bird brain. *Nature* **395**, 11-12.

Goller F. & Suthers R. A. (1995) Implications for lateralisation of bird sound from unilateral gating of bilateral motor patterns. *Nature* **373**, 63-66.

Goller, F. & Suthers, R.A. (1996a) Role of syringeal muscles in gating airflow and sound production in singing brown thrashers. *J. Neurophysiol.* **75**, 867-876.

Goller, F. & Suthers, R.A. (1996b) Role of syringeal muscles in controlling the phonology of bird song. *J. Neurophysiol.* **76**, 287-300.

Goller, F. & Larsen, O.N. (1997a) In situ biomechanics of the syrinx and sound generation in pigeons. *J. Exp. Biol.* **200**, 2165 - 2176.

Goller, F. & Larsen, O.N. (1997b). A new mechanism of sound generation in songbirds. *Proc. Natl Acad. Sci.* **94**, 14787 - 14791

Goller, F. & Daley, M.A. (2001) Novel motor gestures for phonation during inspiration enhance acoustic complexity of birdsong. *Proc. R. Soc. Lond.* B, **268**, 2301-2305;

Goller, F. & Larsen, O.N. (2002) New perspectives on mechanisms of sound generation on songbirds. *J. Comp. Physiol. A*, **188**, 841 - 850.

Goller, F., Mallinckrodt, M.J. & Torti, S.D. (2003) Beak gape dynamics during song in the zebra finch. *J. Neurobiol.* **59**, 289-303.

Goodwin, D. (1970) *Pigeons and doves of the world.* British Museum NH, London.

Greenewalt, C.H. (1968) *Bird Song: Acoustics and Physiology.* Smithsonian institute, Washington DC.

Hahnloser R. H. R., Kozhevnikov A. A. & Fee M. S (2002) An ultra-sparse code underlies the generation of neural sequences in a songbird. *Nature* 419, 65-70.

Hall-Graggs, J. (1979) Sound spectrographic analysis: suggestions for facilitating auditory imagery. *Condor* **81**, 185-192.

Harris, C.M. & Wolpert, D.M. (1998) Signal-dependent noise determines motor planning. *Nature* **384**, 780-784.

Hartley, R.S. (1990) Expiratory muscle-activity during song production in the canary. *Resp. Physiol.* **81**, 177-188.

Henrich, N., Sundin, G., Ambroise, D., d'Alessandro, C., Castellengo, M. & Doval, B. (2003) Just noticeable diffreneces of open quotient and asymmetry coefficient in singing voice. *J. Voice* **17**, 481-494.

Hérissant, M (1753) Recherches sur les organes de la voix des quadupèdes et de celle des oiseaux. *Mém. l'Acad. Sci. Paris*, 279 - 295.

Hersh, G.L. (1966) *Bird voices and resonant tuning in helium-air mixtures.* PhD Dissertation, University of Ccalifornia, Berkely, USA.

Herzel H., Berry D. A., Titze I. R. & Steinecke I. (1995) Nonlinear dynamics of the voice: signal analysis and biomechanical modelling. *Chaos* **5**, 30-34.

Hoese, W.J., Podos, J, Boetticher, N.C. & Nowicki, S. (2000) Vocal tract function in birdsong production: experimental manipulation of beak movements. *J. Exp. Biol.* **203**, 1845-1855

Hofmans, G.C.J., Groot, G., Ranucci, M., Graziani, G. & Hirschberg, A. (2003) Unsteady flow through in-vitro models of the glottis. *J. Acoust. Soc. Am.*, **113**, 1658-1675.

Hsu, H.P. (1967) *Outline of Fourier analysis.* Ass. Educational services New York USA.

Huxley, T.H. (1877) *A manual of the anatomy of vertebrated animals.* London.

Ishizaka, K. & Flanagan, J.L. (1972) Synthesis of voiced sounds from a two-mass model of the vocal cords. *Bell. Syst. Tech. J.* **51**, 1233 - 1268

Johnson, H.W. & Burrows, C.S. (1984) An in-place, in-order radix-2 FFT. *ICASSP-84 Proceedings*, 28A.2.

Johnson, K.P., de Kort, S., Dinwoody, K., Mateman, A.C., ten Cate, C., Lessels, C.M. & Cleyton, D.H. (2001) A molecular phylogeny of the dove genus Streptopelia. *Auk* **11,** 874-887.

Jones, D.L. & Barianuk, R.G. (1995) An adaptive optimal-kernel time-frequency representation. *IEEE Trans. Sig. Proc*. **43**, 2361-2371.

Josephson, R.K. (1985) The mechanical power output from striated muscle during cyclic contraction. *J. Exp. Biol.* **114,** 493-512

Kelly, J.L. & Lochbaum, C.C. (1962) Speech synthesis. *Proc. 4th Int Congress Acoustics.* **G42**, 1-4.

Khanna, H., Gaunt, S.L.L. & McCallum, D.A. (1997) Digital spectrographic cross-correlation: tests of sensitivity. *Bioacoustics* **7**, 209-234.

Kharkevitch, A. A. (1962) *Nonlinear and Parametric Phenomena in Radio Engineering*. John F. Rider Publisher Inc. New York.

King, A.S. (1989) Functional anatomy of the syrinx, In: *Form and Function in Birds*. Vol. 4, Eds: King, A.S. & McLelland, J. Academic Press, New York, 105-192.

Konishi, M. (1994) An outline of recent advances in birdsong neurobiology. *Brain Behav. Evolut.* **44**, 279-285.

Kroodsma, D.E. & Miller, E.H. (1996) *Ecology and evolution of acoustic commmunication in birds.* Ithaca. Cornell Univ. Press.

Lade, B.I. & Thorpe, W.H. (1964) Dove songs as innately coded patterns of specific behaviour. *Nature* **202,** 366-368.

Laje, R., Gardner T. J. & Mindlin G. B. (2001) Continuous model for vocal fold oscillations to study the effect of feedback. *Phys. Rev. E* **64**, art. 056201.

Laje, R & Mindlin, G.B. (2002) Diversity within a birdsong. *Phys. Rev. Lett.* E. **89**, 288102-288106.

Laje, R., Gardner, T.J. & Mindlin, G.B. (2002) Neuromuscular control in vocalizations in birdsong: a model. *Phys. Rev. Lett.* E **65**, 051 921 - 061929.

Larsen, O.N. & Goller, F. (1999) Role of syringeal vibrations in birds vocalizations. *Proc. R. Soc. Lond.* B **266**, 1609-1615.

Larsen, O.N. & Goller, F. (2002) Direct observations of syringeal muscle function in songbirds and a parrot. *J. Exp. Biol.* **205**, 25- 35.

Lavenex, P. B. (1999) Vocal production mechanisms in the budgerigar (*Melopsittacus undulatus*): The presence and implications of amplitude modulation. *J. Acoust. Soc. Am.* **106**, 491-505.

Lehrman, D.S. (1965) Interaction between internal and external environments in the regulation of the reproductive cycle of the ring dove. In: *Sex and Behaviour*. Ed: Beach, F.A., 355-380, Wiley, New York.

Léonard, F. (1997) Referencing the phase to the centre of the spectral window. Why? *Mech. Syst. and Sig. Proc*. **11**, 75-90.

Léonard, F. (2000) Spectrogramme de phase et spectrogram de fréquence. *Traitement du Signal* **17**, 269-286.

Léonard, F., Foata, M., & Paquin, J.Y. (2000) Vibro-acoustic signature comparison and time-warping correction with multi-scale correlation. *Mech. Syst. and Sig. Proc.* **14**, 443-458.

Lighthill, J. (1975) *Mathematical biofluiddynamics*. CBMS-NSF Regional conference series in applied mathematics 17, Society for Industrial and applied mathematics. Philadelphia, USA.

Lillesand, T.M. & Kiefer, R.W. (2000) *Remote sensing and image interpretation*. 4th ed., John Wiley, New York.

Ling, C., Zuo, M., Alvarez, B-A & Cheng, M.F. (1997) Neurogenesis in juvenile and adult ring doves. *J. Comp. Neurol.* **379**, 300-312.

Linnaeus, C. (1758) *Systema naturae per regna tria naturae secundum classes, ordines, genera, spe-*

cies, cum characteribus, differentilis, synonymis, locis. Tomus I. Editio decima, reformata. L. Salvii, Stockholm.

Lous, N.J.C., Hofmans, G.C.J., Veldhuis, R.N.J. & Hirschberg, A. (1998) A symmetrical two-mass vocal-fold model coupled to vocal tract and trachea, with application to prosthesis design. *Acta Acoustica* **84**, 1135 - 1150

Lynes, H. (1925) Birds of North and Central Darfur. *Ibis* **12**, 545-546.

Margoliash, D. & Fortune, E.S. (1992) Temporal and harmonic combination-sensitive neurons in the zebra finch's HVc. *J. of NeuroScience* **12**, 4309-4326.

Main, I.G. (1978) *Vibrations and waves in physics*. Cambridge University Press, Cambridge UK

Mbu Nyamsi, R.G., Aubin, T. & Bremond, J.C. (1994) On the extraction of some time dependent parameters of an acoustic signal by means of the analytical signal concept. Its application to animal sound study. *Bioacoustics* **5**, 187-203.

Méndez, J. & Keys, A. (1960) Density and composition of mammalian muscle. *Metabolism* **9**, 184-188.

Mergell, P. & Herzel, H. (1997) Modelling biphonation - The role of the vocal tract. *Speech Comm.* **22**, 141-154.

Mindlin G. B., Gardner T. J., Goller F. & Suthers R. (2003) Experimental support for a model of birdsong production. *Phys. Rev. E*. **68** art. 041909.

Moon, B.R., Conley, K.E., Lindstedt, S.L. & Urquhart, M.R. (2003) Minimal shortening in a high-frequency muscle. *J. Exp. Biol.* **206**, 1291-1297.

Moreau, R.E. (1966) *The bird faunas of Africa and its islands.* London

Morel, M-Y. (1975) *Oiseaux* **45**, 97-125.

Nelson, B.S. (2004) Dynamics of frequency and amplitude modulation in vocalisations produced by eastern towhees, Pipilo erythrophthalmus. *J. Acoust. Soc. Am.* **115**, 1333-1344.

Nottebohm, F. (1976) Phonation in orange-winged Amazon parrot, *Amazonica amazonica*. *J. Comp. Physiol. A*. **108**, 157-170.

Nottebohhm, F. & Nottebohm, M.E. (1971) Vocalisations and breeding behaviour of surgically deafened Ring Doves, *Streptopelia risoria*. *Animal Behaviour* **19**, p313-327

Nowicki, S. (1987) Vocal tract resonances in oscine bird sound production: evidence from birdsongs in a helium atmosphere. *Nature* **235**, 53-55

Nowicki, S. & Capranica, R.R. (1986a) Bilateral syringeal interaction in vocal production of an oscine bird sound. *Science* **231**, 1297-1299.

Nowicki, S. & Capranica, R.R. (1986b) Bilateral syringeal coupling during phonation of a songbird. *J. NeuroScience* **6**, 3595-3610.

Nussbaumer, H.J. & Quandalle, P. (1979) Fast computation of discrete Fourier transform using polynomial transform. *IEEE Trans. Acoust. Speech Signal Process.* **27**, 169-181.

Oppenheim, A.V. & Schafer, R.W. (1989) *Discrete-Time Signal Processing.* Prentice-Hall. New York.

Parmentier, E., Genotte, V., Focant, B., Goffinet, G. & Vandewalle, P. (2003) Characterisation of the primary sonic muscles in *Carapus acus* (Carapidae): a multidisciplinary approach. *Proc. R. Soc. Lond.* B **270**, 2301-2308.

Paulsen, K. (1967) *Das Prinzip der Stimmbildung in der Wirbeltierereihe und beim Menschen*. Akademische Verlagsgesellschaft, Frankfurt am Main, Germany.

Percival, D.B. & Walden, A.T. (1993) *Spectral analysis for physical applications: Multitaper and conventional univariante techniques.* Univariate Techniques. Cambridge Univ. Press.

Podos, J. (1996) Motor constraints on vocal development in a songbird. *Animal Behaviour* **51**, 1061-1070.

Podos, J. (2000) Correlated evolution of morphology and vocal signal structure in Darwin's finches. *Nature* **409**, 185-188.

Pough, F.H., Janis, C.M. & Heiser, J.B. (2002) *Vertebrate life*. 6th ed. Prentice-Hall Inc. USA.

Press, W.H., Flannery, B.P., Teukolsky, S.A. & Vetterling, W.T. (1990) *Numerical recipes in Pascal. The art of scientific computing.* Cambridge University Press, Cambridge.

Rayleigh, J.W.S. (1945) *Theory of sound.* Dover Publ. New York.

Rodriguez, A.B. & Lea, R.W. (1994) Changes in immune response of the ring dove (*Streptopelia risoria*) during incubation. *Comp. Biochem. Physiol. A*. **109**, 157-166.

Rome L. C., Funke R. P., Alexander R. McN., Lutz G., Aldridge H., Scott F. & Freadman M.A. (1988) Why animals have different muscle fiber types? *Nature* **355,** 824-827.

Rome, L.C., Cook, C., Syme, D.A., Connaughton, M.A., Ashley-Ross, M., Klimov, A., Tikunov, B. & Goldman, Y.E. (1996) The whistle and the rattle: The design of sound producing muscles. *Proc. Natl Acad. Sci.* **93**, 8095-8100.

Rome, L.C. Syme, D.A., Hollingworth, S., Lindstedt, S.L. & Baylor, S.M. (1999) Trading force for speed: Why superfast crossbridge kinetics leads to superlow forces. *Proc. Natl Acad. Sci.* **96**, 5826-5831.

Rüppel, W. (1933) Physiologie und Akustik der Vogelstimme. *J. Ornithol.* **81**, 433-542.

Scala, G., Corona, M. & Pelagalli, GG.V. (1990) Sur la structure de la syrinx chez le canard (*Anas platyrhinchos*). *Anat. Hist. Embryol.* **19**, 135-142.

Seikel, A.J., King, D.W. & Drumright, D.G. (1999) *Anatomy and physiology for speech, language, and hearing.* Singular Publ.

Setterwal, C.G. (1901) *Studies öfver Syrinx hos Polymyoda Passeres.* Ph.D Thesis. University of Lund, Sweden.

Sibley, C.G. & Monroe, B.L. (1990) *Distribution and Taxonomy of Birds of the World.* Yale University Press, New Haven and London.

Slabbekoorn, H. (1998) *Perception of coo variation by the collared dove: a parameter analysis using playbakcs in the field.* PhD thesis, Leiden University, The Netherlands.

Slabbekoorn, H. & ten Cate, C. (1999) Collared dove responses to playback: Slaves to th erythm. *Ethology*, **105,** 377-391.

Smith, D.G. (1977) The role of the sternotrachealis muscles in bird song production. *Auk* **94**, 152-155.

Spiegel, M.R. (1974) *Theory and problems of Fourier Analysis.* Schaum Outline Series. McGraw-Hill, New York.

Staddon, J.E.R., McGeorge, L.W., Bruce, R.A. & Klein, F.F. (1978) A simple method for the rapid analysis of animal sounds. *Zeit. Tierpsychol.* **48**, 306-330.

Stein, R.C. (1968) Modulations in bird sounds. *Auk* **85**, 229-243.

Sturdy, C.B., Phillmore, L.S. & Weisman, R.G. (1999) Note types, harmonic structure, and note order in the songs of zebra finches (*Taeniopygia guttata*). *J. Comp. Physiol.* 133, 194-203.

Suthers, R.A. (1990) Contributions to birdsong from the left and right sides of the intact syrinx. *Nature* **347**, 473-477.

Suthers, R.A. & Hector, D.H. (1982) Mechanism for the production of echolocating clicks by the grey swiftlet, *Collocalia spodiopygia*. *J. Comp. Physiol. A*. **148**, 457-470.

Suthers, R.A. & Hector, D.H. (1985) The physiology of vocalisation by the echolocating oilbird *Steatornis caripensis*. *J. Comp. Physiol. A*. **156**, 243-266.

Suthers, R.A. & Margoliash, D. (2002) Motor control of birdsong. *Curr. Opinion. Nerobiol.* **12**, 684-690.

Suthers, R.A. Goller, F & Pytte, C. (1999) The neuromuscular control of birdsong. *Phil. Trans. Roy. Soc. B* **354**, 927-939.

Svensson, L., Mullarney, K., Zetterstrom, D. & Grant, P.J. (2003) *ANWB Vogelgids van Europa.* Tirion publ., Baarn. The Netherlands.

Tavolga, W.N. (1964) Sonic characteristics and mechanisms in marine fishes. In: *Marine Bio-acoustics,* vol I (ed. W.N. Tavolga), 195-211. New York. Pergamon Press.

Tchernichovski, O., Mitra, P.P., Lints, T. and Nottebohm, F. (2001) Dynamics of the vocal imitation process: How a zebra finch learns its song. *Science* **291**, 2564-2569.

Tchernichovski, O. & Mitra, P.P. (2002) Towards quantification of vocal imitation in the zebra finch. *J. Comp. Physiol.* A. **188**, 867-878.

ten Cate, C. (1992). Coo types in the collared dove Streptopelia decaocto: one theme, distinctive variations. *Bioacoustics* **4**, 161-183.

ten Cate, C., Lea, R.W., Ballintijn, M.R. & Sharp, P.J. (1993) Brood size affects behaviour, inter-clutch interval, LH levels, and weight in ring dove (*Streptopelia risoria*) breeding pairs. *Hormones and behaviour*, **27**, 539-550.

ten Cate, C., Slabbekoorn, H. & Ballintijn, M.R. (2002) Birdsong and male-male competition: causes and consequences of vocal varialbility in the collared dove (*Streptopelia decaocto*). *Advances in the study of Behaviour* **31**, 31-75.

Thompson, D.J. (1982) Spectrum estimate and harmonic analysis. *Proc. IEEE, Vol* **70**, 1055-1096.

Tigges, M., Mergell, P., Herzel, H., Wittenberg, T. & Eysholdt, U. (1997) Observation and modelling of glottal biphonation. *Acustica* **83**, 707-714.

Titze, I.R. (1988) The physics of small-amplitude oscillation of the vocal folds. *J. Acoust. Soc. Am.* **83**, 1536.

Tobalkse, B.W., Hdrick, T.L., Dial, K.P. & Biewener, A.A. (2003) Comparative power curves in bird flights. *Nature* **421**, p363-366.

Todt, D. & Fiebelkorn, A. (1980) Display timing and function of wing movements accompanying antiphonal duets of Cichladusa guttata. *Behaviour* **72**, 82-106.

Van den Enden, A.W.M. & Verhoeckx, N.A.M. (2000) *Digitale signaal bewerking.* 2nd ed. Delta press BV. Overberg, The Netherlands.

Verge, M.P., Fabre, B., Hirschberg, A. & Wijnands, A.P.J. (1997a) Sound production in recorder-like instruments 1. Dimensionless amplitude of the internal acoustic field. *J. Acoust. Soc. Am.* 101 (5), 2914-2924.

Verge, M.P., Hirschberg, A. & Causse, R. (1997b) Sound production in recorderlike instruments .2. A simulation model. *J. Acoust. Soc. Am.* **101** (5), 2925-2939.

Versluis, M., Schmitz, B., von der Heyft, A. & Lohse, D. (2000) How snapping shrimp snap: Through cavitating bubbles. *Science* **289**, 2114-2117.

Vicario, D.S. (1991) Contributions of syringeal muscles to respiration and vocalization in the zebra finch. *J. Neurobiol.* **22**, 63-73.

Vincent, J. (1982) *Structural Biomaterials.* Halsted Press, New York.

Von Békésy, G. (1960) *Experiments in hearing.* McGraw Hill, New York.

Von Rüppell, W. (1933) Physiologie und Akustik der Vogelstimme. *J. Ornithol.* **81**, 433-542.

Wakeling, J.M., Kaya, M., Temple, J.K., Johnston, I.A. & Herzog, W. (2002) Determining patterns of motor recruitment during locomotion. *J. Exp. Biol.* **205**, 359-369.

Warner, R.W. (1972) The syrinx in the family Columbidae. *J. Zool. Lond.* **166**, 285-390.

Watkins, W.A. (1967) The harmonic interval: fact or artefact in spectral analysis of pulse trains. In: *Marine Bio-acoustics Volume 2*. Edited by W.N. Tavolga. Pergamon Press. Oxford.

Wild, J.M. (1997) Functional anatomy and neural pathways contributing to the control of song production in birds. *Eur. J. Morph.* **35**, 303-325.

Wilden, I., Herzel, H., Peters, G. & Tembrock, G. (1998) Subharmonics, biphonation, and deterministic chaos in mammal vocalisation. *Bioacoustics* **9**, 171-196.

Williams, J.M. & Slater, P.J.B. (1991) Computer analysis of bird sounds: a guide to current methods. *Bioacoustics* **3**, 121-128.

Wundelrich, L. (1884) Beitrage zur vergleichende Anatomie des unteren Kehlkopfes der Vogel. *Nova Acta K. Leopold.-Carol. Akad. Naturf. Halle* **48**, 1-80.

Young, I.S. & Rome, L.C. (2001) Mutually exclusive designs: the power otput of the locomotory and sonic muscles of the oyster toadfish (*Opsanus tau*). *Proc. R. Soc. Lond. B* **268**, 1965-1070).

Zar, J. H. (1998) *Biostatistical Analysis*. 4th Int. Edition. Prentice Hall.

Ziemer, R.E. & Tranter, W.H. (1990) *Principles of Communications.* Houghton Mifflin Co., Boston, Mass.

Acknowledgements / Dankwoord

Irony itself wanted me to work on birds. After years of telling my friends there was no point putting a lot of effort in a group of animals that well-studied as the birds, when others were left unexplored, I found this subject and clenched on to it. After two years of looking at vibrating condoms in a dark anechoic room, I thought that most parts were not exactly what I liked about being a biologist and I decided to meet other ornithologists. That's what gave this thesis a happy ending. Without the help of many others, you would not be reading this. Mees talked me into this in the first place and I was delighted and honoured to work together with his creative, indefatigable mind the size of the universe. I would like to thank Ole for his wise words and for being supportive all the time. He somehow managed to know at great distance how I was doing and when I needed a push at exactly the right time. Thanks to Johan for all discussions and many words of advice. Many thanks to my for never crashing on me during the gargantuan thesis-design-task.

Despite the costs of living, it remains realy populair and I would like to thank all the people I have met during the last four years, simply because they were there to have fun with. I would like to thank all my (ex-) colleagues in the Experimental Zoology and the Cellbiology and Immunology Group. Hilda, Willeke, Henk and Anja, hurrah! With many of the (PhD) students and post-docs, I can look back on fun moments: Eshete, Martin, Sander, Talitha, Mark, Joop, Corine, Jochem, Michiel, Paulien, Maaike, Paula, Maria, Arjen, Prescilla. A special thanks to my roommate Igor, the most spicy Limburger I have ever met, for being able to share the office with me, mmmkay..! I had good fun. A very special thanks goes out to Ulrike, without whom my thesis would have written down less sharp for sure. Thanks for all your time, effort, enthusiasm and skills.

The long days turned into long nights during my short visits to the basements of the university building in Odense, sleeping at a LEGO development lab or in town. Many thanks to Marianne, Kenneth and Nicholas for cheering up those days. My visits to Leiden were always fun due to a huge number of nice people. A special thanks to Peter, unfortunately we never finished the experiments, and Gabriel for good discussions. During my stay in Salt Lake City, I enjoyed working in the lab of Franz and loved the great discussions. SLC wouldn't have been the same without Sylvia, Don and Adrian. I want to thank all the people in the lab: Anooshka, Bob, Brent, Kitt, my housemates and colleague reptile snatchers Jason and Jessica, John for his great reptile collection stories, Steve for the rubber boa night cruises, Chad for the capoeira dodge maneuvers. The last weeks were good dance fun thanks to John P. and many others.

After studying in Wageningen, many good friends spread around the globe and I got to meet new great people in Wageningen. Good friends are the most important thing in life, and they make it all worthwhile. Infinite thanks to my dear friends Chris, Arwen, Remko, Joris, Bart, Eva, Erno, Cindy, Tineke, Ruud, Joost, Marleen, Anouk and many others. Staying with friends was always fantastic. I am happy I had the time and was welcome to visit Chris in Frietboer, Switzerland, Remko & Daisy in Moscow, Idaho, Eva in Tarapoto, Peru. My housemates actually had to live with me, all the time: H8; Ruben, Marije, Ingeborg, Joris, Stephan, Esther, Lonneke, Andrea, Birgit, Monique, Marleen, Edo, Charel, Maarten and Stein. Thanks to all people in Wageningen, Dura, too many to mention. The Dutch techno party crew gave every year a special flavour, with the occasional, mindboggingly explosing of energy; Tim, Wouter, Nigel, Josien, Jasper, Roland, Floor, Mirjam, Joost, Marleen, Tineke, Joris. Funny enough, this thesis very likely would not have been here without my car… The Zen-endulged time to fix and restore a 33-year-old beauty took my mind of work, made it fly all over and made my hands very, very dirty. Blood, sweat and tears, great! Thanks to many people this seemingly insane project was a success, Bert, Joris, Arwen, Eric and Evert. A big hurrah to all the people and guides who helped me to find snakes around the globe. I never really liked birds anyway, but admittedly now I do.

Last but not least, I want to thank my parents who always supported and stimulated me whenever I was doing something of the beaten path and went into new, unexplored territory, my sister Ingrid for being back, and Josien for being there, so cool.

I could never identify myself with a spermwhale, which sounds like a perfectly sensible thing to do, but its skeleton would still be a magnificent sight in the Zodiac building. So long, and thanks for all the fish….

Affiliation of co-authors

Franz Goller	Department of Biology, University of Utah, 57 South 1400 East, Salt Lake City, UT-84112. Salt Lake City, United States of America
Kier Heeck	Condensed Matter Physics, Division of Physics and Astronomy Free University of Amsterdam, Amsterdam. De Boelelaan 1081, 1081 HV, Amsterdam, The Netherlands.
Michiel Hendriks	Experimental Zoology Group, Wageningen University, Marijkeweg 40, 6709 PG Wageningen, The Netherlands
Marc Hoffmann	Hydrology and Quantitative Water Management Group, Wageningen University, Wageningen Nieuwe Kanaal 11, 6709 PA, Wageningen, The Netherlands
Ole Næsbye Larsen	Center for Sound Communication, University of Southern Denmark, Campusvej 55, 5230 Odense M, Odense, Denmark
Johan van Leeuwen	Experimental Zoology Group, Wageningen University, Marijkeweg 40, 6709 PG Wageningen, The Netherlands
Ulrike Müller	Experimental Zoology Group, Wageningen University, Marijkeweg 40, 6709 PG Wageningen, The Netherlands
Mees Muller	Experimental Zoology Group, Wageningen University, Marijkeweg 40, 6709 PG Wageningen, The Netherlands
Henk Schipper	Experimental Zoology Group, Wageningen University, Marijkeweg 40, 6709 PG Wageningen, The Netherlands
Igor Spierts	Experimental Zoology Group, Wageningen University, Marijkeweg 40, 6709 PG Wageningen, The Netherlands
Anja Taverne-Thiele	Cell Biology and Immunology Group, Wageningen University, Marijkeweg 40, 6709 PG Wageningen, The Netherlands

Training and Supervision Program

Elemans, C.P.H. Graduate School WIAS

Development and experimental test of a quantitative biomechanical model of avian vocalisation.

Supervisors: van Leeuwen, J.L., Muller, M.& Larsen, O.N.
Project term: March 2000 - July 2004

EDUCATION AND TRAINING

The Basic Package	year	cp
WIAS Introduction Course (mandatory)	2003	1,0
Course on philosophy of science and/or ethics (mandatory)	2002	1,0
Subtotal Basic Package		2,0

Scientific Exposure	year	cp
International conferences		
Society of Experimental Biology, Edinburgh, Scotland. March 29- April 2	2004	1,0
10th Benelux congress of Zoology, Leiden.November 7-8.	2003	0,4
Specialist meeting at the Wissenschaftskolleg zu Berlin, Institute for advanced Science.April 9-12.	2003	1,0
9th Benelux congress of Zoology, Antwerp, Belgium. November 8-9	2002	0,4
International Congress of Ornithology, Beijing, Peoples Republic of China.August 8-17	2002	1,5
Society of Experimental Biology, Swansea, Wales. April 6-13.	2002	1,0
8th Benelux congress of Zoology, Nijmegen. November, 23-24	2001	0,4
Society of Experimental Biology, Canterbury, England. April 2-6	2001	1,0
7th Benelux congress of Zoology, Brussels, Belgium. November 24-25	2000	0,6
Society of Experimental Biology, Exeter, England. March 26-31.	2000	1,0
Seminars and workshops		
Seminar 'Lèvres vibrante et cordes vocales' of the French Acoustical Society, Paris. July 2.	2004	0,2
Next WaVe 'NWO Talentendag' September	2003	0,2
WIAS Science day, May 27.	2003	0,2
Presentations		
Invited speaker at seminar of the French Acoustical Society, Paris. July 2.	2004	0,5
Society of Experimental Biology, oral presentation, March 29- April 2.	2004	0,5
Invited speaker at specialist meeting at the Institute for advanced Science, Berlin, April 9-12.	2003	0,5
Invited speaker at WIAS Science day, oral presentation, March 27.	2003	0,5
International Congress of Ornithology, Beijing, oral presentation, August 8-17.	2002	0,5
Society of Experimental Biology, oral presentation, April 6-13.	2002	0,5
Benelux congress of Zoology Nijmegen, oral presentation, November 23-24.	2001	0,5
Society of Experimental Biology, oral presentation, April 2-6.	2001	0,5
Society of Experimental Biology, poster, April 2-6.	2001	0,5
Benelux congress of Zoology Brussels, oral presentation, November 24-25.	2000	0,5
Benelux congress of Zoology Brussels, poster, November 24-25.	2000	0,5
Society of Experimental Biology, oral presentation, March 26-31.	2000	0,5
Summer School Odense, Denmark, Poster, August 16-27.	2000	0,5
Subtotal International Exposure		*15,4*

In-Depth Studies	year	cp
Disciplinary and interdisciplinary courses		
Aëroakoestiek, TU Twente. September 23 - October 17	2002	4,0
Biology underpinning Animal Sciences	2001	0,8
Acoustical Communication, Odense Denmark, August 16-26	2000	2,0
Avian Acoustical Communication, Copenhagen Denmark, August 27-31.	2000	1,0
Subtotal In-Depth Studies		*7,8*

Professional Skills Support Courses	year	cp
Course Supervising MSc thesis work	2002	0,5
Management and negotiation course, May	1999	1,0
Media training, November	1998	0,5
Subtotal Professional Skills Support Courses		*2,0*

External training period	year	cp
visit Goller lab, Salt Lake City, USA. May 10- August 23.	2003	1,0
visit Center for Sound communication, Odense, Denmark. February 23 - March 12.	2002	0,5
visit Center for Sound communication, Odense, Denmark. October 6 -22.	2001	0,5
Subtotal Research Skills Training		*2,0*

Didactic Skills Training	year	cp
Teaching Assistantships General Zoology I & II	2000-2002	3,0
Teaching Assistantships Human epidemiology & nutrition	2002	1,0
Supervising MSc theses		
Michiel Hendriks		1,0
Paulien Roos		1,0
Subtotal Didactic Skills Training		*6,0*

Education and Training Total	*35,2*

One credit point (cp) equals a study load of approximately 40 hours.

The cover

Nobody actually reads a PhD thesis. Maybe except for the acknowledgements (am I mentioned?) and the curriculum vitae (how does his' compare to mine?). If it is a really good friend, he or she tries to read the Dutch summary. So, I decided if nobody reads it, I wanted a smashing cover to make it look good, or even better.

Since I wasn't too focussed on singing birds with photographing myself, I could not find a photo good enough to satisfy my needs. I wanted a photo of singing birds that gave a crystal-clear impression that it was accompanied by sound. Therefore, I decided to contact Frans Lanting, my favourite wildlife photographer. He has contributed to many National Geographic covers and published beautiful books such as Jungles, Penguin, Living Planet, Eye to Eye, Bonobo, Okavango. When I saw this picture of two Magellanic penguins (*Spheniscus magellanicus*) I knew it was the right one...

Furthermore, the little face on the back cover folding was initially placed on the back cover, but unfortunately it was not allowed there by the Rector Magnificus. Although it looks like a photo of me, it is actually the spectrogram (an 'energy' plot of a time- signal with frequency on the y-axis and time on the x-axis; for more information see Chapter 3) of a sound. Just for the fun of it, I wanted to make sound out of images using the inverse technique that is used to construct a spectrogram from a sound signal. To do so, I took the first column of pixels of a greyscale image and with some scaling and shifting used this one-dimensional string as $g(\omega)$ input for an inverted Fast Fourier Transform (*i*FFT): $G(t) = \frac{1}{2\pi}\int_{-\infty}^{\infty} g(\omega)\, e^{-i\omega t}\, d\omega$.

This resulted in a small piece of time signal. By windowing and adding the *i*FFT of a new column of the image to the growing string of numbers, I ended up with a sound signal. At first, I expected a lot of noise, but funny enough this photo turned out fabulous due to the striped shirt and my glasses.

Curriculum vitae

Coen Elemans werd geboren op 27 februari 1976 te Oss. Hij behaalde zijn Gymnasium diploma aan het Titus Brandsma Lyceum te Oss in 1994. Al vanaf zijn 12e jaar hield hij thuis vissen en toen het dan eindelijk mocht van pa en ma, reptielen. Met een voorliefde voor biologie, nog steeds werkende in de aquariumzaak de Tetra te Oss, begon hij in 1994 aan de opleiding Biologie aan de toenmalige Landbouwuniversiteit te Wageningen.

Al in het eerste jaar van zijn studie werd hij betrokken bij de studenten politiek in de toenmalige Propedeuse Commissie Studiebegeleiding, gevolgde door vier jaar actief lid en voorzitter van de Richting Groep (Rigro) Biologie. In het collegejaar 1998-1999 was hij voltijds bestuurslid van de studentenvakbond, de Wageningse Studenten Organisatie (WSO) tijdens de roerige introductie van het eerste ondernemingsplan van WUR. Met een vriendenclub werd in 1995 het onafhankelijke biologen dispuut Dura Nucleus opgericht.

Na behalen van de propedeuse in 1995, koos hij voor de specialisatie 'Dier'. Tijdens zijn doctoraal, heeft hij twee afstudeervakken gedaan bij de toenmalige leerstoelgroep Experimentele Dierkunde o.l.v. Professor Jan Osse in het Zodiac gebouw aan de Marijkeweg. Het eerste afstudeervak is gedaan onder de bezielende leiding van Mees Muller, en was een vergelijkend morfologisch onderzoek naar de timing van de aanleg van een functioneel hart- en vaatstelsel bij de gewervelde dieren. Het 'veldwerk' werd verricht in de embryocollectie van het Laboratorium voor Ontwikkelingsbiologie, het Hubrecht laboratorium, te Utrecht. Het tweede afstudeervak werd uitgevoerd op het lab van Professor McNeill Alexander te Leeds, Engeland, onder begeleiding van Robert Ker. Om te begrijpen hoe de menselijke voet de enorme klappen verwerkt bij het neerkomen op de grond tijdens rennen, heeft Coen de dempende werking van de menselijke hak gemeten onder verschillende omstandigheden, aan (vers) geamputeerde benen. De resultaten van dit afstudeervak zijn gepresenteerd op een internationaal congres in Exeter (2000). Na een enkele naamwijziging maar nauwelijks cultuurwijzingen van de universiteit behaalde hij zijn Biologie diploma aan de Wageningen Universiteit eind maart 2004.

Enkele weken daarvoor was hij begonnen met de aanstelling als Onderzoeker in Opleiding (OIO) aan de leerstoelgroep Experimentele Zoölogie o.l.v. Johan van Leeuwen. Van maart 2000 tot juli 2004 heeft hij hier zijn promotie onderzoek verricht. Dit onderzoek werd begeleid door promotor Johan van Leeuwen en copromotoren Mees Muller en Ole Næsbye Larsen. Het proefschrift in u handen, wat u zou kunnen lezen, is het resultaat van dit onderzoek. Tijdens zijn onderzoek heeft hij gewerkt in groepen in Odense, Denemarken en Salt Lake City, USA. De resultaten zijn gepresenteerd op internationale congressen in Brussel (2000), Canterbury (2001), Nijmegen (2001), Swansea (2002), Beijing (2002), Antwerpen (2002), Leiden (2003), Edinburgh (2004) en werd hij uitgenodigd lezingen te geven in Berlijn (2002), Wageningen (2003) en Parijs (2004).

Tijdens zijn studie begon hij met fotografie en was hij veel buiten op de mooiste plekjes van Nederland om planten en dieren te zoeken. Ook begon het zoeken naar reptielen ernstigere vormen aan te nemen. Vele reizen naar uithoeken van de wereld brachten hem, naast Europa, in Tunesië, Canada, Israël, Jordanië, Thailand, in de Amazone van Peru, op zoek naar de bijna uitgestorven Jangtzé alligator in China, Turkije en de woestijn systemen van de Verenigde Staten. Diverse pogingen om het Zodiac wat op te fleuren leiden niet tot een skelet van een potvis, wel eentje van 12 meter piepschuim, en het kunstexpositie project ExpoZ'd, welke nu nog loopt. Hij heeft daarmee het felbegeerde record 'Zodiac kantine-verbouwen' nog steeds in handen.


scienzz
Geluidnieuws
SCIENCE NEWS Online
ulmer online
The Animal Communication Project
scienceticker.info


Opmerkelijk
VARA
Berliner Zeitung
HindustanTimes.com
call 083 12 FELIX
Science now
stke members
bridgeles.nl
N24
DUIVENVIBRATO
morgenwelt

Coverphoto: ©Frans Lanting\www.lanting.com

Other photos: Coen Elemans

Design: Coen Elemans

Print: Ponsen & Looijen Wageninggen

This study was carried out at the Experimental Zoology Group, Department of Animal Sciences, at Wageningen University.

This study was supported with a grant from NWO/ALW.